Fabrication And Electrical Characterization of Organic Neuromorphic Memory Devices

Master thesis by : Rabiul Islam
1. Supervisor : Dr. Paschalis Gkoupidenis
2. Supervisor : Prof. Dr. Wolfram Jaegermann

TECHNISCHE
UNIVERSITÄT
DARMSTADT

MAX-PLANCK-INSTITUT
FÜR POLYMERFORSCHUNG

MAX-PLANCK-INSTITUT
FÜR POLYMERFORSCHUNG

TECHNISCHE
UNIVERSITÄT
DARMSTADT

Fabrication and Electrical Characterization of Organic Neuromorphic Memory Devices.

Final Thesis Report
to achieve the university degree of Master of Science in Materials Science
Study program: Materials Science

Submitted by:
Rabiul Islam,
Matriculation No.: 2997810,
Department of Materials Science,
Technische Universität Darmstadt, Germany.
robi.physics@gmail.com

Submitted to:
Department of Materials Science,
Technische Universität Darmstadt,
Alarich-Weiss-Straße 2,
64287 Darmstadt, Germany.

And
Department of Molecular Electronics,
Max-Planck-Institute for Polymer Research,
Ackermannweg 10,
D-55128 Mainz, Germany.

Supervisor:
Dr. Paschalis Gkoupidenis,
Department of Molecular Electronics,
Max-Planck-Institute for Polymer Research,
Mainz, Germany.

Co-Supervisor:
Prof. Dr. Wolfram Jaegermann,
Department of Materials Science,
Technische Universität Darmstadt,
Darmstadt, Germany.

Tag der mündlichen Präsentation: 16 July, 2019
Tag der Einreichung: 15 Oktober 2019

Declaration

I declare that I have authored this thesis independently, that I have not used other than the declared sources/resources, and that I have explicitly indicated all material which has been quoted either literally or by content from the sources used.

Darmstadt, Germany 15. October 2019	(Rabiul Islam)
.....	.....
Place & Date of Submission	Signature

Acknowledgements

This thesis protocol material is based upon the work supported by the Department of Molecular Electronics, Max-Planck Institute, Mainz. First, I would like to thank Dr. Paschalis Gkoupidenis from MPIP, Mainz, for allowing me to work in this research project. I am very much grateful to him for his regular discussions, guideline, and encouragement throughout the thesis study that helped me a lot to cope-up with the work efficiently. Besides of it, thanks to him for officially refereeing my thesis.

I would also like to express my gratitude to Prof. Dr. Wolfram Jaegermann from the Materials Science Department, Technische Universität Darmstadt, for approving and allowing me to pursue my thesis. His valuable suggestions were guided me to finish this thesis work successfully.

I want to thank Dr. Dimitrios A. Koutsouras from Max Planck Institute, Mainz, for providing me hand-to-hand experience on the cleanroom-based OECTs device fabrication process. Beside of it, thanks to Frau Michelle Beuchel and Mr. Christian Bauer for their friendly co-operation during the device fabrication process.

Also, thanks to Prof. Dr. Paul W.M. Blom, director of the Molecular Electronics Department at MPIP, for his constructive comments during the group meeting. However, a special thanks to Frau Petra Pausch at MPIP for arranging all the appointments during my thesis study.

I would also like to convey my thanks to all members of the Molecular Electronics Department at MPIP for supporting by giving a friendly environment. Along with, thanks to all members of the Institute of Surface Science at TU Darmstadt.

Last, but not least, I want to give thanks to my family and friends for their constant support from the beginning of my thesis work.

Abstract

The organic polymer has gained considerable interest in the field of bioelectronics during the last few decades. Organic materials based devices have several unique characteristics; low-cost and low thermal budget fabrication processes, tunable properties through chemical synthesis, flexibility and biocompatibility. Those entire features make organic materials suitable for new functionalities in comparison to their inorganic counterparts. Moreover, the attributes mentioned earlier give an additional degree of freedom to use organic materials in neuromorphic devices whose functions have the potential to induce biological realism in brain-inspired information processing. Nowadays, neuromorphic devices have attracted the interest in research and industry. The use of organic materials might lead to a new class of neuromorphic devices that has several applications in areas that range from brain-computer interfaces to circuits for local data processing in energy restricted environments. However, flexibility and biocompatibility helps to optimize the mechanical mismatch between electronics and biological substances that might be a new way of signal processing at the interface with biology.

In this thesis project, three-terminal organic polymer-based Organic Electrochemical Transistors (OECTs) have fabricated in cleanroom-based fabrication process. PEDOT:PSS and p(g2T-TT) thin-film polymers were used as active channel materials in OECTs. Ions inject from the liquid electrolytes by using a specific gate bias. The migrated ions modulate the entire bulk-volume conductivity of the organic polymer channel due to the strong coupling between ionic and electronic charges within the channel. Several electrical characterizations of OECTs were investigated in the presence of liquid electrolytes. The memory phenomena of PEDOT:PSS and p(g2T-TT) polymer-based OECTs were systematically studied in this work. It was observed that PEDOT:PSS organic polymer shows no memory properties/negligible memory, and p(g2T-TT) polymer exhibits memory phenomena due to its unique polymer structure. It also seen that the memory process in p(g2T-TT) polymer is a reversible process that can be return to its initial state by applying opposite gate bias. Beside it, the polymer's behavior also was investigated in contact with and without aqueous solutions. Additionally, it observed that p(g2T-TT) polymer is less hydrophilic compared to PEDOT:PSS due to its intrinsic properties. Multiple memory devices were fabricated at different times and reproducible memory phenomenon was observed in OECTs.

1. Table of Contents

1. Introduction

Computers and microelectronics have changed our way of everyday life. Massive integration of semiconductor chips has given us a wide range of freedom to fabricate a large variety of portable electronic devices. All conventional computer CPU architecture relies on semiconductor base transistors, which miniaturization structure followed by Moore's Law [53]. After a certain level of miniaturization, CPUs lose their most important properties across such minuscule distances and lets electrons pass the so-called quantum tunneling effect [29, 35]. Due to this effect, a minimal current leakage occurs in the tiniest circuits, which, increases power consumption as well as generates heats, which affect the functioning and reduce their efficiency. However, the electronic circuits-based modern PC chips rely on complementary metal-oxide-semiconductor (CMOS) technology, and they designed according to John von Neumann architecture [1]. This architecture describes in the First Draft how computational and memory units have to interact to execute any program. A von Neumann computer consists of computational and memory units [29] as a repository for both programming instructions and data. The physical separation of the computational and memory unit at the same time, however, quickly draws a limitation so-called von Neumann bottleneck [29]. That's because every time an instruction read, the CPUs cannot process data. On the other way around, if data read, the CPU has to wait for instructions. There are only switches designed to solve a specific problem, meaning it required much work to change them over to solve a different calculation. The new technological developments in the field of electronics demand faster signal execution and memory. Nowadays, it well recognized that von Neumann architecture base traditional computer is not well-adapted to understand and capture the information of the biological nervous system [6] due to the von Neumann bottleneck [6, 29]. The challenges of von Neumann bottleneck can solve through a new computational concept, which is inspired by the biological neural network [6].

The biological nervous system does parallel signal processing, which is much faster than the series signal processing that has been using in conventional computers. In parallel signal processing, multiple data can process at the same time that gives the faster performance of a device, which is pretty much similar to the biological neural network in an animal's brain. The human brain contains a large number of various types of neurons [1]. Every neuron connects, see figure 1, through a tiny biological channel so-called synapses. Figure 1 shows that each neuron connects with multiple neurons through the synapses means every neuron can do multiple signal processing and memory tasks throughout the entire neural network at the same time without any time lag [1]. The human brain's computing system has some unique advantages. For example, it is an energy-efficient cognitive system and equipped with a figure of merit of highly fault-tolerant and parallel computation, self-learning, and updating itself [1].

All the above advantages of biological neural network inspired the scientists to develop an artificial neural network in where inbound impulses are accumulated spike by spike just like inside a biological neuron and then sent along the conductive channel to connected artificial neurons. Thus, concepts of artificial neural networks are, artificial nodes used instead of neurons, somewhat analogous to the function of the brain. This biologically inspired system could finally break the von Neumann bottleneck [30]. In the late 1980s, the concept of neuromorphic engineering, also known as neuromorphic computing, was established through the work of Carver Mead [1, 6], one of the pioneers of semiconductor electronics [30]. He proposed a very-large-scale integration (VLSI) system, which mimics the neuro-biological architectures with a silicon-based electronic analog circuit [6, 31]. Initially, he has proposed an artificial synapse by using floating-gate silicon transistor [1].

Nowadays, neuro-inspired multi-core chips with standard CMOS technology are successfully applied in the conventional computing system [6]. The hardware-level implementation of neuromorphic computing can realize through some solid-state technologies, including oxide-based memristors, transistors, spintronic, and ferroelectric memory devices, which are basic functional building blocks of neural processing and neuroplasticity [1, 6].

Recently a breakthrough was made in neuromorphic computing by engineering new learning organic electronic materials. Those organic electronic materials have taken the attention of researchers due to their intrinsic properties, for example, exceptional interfacing abilities between electronics and biological substances, low production cost, flexibility, and biocompatibility. All those features make organic materials desirable to use in organic bioelectronics devices. A particular example is Organic Electrochemical Transistor (OECT), a device whose channel made from organic conducting or semiconducting polymer such as poly(3,4 ethylenedioxythiophene):poly(styrene sulfonate) (PEDOT:PSS) [1, 3, 6]. An organic electrochemical transistor can amplify or switch electron signals and power through the injection of ions from an electrically conducting solution (electrolyte) into its conducting/semiconducting polymer channel; hence, the conductivity of the polymer channel tunes. Here, the electronic charge carrier density of the channel has been modulated by the ionic charges due to the strong coupling between electronic and ionic charges within the entire bulk-volume of the channel; hence, the transconductance of OECT has been improved compared with its counterpart field-effect transistors (FET) [3, 6]. On the other-hand, FETs devices operate in the interfacial doping regime which cannot provide good transconductance as OECT does. The strong coupling between ionic and electronic charges in OECT makes excellent interfacial cooperation between electronics and biological systems [6]. OECT also has been enabled to behave in a manner that is similar to short-term and long-term neuromorphic functions of the brain.

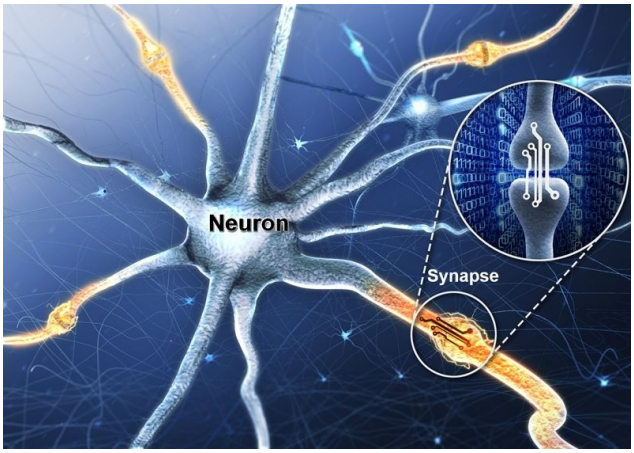

Figure 1: Representation of the biological neurons and synapses. Each neuron connects with multiple neurons through synapses. The magnified synapse represents the portion mimicked using solid-state devices [32].

In this master thesis study, three-terminal organic electrochemical transistors were fabricated whose channel was made from PEDOT:PSS conducting polymer and p(g2T-TT) semiconducting polymer. Liquid sodium chloride-based electrolyte provides the modulator ions in the channel. The p(g2T-TT) polymer made transistor can store ions even behind its operation period that can be used as a neuromorphic memory device. Different electrical characterization has been performed to observe the memory phenomenon of OECT to use them in hardware-based neuromorphic circuit applications.

2. Theoretical Background of Organic Electrochemical Transistor.

2.1 History of OECTs Technology

In the modern era, all electronic devices are usually referring to things containing transistors. After the successful invention of the transistor by William Shockley and his colleagues in 1947 [35, 38], the reliability of vacuum tubes for the more massive sized computer was replaced by tiny transistors [3]. Conventional transistors employ inorganic semiconductor materials such as mono-crystalline silicon or gallium arsenide, dielectrics, and metals, which allow a control flow of electrons through this tiny solid-state-device [3, 35]. However, its miniaturization leads to the development of integrated circuits results in the portable electronic device. All modern transistors use an electric field to control the current following through the device. The flow of current relies on field-effect doping: the number of mobile electrons or holes within the semiconductor channel is modulated by the voltage applied to the gate electrode. The metallic gate electrode also can be referred to as the control electrode, is separated from the semiconductor channel by a dielectric. This type of transistor is called metal-oxide-semiconductor field-effect transistor or MOSFETs. Over the last several decades, field-effect transistors have widely been used in many portable electronic devices. However, FETs using various types of inorganic semiconductors as their active channel materials are disadvantageous in that they are expensive, nonbiodegradable, and in many cases are complex fabrication processes. More recently, two dimensional or nanoscale materials, such as graphene, were introduced in the FET channel.

In parallel, over the past few decades, organic electronic materials such as small molecule semiconductor or conjugated conducting polymer offer an alternative to inorganic devices which can meet unique demands, for instance, biocompatibility, mechanical flexibility, large scale easy solution processibility, etc. [37]. Organic conducting polymer-based transistors are widely investigated with the discovery of conducting conjugated polymer in the late 1970s [38]. Among them, steady progress has been achieved on organic thin-film based transistors has excellent attention due to their broad range of applications, especially in the biological systems. Organic thin-film based transistors can be subclassified into organic field-effect transistors (OFETs) and organic electrochemical transistors (OECTs) [33, 34]. Organic conjugated macromolecules and small organic molecules are used as a semiconductor in OFETs operations, in which the gate voltage is applied across the gate insulator and through field-effect doping the gate electrode modulates the channel current.

In the mid- of 1980s, organic electrochemical transistors (OECTs) was developed by Wrighton and colleagues, as an extraordinary modality of organic FETs. It was the first time-reversible electrochemical switching of electric conductive polypyrrole was reported by them [3]. A few years later, in 1984, the first successful OECT was built (see in figure 2) by Henry S. White *et al.* at Massachusetts Institute of Technology [38, 39]. They had reported a device with a chemically derivatized microelectrode array that had similar functionality of transistors to amplify and control a tiny current when it was immersed in a liquid electrolyte solution. Their device was mimicked the fundamental characteristics of solid-state transistors. In their device, three independent gold microelectrodes are separated by 1.4 μm gaps. A polypyrrole polymer makes a bridge allowing a current pass between source and drain. It is the first time the gate electrode was separated from the semiconductor channel interface with electrolyte [38]. In their designed OECTs, the gate electrode was controlled by a traditional gate-counter-reference electrode probing approach [3, 39] in where the counter and reference electrodes were used to establish the current circuits to ensure the stability of the different external cyclic gate potentials. At a constant gate voltage, the gate electrode can be simplified into only one

electrode because the transfer curve or transconductance curve would not change due to the constant gate voltage [40].

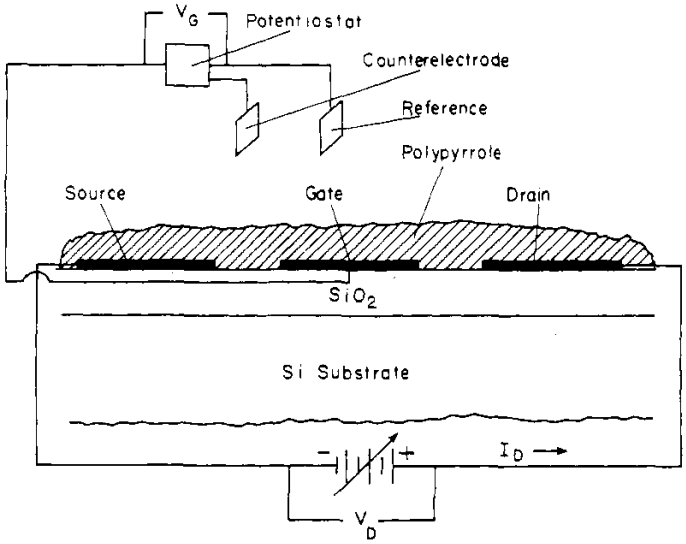

Figure 2: Schematic cross-section view of the first successful build polymer channel-based OECT, which shows the circuit elements used to characterize it [39]. The device was fabricated on SiO_2 (~0.45µm thick) coated Si <100> substrate. The source, gate, and drain are Au with the dimension of width × length × thickness (3×140×0.12) μm^3 coated with polypyrrole. During its operation, the microelectrode array, counter, and reference electrodes were placed in an electrolyte solution.

From then on, various probing setup on the configuration of the separated gate and channel interface was developed for electrochemical and biological applications [3, 38]. Besides it, some other polymers, such as polyaniline, polypyrrole, poly(3-methylthiophene)[41], have been investigated as the active channel material in electrochemical transistors. However, various configurations of gate electrodes, tiny scale integration facilities and advanced printing technology enables the OECTs to use in massive area computing.

The first printing technique based electrochemical transistor was reported in 1994 [3, 42]. Source and drain electrodes were carbon-based materials, and they were printed on polyvinyl chloride by using screen-printing technology. Liquid nitrogen has been used to make the cracked on the device and polyaniline was grown along the fractured edge and coated with glucose oxide immobilized in poly(1,2-diaminobenzene. This transistor was used for glucose and peroxide sensing [46, 47]. In 2002, the first PEDOT:PSS organic polymer-based transistors were reported. The source, drain, and gate of OECTs were laterally configured with a screen-printed technique, and the gel electrolyte on the top of the channel was used, which can be achieved up to 1.2 mS of transconductance [3, 43, 44]. Beside of it, PEDOT:PSS-NFC channel OECTs also has been demonstrating with transconductance beyond 1 S [3, 45]. Recently, p(g2T-TT) polymer has been used in both lateral and floating gated; OECT exhibits a unique memory phenomenon, which is described in section 2.4 of this report.

2.2 Polymer Materials for OECTs Channel.

The channel for OECTs is generally fabricated by electrically conducting or semiconducting polymers, which has excellent redox activity. Past few decades, organic semiconducting polymers have attracted intense interest because of their potential use in mechanically flexible, lightweight, and low-cost fabrication processes. So far on, various types of conjugated conducting and semiconducting polymers have been studied for OECTs channel such as PEDOT:PSS, PEDOT:TOS, PTHS, PEDOT-S, p(g2T-TT), p(gNDI-g2T) [3], etc. Among them, PEDOT:PSS is the most popular conducting polymer used for the OECTs channel. Following this thesis study protocol, two types of organic polymer were used: PEDOT:PSS conducting and p(g2T-TT) semiconducting polymer.

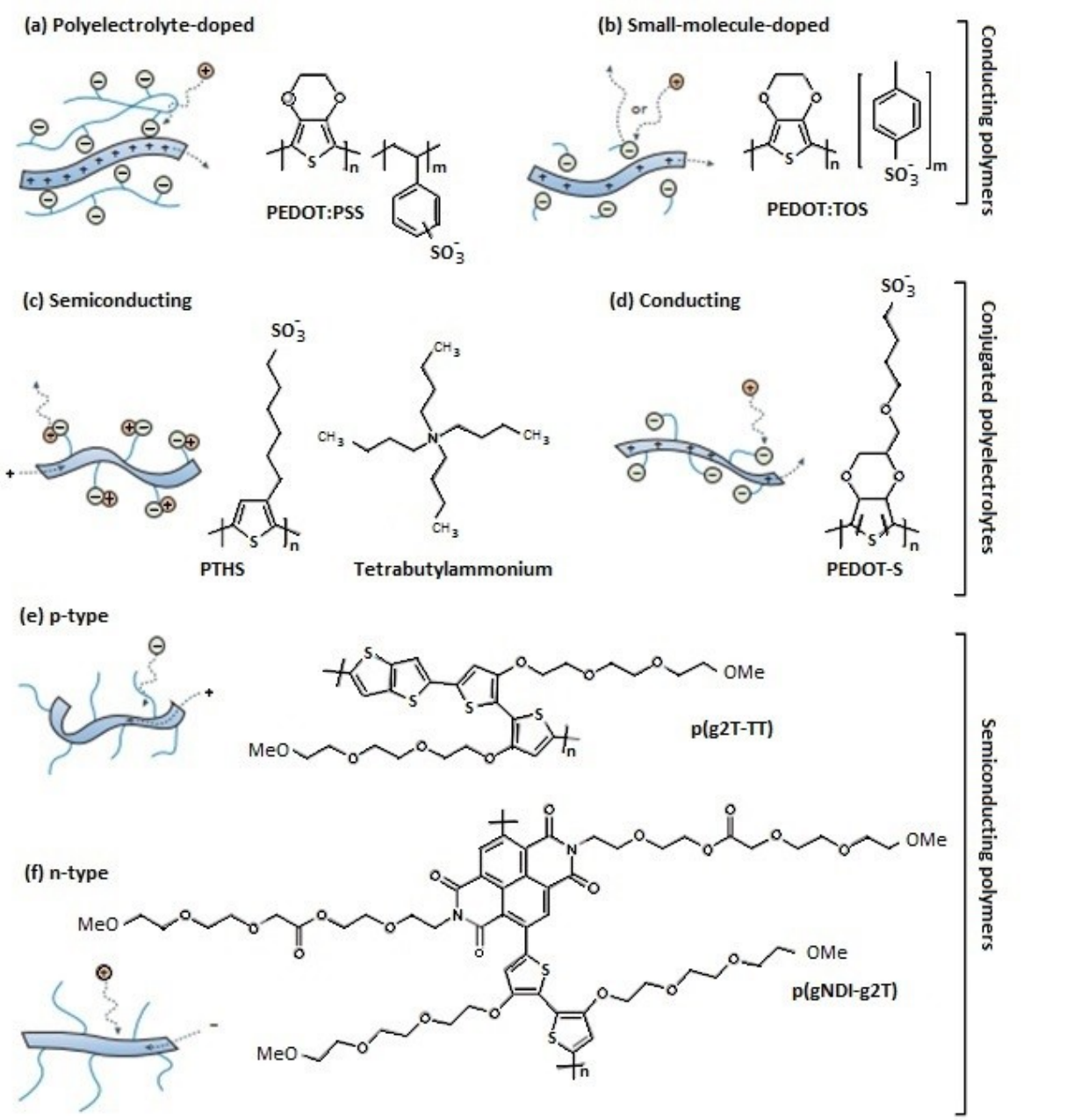

Figure 3: Schematic diagram and molecular structure of different kinds of polymer materials used in OECT channels [3].

2.2.1 PEDOT:PSS Conductive Polymer.

The first poly(3,4-ethylenedioxythiophene) polymer was synthesized at the Bayer Laboratories in Germany [66]. The monomeric unit of PEDOT is the 3,4-ethylenedioxythiophene or EDOT. The electrical properties of this polymer can be dramatically enhanced by adding poly(styrene sulfonate). Poly(3,4-ethylenedioxythiophene):poly(styrenesulfonate), abbreviated as PEDOT:PSS is an electro-chemically stable conjugated polymer which has high electrical conductivity by doping with p-type dopants such as small anions (PSS) or polyanions (see in figure 3 a & b). When PEDOT is doped with Poly(styrenesulfonate), the sulfonate anions of PSS introduce some holes in the PEDOT polymer chain. Due to the doping, holes can hop throughout the polymer chains which play an essential role to make this polymer highly conductive of more than 1000 S/cm at room temperature [38, 48, 49, 51], makes it a potential candidate to use in a variety of applications. PEDOT:PSS polymer is synthesized by solution, vapor-phase or electrochemical polymerization. It is available in the form of a liquid solution, and its aqueous dispersions allow a smooth deposition of polymer thin film using a solution-processing technique [52], which was used during the fabrication of the OECTs channel of this thesis work. The dispersion starts by polymerizing EDOT (the monomer of PEDOT) in the presence of PSS [52]. The solution-based easy fabrication process makes it a potential candidate for using, for example, in electrostatic coatings, anodes for light-emitting diodes, solar cells, etc. [51, 52].

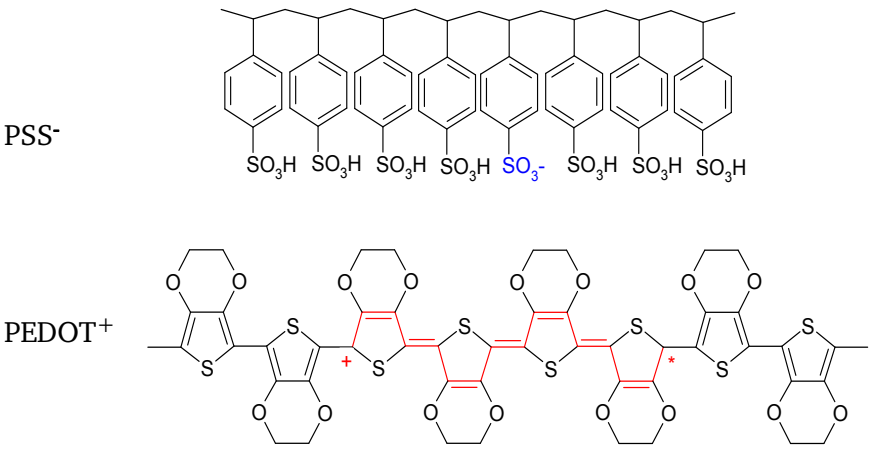

Figure 4: Chemical structure of PEDOT and PSS. The hole on the PEDOT polymer chain represents a positive polaron, which is compensated by a sulphonate ion on the PSS chain [57].

The PEDOT:PSS has a complex polymer structure. Figure 4 shows the chemical structure of PEDOT & PSS polymer. When PEDOT was doped with PSS molecules in the form of liquid, a sequence of hierarchically structured monomers of PEDOT:PSS was formed. Hierarchical is the primary structure of PEDOT:PSS that leads towards the final solid thin film growth. The secondary structure is a polyion complex where PSS molecules combined with PEDOT through electrostatic interactions. In this secondary structure, the PSS molecule plays a role as a counter-ion for balancing the charge transfer that leads to the formation of holes in PEDOT films. The PEDOT:PSS in water was formed a colloidal gel having a micelle structure or tertiary structure [51]. So finally, a solid thin film is formed through the spin coating process, which enables us to achieve high electronic conductivity in the solid film. The structure of the hierarchical configuration has not been understood well; as a consequence, there is little progress for understanding the electronic conduction mechanism at the microscopic level [51].

However, recently, it has been reported that the conductivity of PEDOT:PSS solid thin film can be rapidly enhanced by adding some other solvents, for example, dimethyl sulfoxide, N-N dimethylformamide or tetrahydrofuran [51, 54]. It has also been reported by Okuzaki *et al.* that the addition of ethylene glycol (EG) can dramatically enhance the electrical conductivity of the solid PEDOT:PSS thin films [55]. Besides those solvents, there is some other variety of additional solvents used to enhance its electrical conductivity. However, due to the poor understanding of the structure, there is little information about the origin of its high electrical conductivity by the addition of solvent [51].

PEDOT:PSS polymer-based OECTs exhibits very high transconductance, in the range of millisimiens/µm [1], and short response time, which makes this conducting polymer desirable for many bio-electronic applications pursued OECTs. Besides those unique properties and excellent performance of PEDOT:PSS in OECTs, using this polymer has some challenges. For example, in the sense of electrical properties, PSS molecules have massive structure affects the volume fraction of PEDOT thin film which leads to the smaller volumetric capacitance [56]. However, PEDOT:PSS polymer has higher Young's modulus compared to biological tissues. This mechanical property limits this polymer for using in biological applications [58, 59]. Furthermore, its high acidic properties hinder processing via a different technique such as inkjet printing.

2.2.2 p(g2T-TT) p-type Semiconducting Polymer.

Previously it was reported that p(g2T-TT) polymer channel-based OECT device exhibits better performance in terms of transconductance than PEDOT: PSS-based devices [63]. Beside it, PEDOT:PSS is a two-phase polymer salt that allows only depletion mode of OECTs operation, whereas p(g2T-TT) is a single-phase polymer without any native dopants. Due to this material distinction, the p(g2T-TT) polymer-based OECTs can be operated in both depletion and accumulation mode[61].

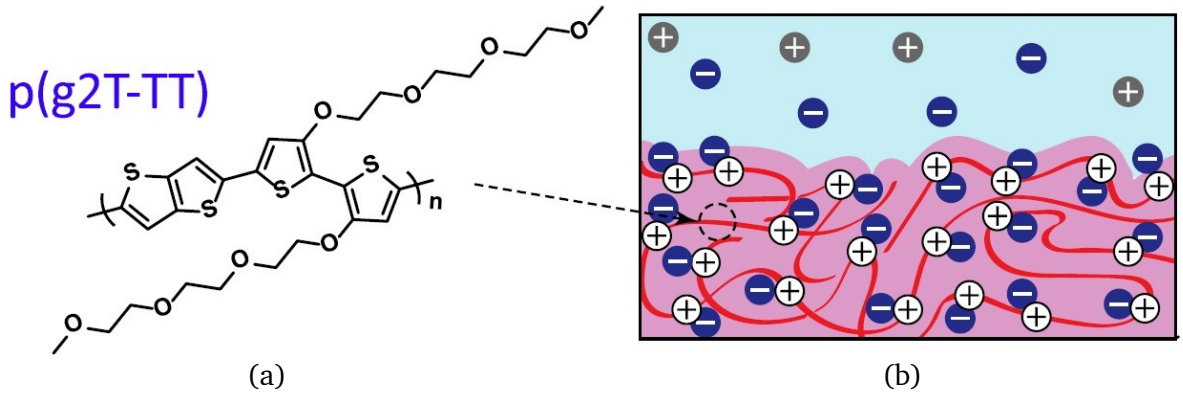

(a) (b)

Figure 5: (a) The molecular structure of p(g2T-TT) polymer contains bithiophene-thienothiophene (2T-TT) polymer backbone holds ethylene glycol side chain. (b) Schematic presentation of interactions of ions with glycolated p(g2T-TT) polymer. Anions (Cl^-) from NaCl electrolyte (green color) are shown in blue; cations (Na^+) in gray and holes along the polymer backbone chain are shown as white spheres [60].

Figure 5(a) shows the molecular structure of p(g2T-TT) semiconducting polymer, which contains triethylene glycol side chains [$CH_3(OCH_2CH_2)_3O$-]. The chemistry of this side chain effectively

influences several physical and electrical properties of this polymer, such as memory stability or memory retention time in the OECT memory devices [60]. However, this glycol side chain plays a vital role in storing the ions inside the polymer which makes this p(g2T-TT) polymer suitable candidate for the OECT memory device. The glycol side chain allows for swelling of the overall polymer, and thus ions from liquid electrolyte can penetrate it for necessary electrochemical doping. The backbone of the polymers consists of the bithiophene-thienothiophene (2T-TT) unit which provides its rigidity and potential for high hole mobility [60, 64]. Moreover, the bithiophene-thienothiophene (2T-TT) polymer backbone is functionalized with ethylene glycol (EG) side chains at the position of 3,3′ on the bithiophene unit which finally leads to the formation of p-type semiconducting p (g2T-TT) polymer structure [60], shown in figure 3(e) & 5(a). The interaction between the sulfur and oxygen in the head-to-head coupled bithiophene unit induce a backbone co-planarity and increase the sufficient conjugation length of the polymer, which is more favorable for charge transport in the polymer [60, 65].

2.3 Working Principle of OECT

2.3.1 Structure and Operation of OECTs.

The OECT is a three-terminal device, and they are labeled as to the source, drain, and gate. Among them, source and drain electrodes are connected by an organic conducting or semiconducting polymer, which is the heart of this device. There is a liquid electrolyte on top of the polymer channel, which contains anions and cations. The third one is a gate electrode which is separated from the polymer channel through the electrolyte. Fig. 6 (a) represents the schematic diagram of a typical OECT. The working principle of OECT is based on changes in the channel's doping state, and hence its conductivity, by the application of a suitable gate bias which able to switch the polymer between an ON (conductive) and OFF (non-conductive) states [6, 8, 65, 66]. In OECTs, the source electrode is grounded so that the applied voltage to the drain and gate electrodes are against the source [65]. The PEDOT:PSS conducting polymer channel -based OECT work in depletion mode. By contrast, p(g2T-TT) semiconducting polymer channel-based OECT can work both in depletion and accumulation mode [61].

In depletion mode of OECTs operation (shown in Fig. 6 b), the current conduction through the channel is mainly due to the contribution from holes, so electrons' contribution to the channel conductivity is neglected. At zero gate voltage, the transistor is in its ON state, which leads to high current flows through the channel from source to drain under external polarization of the drain contact. The ON sate happens without gate biasing because of the presence holes in the polymer due to the p-type PSS dopant molecules. When applying a positive voltage pulse at the gate electrode (V_g>0 against the source), cations are entered from the liquid electrolyte to the PEDOT:PSS polymer channel and compensate the negatively charged sulfonate ions on the PSS, resulting in the de-doping (electrochemical doping) the polymer channel [8, 65]; this is so-called depletion mode of operation, illustrated in figure 6 b. The holes in the channel are extracted at the drain which is not replenished at the source. These ionic interactions reduce the density of charge carrier (hole polarons) in the channel which leads to the smaller drain current. That means OECTs can convert ionic currents into electronic currents through the electrochemical doping process [65]. After cut-off the gate pulse, the injected ions may or may not return to the electrolyte depend on the types of the polymer. For example, after removing the gate voltage, the injected ions are returned to the electrolyte in PEDOT:PSS polymer channel-based OECTs. For p(g2T-TT) semiconducting polymer-based OECTs, the injected ions are

trapped or stored in the polymer backbone chain and does not go back to the electrolyte even after removing the gate voltage which is attributed to the memory phenomenon.
Accumulation mode OECTs made of semiconducting polymers, such as p(g2T-TT), usually are in the OFF state due to the negligible number of mobile holes in the channel, shown in Fig. 6 c. Application of negative gate voltage causes the injection of anions into the polymer channel which leads to the unbalanced charging environment in the polymer channel. To maintain the charge balancing conditions, the holes are accumulated from the polymer backbone chain result in the formation of a larger number of more significant carrier density, leading to the ON state of the OECT [3, 5, 7, 8].

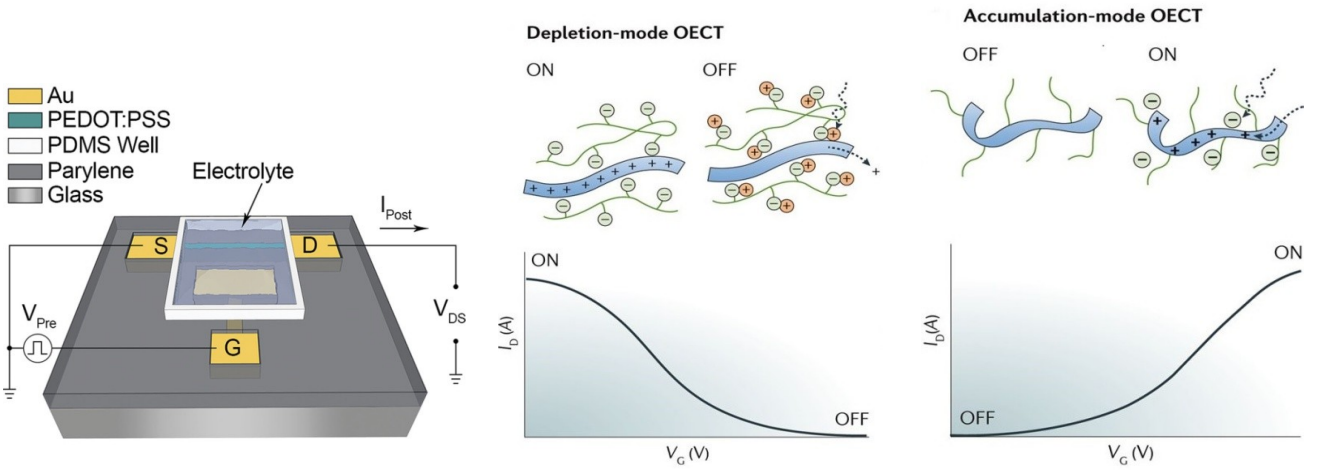

(a) (b) (c)

Figure 6: **(a)** Schematic diagram of an OECT, showing source (S), Drain (D), gate (G), and liquid electrolyte (NaCl), Fig. adapted from Paschalis Gkoupidenis *et al.* [8]. **(b)** Transfer curve of a conducting organic polymer-based OECT showing its depletion-mode operation. **(c)** Transfer curve showing the accumulation-mode operation of an OECT with semiconducting polymer channel [3].

2.3.2 Device Physics of OECTs

The most crucial feature of OECTs is its signal amplification properties; small voltage signals applied to the gate electrode can amplify to the drain current. The figure of merit corresponding to amplification is called gain. A high gain OECTs is more favorable for practical application due to the high sensitivity, low limit of detection, and excellent signal-to-noise ratio. The efficiency of the amplification of OECTs can be observed from the slope of the transfer characteristics curve, so-called transconductance: $g_m = \delta I_D/\delta V_G$ (I_D & V_G are drain current and gate voltage respectively) which is an essential figure of merit for a transistor [8, 65]. A high transconductance OECTs can be operated efficiently even at shallow gate voltage leads to low power consumption. Generally, organic polymer-based OECTs has very high transconductance due to the volumetric nature of the polymer channel [3, 65, 66]. An essential model was introduced by Bernards and Malliaras in 2007 which describe the complete behavior of OECT [68]. According to this model, the change of electronic conductivity occurs throughout the entire volume of the OECTs channel result in high transconductance, g_m [3]. Beside it, this model reproduces the transient response and the steady-state by considering OECTs as a combination of two equivalent

circuits: an ionic and an electronic circuit. Figure 7 (a) & (b) shows the equivalent electronic and ionic circuit used to model OECTs.

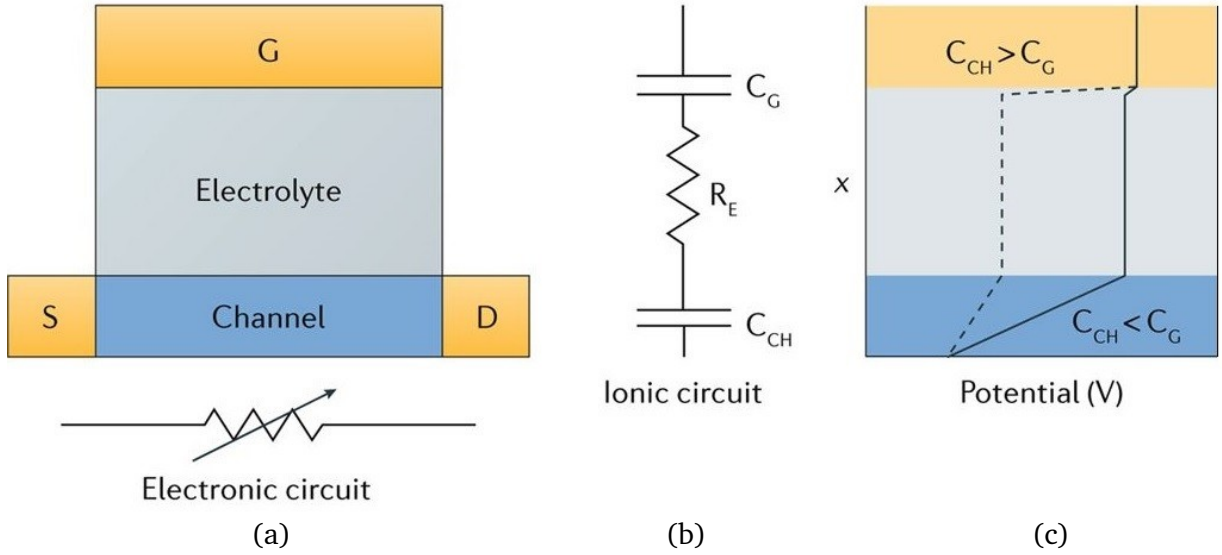

Figure 7: Schematic diagram of Bernards model used to describe the physics of OECTs. (a) The electronic circuit, shown below the device layout on the left. (b) The ionic circuit consists of resistor R_E of the electrolyte, capacitors C_G & C_{CH} corresponds to the gate and channel, respectively. (c) Distribution of the gate voltage in the ionic circuit. The dashed line represents the deficient gating; the solid line corresponds to the efficient gating [3].

Figure 7 (a) (below the device layout) represents the electronic circuit, which is modeled as a resistor with a resistance. This resistance controls the flow of electronic charge in the source-channel-drain structure according to Ohm's law, and it varies upon the de-doping process. In contrast, the ionic circuits describe the flow of ions in the gate-electrolyte-channel structure, shown in figure 7 (b) [3]. It is possible to describe the ionic circuit as a series of resistor R_E and capacitor C_G & C_{CH}. In this model, the resistance R_E corresponds to the electrolyte conductivity, and it is an indication of its ionic strength. The capacitor C_{CH} is describing the storage of ions in the channel. The channel-electrolyte interface has greater capacitance than the gate-electrolyte interface due to the high capacitance of PEDOT:PSS or p(g2T-TT) channel polymer [65, 66]. The effective gate voltage at the OECTs channel can be changed due to the change in the gat-electrolyte interfacial capacitance. As a result, the device properties may influence by the type of materials, size, and geometry of the gate electrode. For example, the fraction of the gate voltage can be dropped across the channel-electrolyte interface, which can be controlled by the type of material and geometry used in the gate electrode. The polarizable material-based gate electrode, such as Pt or Au, may result in the formation of two capacitors in the ionic circuit; one capacitor at the channel- electrolyte interface and another one is at the gate-electrolyte interface, and they are in series connection. As a result, the applied gate voltage drops across the smaller capacitor (gate-electrolyte interface), shown in figure 7(c) with a dotted line, which is not favorable for low operating voltage OECTs application. This problem can be overcome if the capacitance of the gate electrode is ten times larger than the capacitance of the channel. Such larger gate geometry is difficult to use in some applications. Alternatively, a non-polarizable gate electrode, such as Ag/AgCl, induces a negligible voltage drop at the gate-electrolyte interface [3, 71]. In this way, an effective gating mechanism is achieved.

2.4 Memory and Neuromorphic Functionalities of OECTs.

Neurons in the brain are connected through several synaptic connections. The efficiency of the connection changes over time; this phenomenon is referred to as synaptic plasticity. The plasticity can be divided into two categories named: short-term plasticity (STP, range <ms to min) assist to perform various computational tasks in the brain and long-term plasticity (LTP, range> min, days or even week) is attributed to the memory and learning [8, 70]. The essential synaptic functions, such as potentiation and depression, short-to long-term memory transition & spike-time-dependent plasticity (STDT), are commonly termed as neuromorphic because they mimic the structure and function of the nervous system [1, 8]. Moreover, the neuromorphic functionalities can be mimicked with OECTs to develop artificial neural networks involving the co-location of computation and memory that is the way of parallel neuromorphic computing.

Recently it has been reported by Paschalis Gkoupidenis *et al.* [5, 8]. that an OECT can replicate the synaptic integration and biological memory behavior, Follow-Up his work, a synaptic transistor can be used to reproduce the synaptic functions (similar to biological synaptic behavior) by applying a voltage at the gate electrode, which is termed as pre-synaptic stimulus, and simultaneously the resultant post-synaptic drain current has been measured, shown in Figure 8.

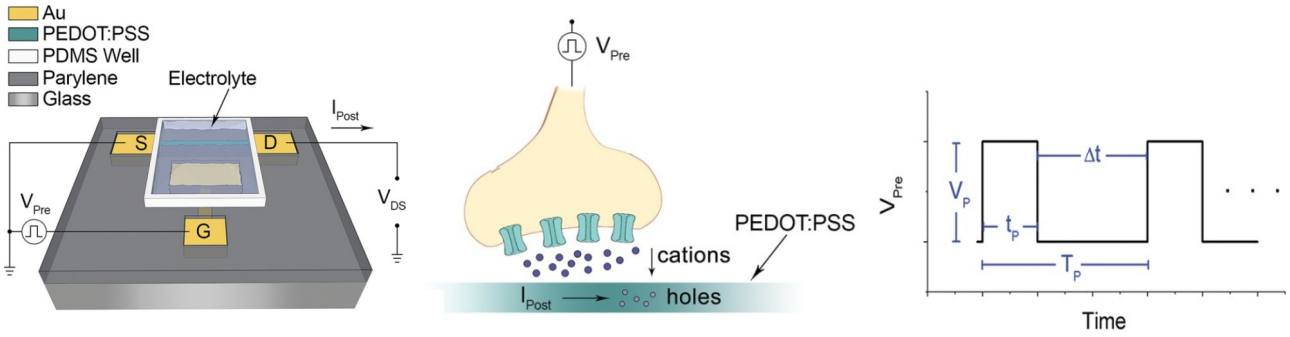

(a) (b) (c)

Figure 8: Schematic diagram of (a) an OECT, the channel is covered by a liquid electrolyte, (b) synaptic OECT having similar functionalities to a biological synapse, and (c) characteristics patterns of pre-synaptic gate pulses. Figure adapted from [8].

A pre-synaptic positive gate pulse (V_{pre}) has been applied to the gate electrode with the following parameters: amplitude of the pulse V_p, pulse width t_p, pulse period T_p, and the difference between two pulses $\Delta t = T_p - t_p$, shown in Fig. 8 c. At the same time, the post-synaptic pulse I_{post} (drain current) was measured. Short-term synaptic behavior can be realized from this device by applying a series of pre-synaptic pulses with variable V_p, t_p and T_p values [8]. The polymer is de-doped due to the applied pre-synaptic positive gate voltage (the details working principle was described in the section of 2.3 in this report). For PEDOT:PSS polymer channel-based OECT, this de-doped state remains as long as the pre-synaptic pulses present at the gate electrode. After removing the gate pulse, the PEDOT:PSS polymer was reversibly doped to its initial state result in the post-synaptic current jump to its initial level too [8]. That means I_{post} spike-and-recovery behavior of this polymer is the temporary event. This phenomenon can be attributed to short-term plasticity, STP. On the other hand, after removing the pre-synaptic pulse in the p(g2T-TT) channel-based OECTs, the polymer is not reversibly doped to its initial state and post-synaptic current does not go back to its initial state as well. It happens because the injected

ions are trapped/stored for a certain period of time due to the unique memory property of this polymer. This memory phenomenon of OECTs can be attributed to the long-term plasticity, LTP. OECTs can behave as a low-pass filter, which is related to the synaptic depression.

2.5 Applications of OECT.

Due to the unique electrochemical properties, organic semiconducting materials are sensitive to some external stimuli such as light, heat, chemicals, or even magnetic fields [1]. The ion-sensitive properties make the OECTs to use in many biological applications. Flexibility and biodegradable properties of the organic materials make this device compatible with a large variety of applications in the field of bioelectronic, for example, devices for healthcare-related uses and biomedical research especially biosensors. On the other hand, the high transconductance of the channel materials and its on-off ratio over low-operating voltage makes OECTs as a potential candidate in the field of an electronic circuit. Based on those above attributions, OECTs can be used in two major fields: Bioelectronics and Circuits & Logic.

2.5.1 OECTs in Bioelectronics

Organic materials based OECTs have potential applications in the field of bio-electronic such as bio-sensing, biomedical devices, and even wearable medical devices [1, 3]. For example, the heart rate and body temperature can be measured by this device in real-time. The ion-sensitive properties of the organic channel materials make an OECT suitable for electrochemical biosensors, which are based on the interaction between the bio-molecules and channel materials. The bio-molecules for the sensors can be classified into electro-active (i.e., dopamine) and electro-inactive (i.e., glucose, lactate) species that are responsible for changing of doping state of the conducting polymers [38, 72]. The biosensors can be mainly subdivided into the enzymatic sensing, immune-sensing and aptamer sensing [73].

OECTs Based Enzymatic Biosensors:

In biosensors, OECTs play a role as a transducer that can monitor the concentration of electrolytes and metabolites, such as glucose and lactate, in our human body [3, 38, 65]. The basic operation principle of such an enzymatic biosensor relies on the selective interaction between redox enzyme and metabolite molecules. The metabolite molecules are catalyzed by the selected enzyme on the gate electrode, which results in the enzymatic product. The metabolite molecules and the enzyme interacts through which either they gain or lose electrons on the gate electrode that results in the changing of channel current. The charge neutrality condition is maintained in the whole circuit (both in ionic and electronic circuit, described in the section 2.3.2) by entering the cation into the polymer channel which is the replacement of cationic polymer (e.g., $PEDOT^+$) compensating the anionic polymer (e.g., PSS^-) result in the reduction of the drain current. The changing of drain currents is logarithmically proportional to the concentration of metabolite molecules [3, 38]. The mobilized enzyme can be absorbed by the channel or dissolved in the electrolyte that reduces the sensitivity of the sensors. The sensitivity and selectivity of the device can be improved by using an immobilized enzyme on the gate electrode [3]. The principle stated above is applied for glucose or lactate monitoring in our body.

Beside it, OECT-based enzyme-free biosensors have already been developed to detect some biological substances such as ascorbic acid (AA), dopamine (DA), etc. Recently it has been reported by Fabio Biscarini *et al.*[74] that the synaptic response of the PEDOT:PSS channel-based OECTs are changes with

the concentration of dopamine, which is one of the most critical neurotransmitters in the human body. OECT can be used to selective sensing of dopamine that can dramatically improve the diagnosis of neurological diseases such as Parkinson's disease and autism [1, 65, 74].

OECTs Immunosensors:

OECTs can be used for detecting or measuring a specific protein or other substances through their properties as antibodies or antigens. Antibodies of the immune system are known as the bio-recognition element. The antibody leads to the development of the highly specific and sensitive OECTs immunosensor. Generally, competitive and sandwich types are widely used immunosensors [38].
In competition reactions, antibody or antigen is treated as immobilized immunoreagent onto the electrode surface is a great challenge for the development of OECT immunosensors [75]. On the other hand, a primary antibody uses for the sandwich-type immunosensor, and a specific antigen marker is used as a sample solution. The chemical reaction between the secondary antibody and antigen results in the formation of the detectable and low-noised signal. This fundamental principle has been used to develop the OECT immunosensor to detect the prostate-specific antigen (PSA) [38].

OECTs Aptamer Sensors:

Aptamer sensors are a highly specific sensor that has potential applications in clinical diagnoses, such as sensing of deoxyribonucleic acid (DNA). An OECT-based DNA sensor is integrated with a flexible microfluid device. In aptamer sensors, the ionic concentration of the electrolyte does not affect the gate potential [38]. In 2018, Peng *et al.* [75] have developed an OECT to be suitable for the sensing and analysis of micro RNA.

Beside of those applications, OECTs is used as artificial receptors. The chemical stability of an OECT-based artificial receptor is comparatively higher than natural receptors [38]. An artificial receptor-based wearable OECT device shows great potential in the field of stretchable devices. Many applications of OECTs have focused on cell monitoring in where the coupling of OECTs with live mammalian cells can monitor toxicology and electrophysiological activity [38]. The basic principle of this technique is the growth of monolayer cells between the channel and gate, which makes a potential barrier of the movement of electrolyte ions; thus, changes the behavior of OECTs. OECTs can also be used as an ion sensing device [3].

2.5.2 OECTs in Circuits and Logic

Compared to MOSFET technology, OECTs have low switching speed obstruct this device to use in digital signal processing and computation. Despite this disadvantage, a combination of OECTs with typical integrated circuits enhances the efficiency of existing technology and introduces new opportunities, such as internet connectivity, at an electronic level [3]. It has been reported that the negative- AND/NAND and NOR logic gates can be achieved through PEDOT:PSS channel-based OECT circuits [76]. OECTs can also be used in the circuit of display pixels. Sensors and detectors are arranged in matrices on display pixels where OECTs play a role as a switch to drive individual sensors on the x-y plane. PEDOT: PSS-based OECTs tenfold increase the sensitivity of the output signal in a sensor circuit. A typical example of the sensor circuit is a Wheatstone bridge, shown in figure 9(b), consisting of two PEDOT:PSS channel-based OECTs that behave as a sensor circuit to detect metabolite molecules [77]. When a high transconductance OECT combined with a resistor, this simple circuit significantly amplifies the input signal to output compared to conventional electrodes. Organic materials based

OECTs have high transconductance which can be the key point to use it in the energy-storage circuits. The energy storage technology uses a supercapacitor that needs high-transconductance switches to balance charging and discharging. In this case, high transconductance OECTs can be used as an effective switching device [3].

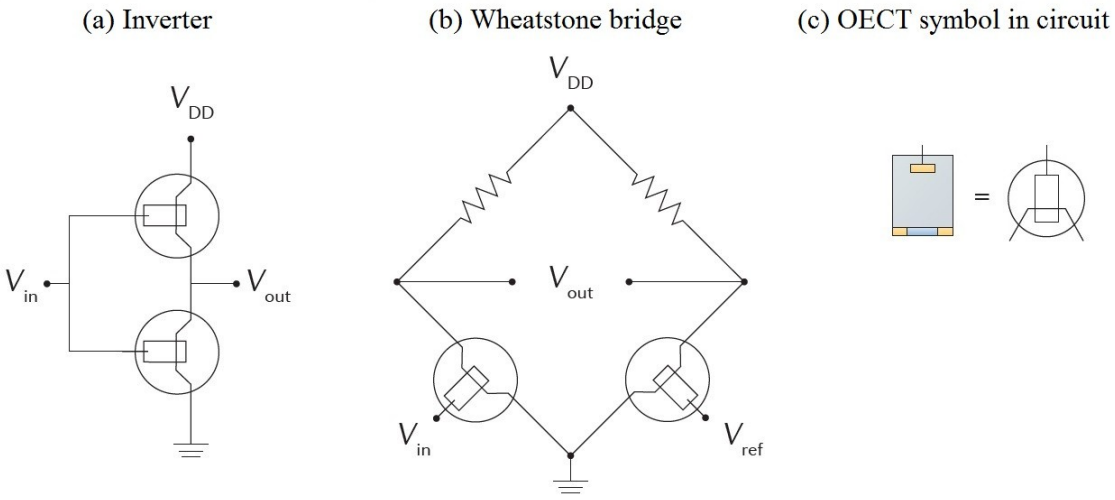

Figure 9: Application of OECTs in a variety of circuits, such as (a) inverter and (b) Wheatstone bridge. (c) the equivalency of OECT in the circuit [3].

Recently, it has been reported that OECTs can be used in machine learning applications [2,8,9]. It has been observed the semiconducting polymer-based OECTs exhibits memory phenomenon. This property of OECTs can be used to develop the hardware-based artificial intelligence and deep learning algorithm devices. For example, the combination of OECTs memory device and typical OECTs can be used for the learning and memory of artificially intelligent robots.

3. Fabrication Approaches of OECTs Memory Devices

The entire fabrication process of OECTs consists of several fabrication methods. The basic fabrication techniques of OECTs are given below.

- **Spin coating:** The process for producing a thin and uniform polymer film on a substrate.
- **UV photolithography:** The way used in microfabrication to define a pattern in a thin photosensitive polymer layer.
- **Reactive ion etching:** The method of removing unwanted materials, such as dust, from the surface of the substrate. This process is also called dry-cleaning. This method uses reactive species, for example, oxygen ions, to remove the dust.

- **Metal evaporation technique:** One of the widely used techniques to deposit a metallic thin film on the substrate.
- **Thickness measurement method (profilometry):** The process used to observe topographical information from a surface and measure the thickness, exceptionally thin film.

This section describes the basic working principle of those methods.

3.1 Spin-coating

Spin-coating is a well-known transient process of flow and mass transfer. It is one of the traditional techniques of depositing dilute solution to a thin film on a planar substrate that offers uniformity, reproducibility, and control of the precise film thickness. This depositing technique applies to both inorganic, organic, and inorganic/organic mixture solvent. However, this section of the report will focus only on the spin-coating deposition of photoresist and polymer thin film. Due to the smooth processing method, spin-coating deposition has become the method of choice for the formation of thin-film especially in the fabrication of microelectronics devices.

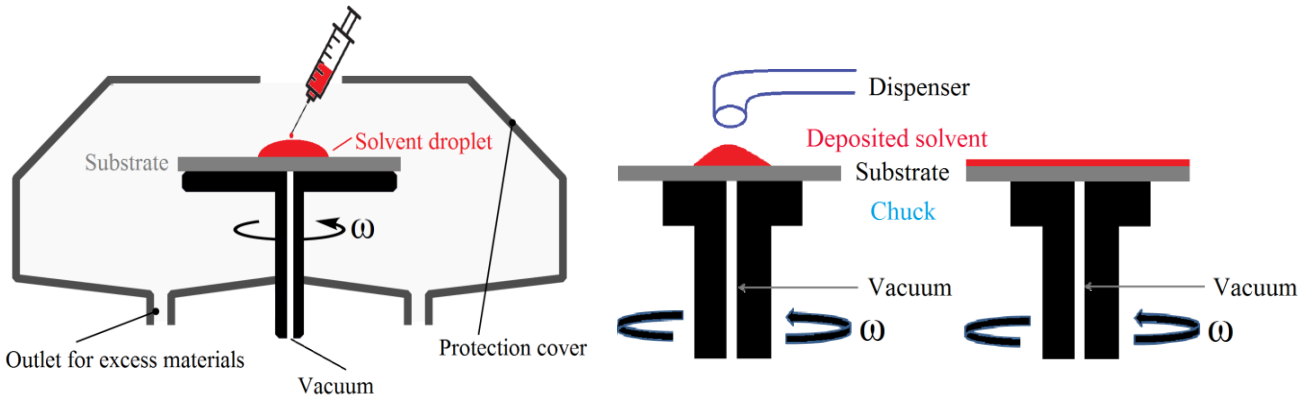

(a) (b) (c)

Figure 10: Schematic diagram of the spin coating technique. (a) A typical spin-coating system [79]. Vacuum drawn down and firmly holds the substrate with the chuck during the angular rotation. The protection cover traps the excess solvent droplets and prevents their spreading surroundings the system. (b) A droplet of the solvent is placed on the substrate through the dispenser. (c) Thin film is formed due to the angular rotation as well as the centrifugal force. Figure (b) & (c) adapted from [79].

In the spin-coating deposition approach, a horizontal rotating chuck firmly holds the substrate via a vacuum. Figure 10 shows the schematic diagram of a typical spin coating system. A few droplets of a dilute solution, that to be formed as a thin film, is placed in the middle of the substrate. The substrate is then rotated rapidly at a predefined acceleration that generates a centrifugal force on the droplet. The adhesive force holds solvents with the substrate. However, the action of centrifugal force leads in strong sheering of the solvent, which causes a quick radial flows of liquid that to be deposited [10,12,78]. Due to the radial flow, the majority of the processed material is ejected off the substrate in the first

couple of seconds of the process. Recently it has been reported by Dimitrios A. Koutsouras *et al.* that almost 98% of the initial material is wasted in this method [10]. The exhaust suction takes them out of the rotating chamber and prevents droplets from re-circulating and hitting the wafer — rest of the material form a thin layer of the desired film. At a specific acceleration and number of rotations, the thinning process of the volatile solvent continues until the equilibrium film thickness achieved causes of disjoining pressure effect [12]. The disjoining pressure refers to the Gibbs energy/force of injection per unit area on the two flat and parallel surfaces. The final thinning process is then dependent on solvent evaporation.

Depending on the thickness, the film can be divided into a thin film and ultra-thin film ≤ 10nm [13]. The thickness of the film can be controlled by controlling some specific deposition parameters such as angular spinning speed ω, evaporation rate e_r, the solvent density ρ, time of total rotations t, and the solvent viscosity η. Among them, two parts strongly affect the film thickness over the time: effect of angular speed ω and the evaporation rate of the solution e_r [10,13,78]. Highly volatile solvents evaporate rapidly results in thicker films compared to the lower volatile solvents. Beside it, the solution's viscosity and concentration significantly affect the film thickness [12]. Figure 11 shows how film thickness is affected by the angular spinning speed. The higher the angular speed means the thinner the film.

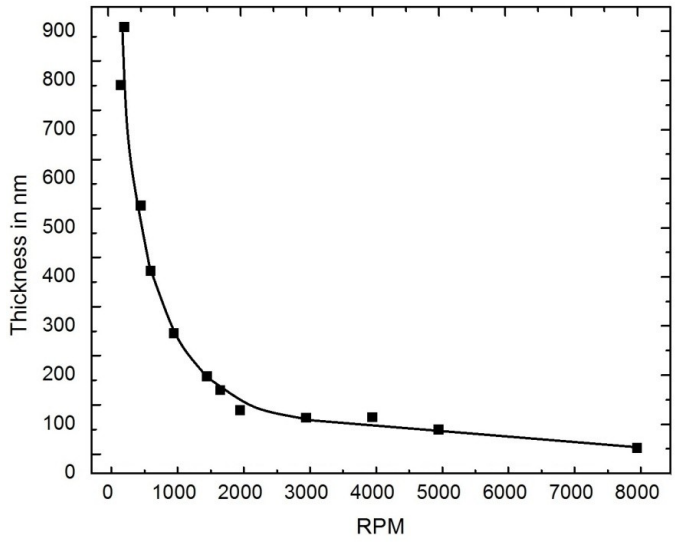

Figure 11: Figure shows the relationship between angular speed and film thickness of PEDOT:PSS polymer thin film. The average film thickness is a function of the rate of angular spinning speed ω. The spin coating time was 30 seconds, and the drying time was 60 minutes.

The film thinning process occurs through two distinct stages. A very first coating stage and finally longer drying stage [10,12]. In the first stage, film thinning is the only cause of the radial outflow due to the effect of angular spinning. In this early stage, the solvent evaporation is neglected, and it is assumed that the solution concentration stays constant. The solution in the early stage is analogous to the thinning of a Newtonian fluid on the rotating substrate (i.e., the linear relationship between shear stress and shear rate) [12, 78]. The second stage is the more prolonged drying stage in which film thinning is exclusively occur due to the solvent evaporation. This stage corresponds to the complex

mechanism of coupling between fluid rheology and solvent evaporation. The physical and rheological behavior of the solvent is changed by solvent evaporation during the coating process which is analogous to the non-Newtonian fluid behavior. It is thus, truly challenging to understand how solvent evaporation affects the fluid rheology and vice versa. Many assumptions and sophisticated numerical methods have been applied to model this process [78]. However, the film thickness can be easily expressed by an empirical expression (3.1) given below [80].

$$h = \frac{K C^{\beta} \eta^{\gamma}}{\omega^{\alpha}} \qquad \text{..... (3.1)}$$

K, C, and η are the calibrations constant, polymer concentration, and viscosity of the solution, respectively. α, β, and γ is called exponential parameters, which can be calculated experimentally. By knowing those parameters, the above model can provide the film thickness of a given polymer. Generally, the film thickness can be expressed by equation (3.2) as well [80].

$$h = \frac{\eta^{0.4-0.6}}{\sqrt{\omega}} \qquad \text{..... (3.2)}$$

There are two common ways of solvent dispersion on the substrate during the spin coating: The static and dynamic dispense. In the static dispersion, first, the solvent is placed on the stationary substrate, and then the angular rotation is started. The de-wetting issue with the substrate is present in this operation mode [13], leading to more deposited materials required for highly viscous solvent during the deposition process [10]. In the dynamic dispersion mode, the solvent is dispensed when the spin-coater motor, as well as the substrate, is already operating at a low angular speed, which is followed by the rapid acceleration of predefined angular speed. This process is also called the on-the-fly-dispensing spin-coating approach [13]. Theoretically, the static wetting balance is broken by the tangential force of the droplet results in the quick solution spreading over the substrate. This approach requires fewer materials compared to the static dispersion. However, in both approaches, the final film thickness is greatly affected by the angular rotational speed and the total spinning time.

There are some challenges in the spin coating deposition process. If the substrate belongs to a non-rotation-symmetric shape, a sidewall of the deposited material is formed due to the strong air turbulences. Thus nonuniform film may create.

3.2 UV Photolithography

History of Photolithography:

Photolithography is a microfabrication technique that is often used for defining an intricate 2D geometric pattern on a substrate via light. The word 'photolithography' consists of three Greek words, namely *photo* (Φως), *litho* (λίθος) and *graphy* (γραφή) with the meanings light, stone and writing, respectively [10,81]. The first understandable photolithography technique was invented in 1796 by German author and actor Aloys Senefelder [81]. After his work, much development on photolithography has introduced over time. The modern photolithography technique is based on two remarkable historical developments in the photoresists. In 1782, the first experiment was done by the Swiss pastor Jean Senebier (1742-1808) of Geneva with the property of resins. He observed that some resins become insoluble after the sunlight incident on it. The second historical landmark of photolithography

came with the work of Nicéphore Niépce in 1826. He was inspired by Senebier's resins experiment. Niépce used various resins in sunlight and first time able to produce a photolithography image using light. He used a pewter plate coated with bitumen of Judea (a form of asphalt) dissolved in lavender oil. Then he placed an etched print on oiled paper over the bitumen-coated glass plate. In his work, etched, printed oiled papers worked like a mask on top of the pewter plate that was exposed to sunlight for three hours. After the exposure time, the exposed regime of the photoresist (bitumen) becomes harder and insoluble; in contrast, the shaded regime of bitumen could be washed away by a solvent of turpentine and lavender oil mixture. Later, this behavior of photoresist was classified as a negative photoresist [10,81].

In 1935, the first synthetic photopolymer/photoresist was developed by Louis Minsk. His developed polymer name is poly(vinyl cinnamate), which is the basis of the first negative photoresist [10]. In his approach, the desired pattern corresponds to the dissolved part of the photoresist. In 1940, Oskar Süß first invented the positive photoresist named diazonaphthoquinone [84]. Later on, the photolithography technique becomes popular in microelectronic research and industry. The first time the photolithography technique was used to fabricate the integrated circuits in the late 1950s [81,82]. Nowadays, various radiation sources have been used in lithography, such as UV light, X-ray, charged particles, etc. This section of this report is briefly describing only the ultraviolet photolithography.

Basic Principle of Photolithography:

The basic principle of a photolithography process is simple. It is a photographic process by which a light-sensitive organic polymer, so-called photoresist, goes through a series of complex photochemical reactions when exposed to sufficiently energetic radiation, results in alters the solubility of the photoresist. A mask is used on top of the photoresist to transfer the predefined pattern in the thin film of photoresist. The mask is designed in such a way that a part of the photoresist is exposed to the UV light, and the rest of the photopolymer is untouched by the light. Generally, photolithography refers to the use of ultraviolet light (wavelengths 436 nm to 365 nm). However, deep ultraviolet light (DUV wavelengths 248 nm to 193 nm) and extreme ultraviolet (EUV wavelengths 5 nm to 100 nm) can also be used in photolithography [10].

Photoresist plays a role as a patterning medium in the substrate that can be subdivided mainly into two types: positive and negative photoresist. They exhibit different properties in contact with radiations. When positive photoresist exposed to radiation, a chemical reaction within the exposed regime makes it more soluble to an organic developer (shown in Fig. 12b). The mechanism behind this phenomenon is either due to the polymer chain scission by the effect of radiation, or due to the polarity of the molecule is changed due to the light photons.

In contrast, the negative photoresist exhibits precisely the opposite behavior of its counterpart. A negative photoresist becomes insoluble in organic developers under exposed to UV radiation. It's happening because the UV radiation promotes polymer cross-linking or starts the polymerization of the monomer, thus makes it less soluble to solvents. Therefore, the exposed negative photoresist remains and unexposed part of photoresist film are removed during the development, shown in figure 12a. As a consequence, the exposed regime of the photoresist forms a negative image (patterns) as in photomask [81,82,83]. The main difference between them is the positive photoresist is costly compared to negative ones but offers higher resolution. Figure 12 shows the effect of UV radiation when a positive and negative photoresist exposed to it.

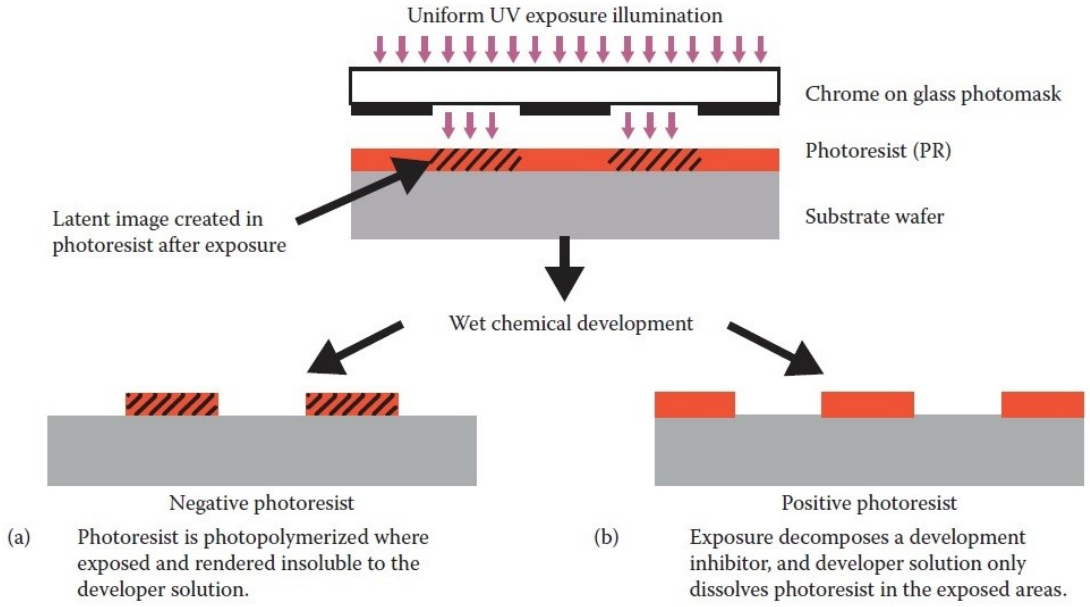

Figure 12: Schematic illustration of the effect of positive and negative photoresist under UV exposure. (a) The exposed region remains after the development of negative photoresist due to the polymer cross-linking. (b) The exposed region is removed after the development of the positive photoresist. Figure adapted from [81].

Mask alignment and exposure mode:

Generally, the mask is made of transparent glass, which is coated with a patterned thin chrome layer. The radiation can pass through the transparent glass while the opaque chrome layer stops the incident radiation and protect the photoresist underneath the mask [82]. The mask pattering/designing is performed by electron beam lithography. Care should be taken during the mask alignment to perform precise radiation into the photoresist. The three major radiation exposure modes are Contact mode, Proximity mode, and Projection mode, shown in figure 13.

(a) Contact Mode:

In contact mode photolithography, the substrate and mask physically contact each other during the radiation exposure. However, a small spatial gap is necessary to avoid the mask damaging while the mask alignment process. The resolution is high in the contact mode. In this mode, the final resolution of the patterns can go down to the wavelength of the radiation used. The main challenges are the high possibilities to damage the mask and make accidental scratching on the photoresist film.

(b) Proximity Mode:

In proximity mode of alignment operation, a small gap is maintained between the substrate and the mask. This mode reduces the resolution because of diffraction effects but protects the mask from damage. The contact mode and proximity printing modes are called together as shadow printing since the substrate is just underneath the mask.

(c) Projection Mode:

This mode is accessible in the semiconductor industry. In this mode, there is a large gap between the mask and the substrate. The radiation is projected through a lens placed between the mask and the substrate surface. This approach can offer demagnification of the mask pattern on the photoresist, see in Fig 13c.

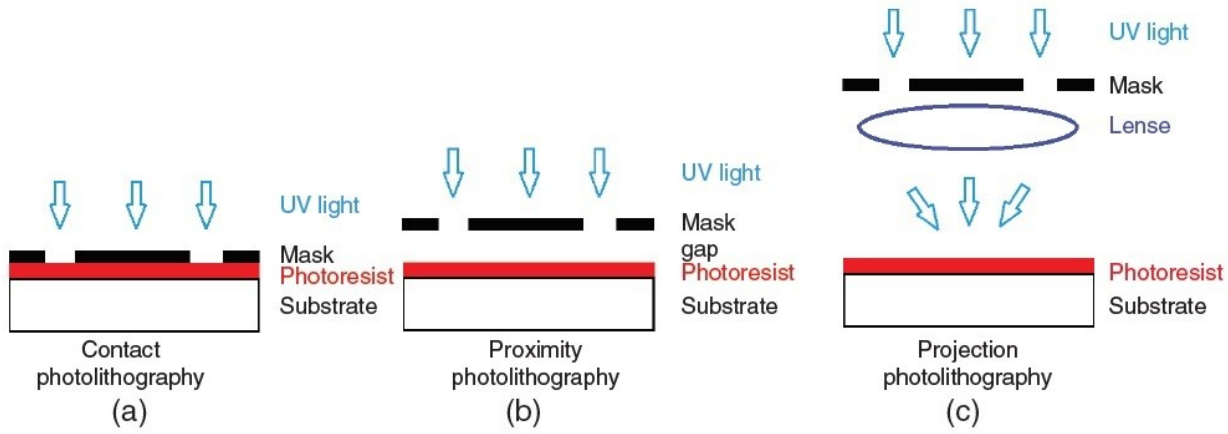

Figure 13: Schematic illustration of the three basic exposing modes of radiations. (a) Contact mode, (b) Proximity mode, and (c) Projection mode photolithography. Fig. adapted from [10].

Overall, the general sequence of UV photolithography processing steps is as follows. First, the substrate is cleaned to remove organic contaminants. To begin photolithography, a layer of photoresist is spin-coated to a uniform thickness on the substrate. The photoresist coated substrate is then exposed to intense UV radiation through a precisely patterned stencil called the photomask. The soluble part of the photoresist is then washed off using a developer solution leaving behind patterned and exposed substrate regions in the photoresist thin film. The pattern is then etched by a dry etching technique called reactive ion etching, which uses chemically reactive plasma to remove unwanted material deposited on the substrate. The etching technique may vary depending on the material being processed. Finally, the remaining photoresist leaves a precisely patterned microstructure. This structure can then be used directly or as a mold for the fabrication of OECTs channel and electrodes. The complete photolithography process is exclusively done in the cleanroom-based environment to avoid contaminations. All those steps are described in the experimental procedure section 4 in this report.

3.3 Reactive Ion Etching

Etching technology has been used to remove the layer of material from the surface. The etching process has traditionally been divided into dry etching and wet etching. This section of this report deals with dry etching, especially the reactive-ion etching (RIE) technique that is used in microfabrication research and industry. RIE uses chemically reactive plasma to remove unwanted materials on the substrate. The plasma, such as O_2 plasma, is created in a vacuum by a highly oscillating electromagnetic field. Plasma in the vacuum chamber aggressively etches the targeted surface in the vertical direction; thus, it is the directional etching process. A brief description of the RIE generation process and its working principle is given below.

RIE Equipments:

RIE technique is consists of a vacuum chamber equipped with two parallel plate electrodes separated from each other. One electrode is called the ion trapping metal plate, which is grounded, and another electrode on the bottom of the chamber called the wafer platter. A highly oscillating radio frequency (RF) generator is connected with the bottom electrode, which discharges the gas molecules into ions. The separated electrodes create electric field results in the acceleration of the ions towards the substrate surface. The wafers are placed on top of the bottom electrode, which has direct contact with

the plasma glow. The wafer platter holds materials to be treated electrically isolated from the rest of the equipment in the vacuum reactor chamber. The process gasses enter the reactor chamber through a gas control valve situated on top of the chamber, and they are evacuated by a vacuum pump through an outlet on the bottom. The provided gas plays a vital role during the etching process. The type and amount of gas used in the reactor chamber vary depending upon the different factors such as type of etching, rate of etching, types of materials that to be etched, etc. For example, oxygen plasma is used to etch parylene C polymer, and sulfur hexafluoride gas is used for the silicon etching process [10,21]. The gas pressure in the reactor is maintained by adjusting the inlet and outlet control valve. Figure 14 shows the basic structure and working principle of a reactive ion etching system.

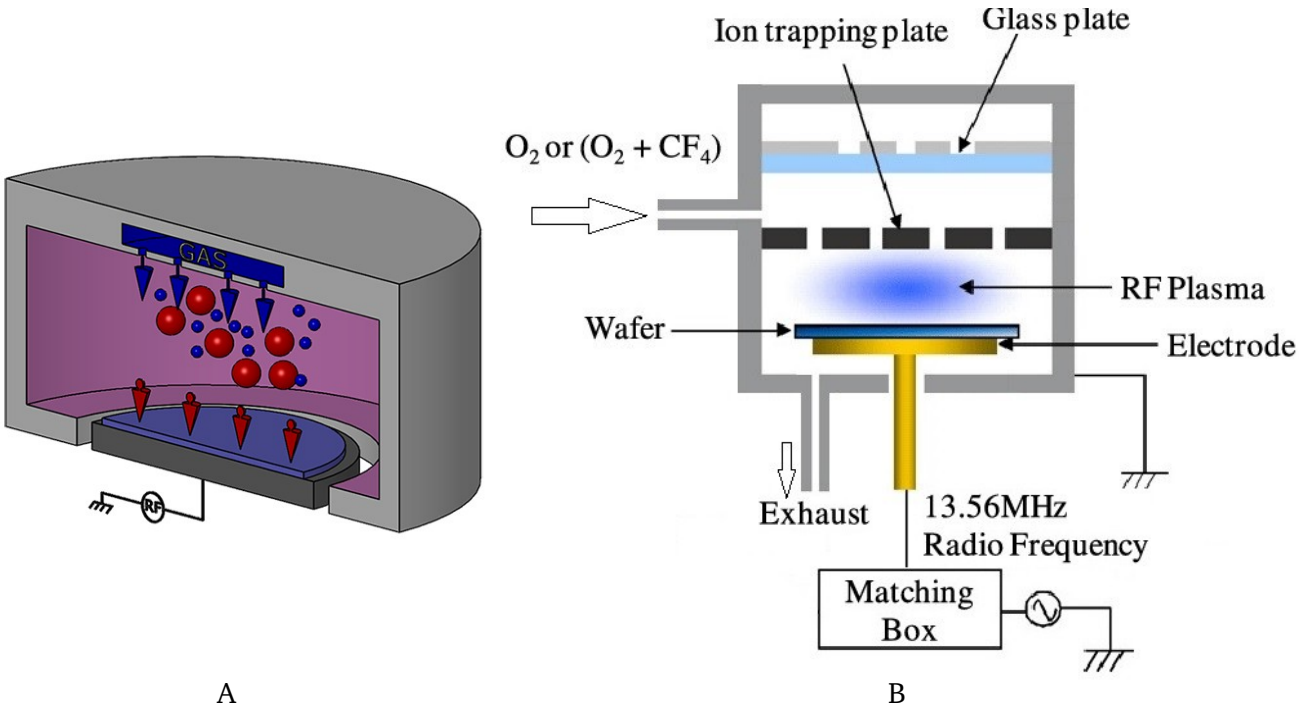

Figure 14: Schematic presentation of the RIE plasma technique. (A) The cross-sectional view of an RIE reactor chamber [34]. The red circle represents the plasma, and the small blue circles are the removed targeted materials. (B) The schematic presentation of the inside view of the RIE system. O_2 or a mixture of gases entered into the chamber and created plasma. The ion trapping metal plate is grounded [25].

Other types of RIE systems are possible, for example inductively coupled plasma RIE or ICP-RIE technique, which also known as deep reactive ion etching (DRIE). In DRIE, ICP torches are used for plasma generation. In the DRIE technique, the ICP torch generates plasma that is one to two orders of magnitude higher than RIE. As a result, DRIE provides higher etching rates and selectivity than RIE.

Working principle of RIE:

The basic principle of the RIE process is based on creating gas plasma and its quick circulation in the reactor chamber. An energetic radio frequency (RF) is applied in the wafer platter by a radio-frequency generator, which generates an oscillating electromagnetic field to the bottom electrode (wafer platter). Typically RF is set at 13.56 MHz and 600 W, other frequencies are also available, but this 13.56 MHz provides the best results for organic polymer etching process [25, 92]. Since one electrode is grounded and another one is energized by the RF generator, the capacitive coupling between the electrodes excites

the gas, generating gas plasma. The principle behind the production of gas plasma is the high oscillating electromagnetic field adds energy to the gas molecules or atoms. Due to the energy consumptions by atoms, electron transition occurs from their ground energy state to the excited state and sets them free from atoms result in the creation of gaseous ions, so-called reactive ions, and free electrons.

$$O \rightarrow O^{+} + e^{-}$$

These free electrons are electrically accelerated throughout the vacuum chamber in up and down cycles. The resistance of the electrons to move with the electromagnetic field resulting in the formation of enormous heat; thus, plasma generation occurs. Some electrons bombardment occurs on the walls of the chamber, and they are absorbed into the chamber wall. The chamber is made of metal and grounded, so they are fed out to the ground, and thus, possibilities to change the electronic state of the system are reduced. However, a negative charge is created into the wafer platter due to the electron deposition into it. Since the wafer platter is isolated from the system, a significant negative voltage is developed on the platter, about a few hundred volts. On the other hand, due to the high concentration difference between positive ions and free electrons, the plasma itself contains a slightly positive charge [25].

That means, the plasma and the wafer platter contains a massive voltage difference. This substantial potential difference influences the reactive ions (positive ions) rapidly accelerates towards the wafer platter and collide with the sample materials that to be etched. The reactive ions chemically react with the targeted surface materials but also remove the impurities and radicals on the surface of the sample by transferring their kinetic energy. The result is a surface without impurities and with few nanometer layers of free radicals. Since the reactive ions mostly move in the vertical direction in the reactor, the RIE process provides a highly anisotropic etch profile compared to the wet chemical etching.

It is known that the RIE process consists of both physical and chemical etching. It is difficult to control the physical and chemical components of the etching independently. The physical etching effect, namely sputtering, decreases with increasing chamber pressure. Etching conditions in an RIE technique can be adjusted by adjusting various deposition parameters such as types and amounts of gas flows in the chamber, pressure, RF power, etc. For example, faster etching can also be achieved by raising the temperature of the reaction chamber.

3.4 Metal Evaporation Method

OECTs require thin-film metal electrodes, generally gold. Evaporation is a commonly used technique in the field of microfabrication for the metal thin film deposition. The metal electrodes of OECT are fabricated using the evaporation technique. Thermal evaporation is the most straightforward technique of evaporation where the target atoms or molecules are transferred from a heated source to a substrate. The process is started by the creation of a vacuum, and the source material is heated to its evaporation temperature. The rate of evaporation, as well as the film thickness, is greatly influenced by few deposition parameters, such as the amount of vacuum, current for heating, the time of evaporation, geometrical relation between target materials and substrate, etc. Generally, the target material is heated in a vacuum chamber because the vacuum environment allows the target particles to travel directly to the substrate without any internal collisions between vapor particles and background

gas. Pressure in the chamber plays a vital role in a deposition. Higher the pressure leads to the smaller mean free path results in the more internal collisions of vapor atoms, thus disturbing its direction of atom's movement to some degree, which reduces the deposition rate. Due to this reason, the vacuum pressure should be below at a certain point for which the mean free path is longer than the distance between metal vapor source and the target object (substrate).

Physical Principle:

The thermal evaporation consists of two basic processes: evaporation of target material and condensation of the vapor on the substrate. The entire process takes place in a vacuum chamber. A high vacuum is obtained by a two-stage pumping system. First, a rotary pump that initiates a pre-vacuum environment and then a turbo molecular pump allows achieving a high vacuum reactor. A high flow of a significant current is passed through a refractory heating filament that plays a role as a controllable heating source (e.g., tungsten, molybdenum, etc.) result in the formation of plasma-like heat. In this process, the heating source can be resistance wire or a dimple shaped ribbon of refractory metal that can hold the pellet of the target materials. The target material is evaporated feds in a boat like shaped ceramic evaporator so-called boat, as shown in Fig. 15.

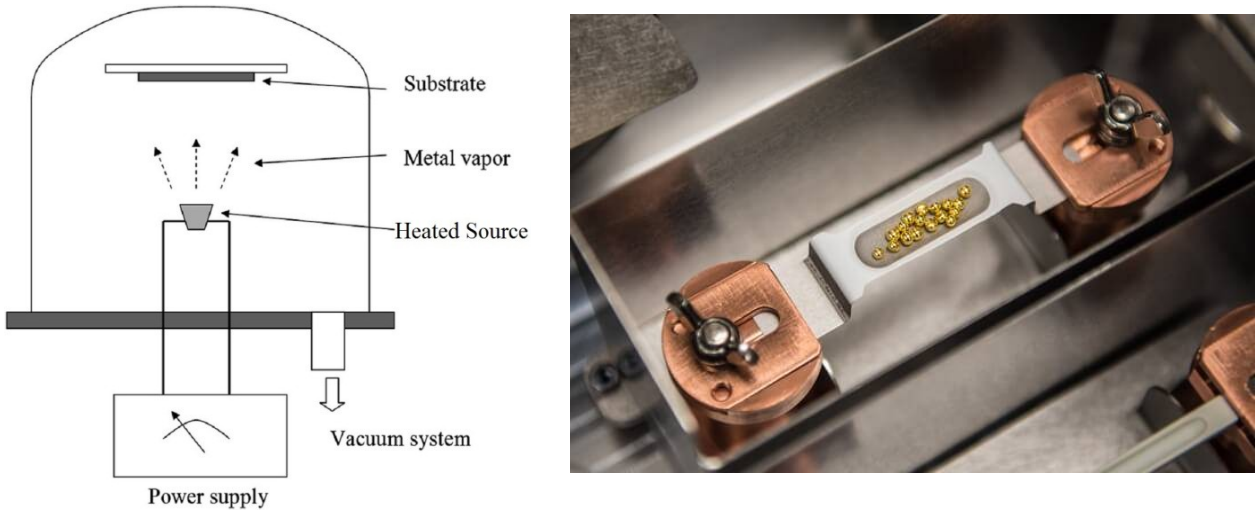

(a) (b)

Figure 15: (a) The schematic presentation of the metal evaporation reactor chamber. This illustration briefly shows the basic components of a metal evaporator [66]. (b) A dimple shaped ribbon of refractory metal that generates resistive thermal evaporation of target metal, i.e., gold [86].

The hotter boat melts the target material and eventually evaporated; forms a cloud of evaporated metal atom above the source. The evaporated target atoms transfer their energy to the substrate where the condensation occurs and form a thin metallic film. Since the evaporation process requires energy, a stabile evaporation process demands the constant flow of current during the entire process. The rate

of evaporation is increased by increasing the current and vice versa. Thus the current flow is one of the functions of the evaporation rate [66]. The evaporation is also possible by shaping the source material into a small horseshoe shape and hangs it over the heating filament coil. As long as the source material is heated and melts by the coil, subsequent evaporation occurs in all directions. This method is less efficient than the boat method. However, the filament-based heating source limits the thickness of the thin film. Because the size of the filament usually is small, which can melt a certain small amount of targeted material; hence thick film deposition is not possible using filament base heating source; instead of the evaporation boats and crucibles can perform it.

The quality of the vacuum and the purity of the source material define the purity of the deposited film. Several conditions have to maintain to obtain pure films. The first condition is the source material should be highly pure; at least 99.99% pure because impure source material dramatically affects the quality of the deposited thin film. The second important aspect is the contamination of vapor with other elements. The unwanted vapors from other elements (e.g., heating filaments) can affect the purity of the vacuum. For example, if the heater element is made of a material with low diffusion will not contaminate the process. Another condition concerns to the vacuum level. If the vacuum level is low or close to the atmospheric pressure in the reaction chamber, in that case, the evaporated atoms collide with other particles, or they may react with each other and hence reduce the amount of vapor on the substrate; thus, thickness control is difficult. As a result, non-uniform or fuzzy thin film deposition appears on the substrate. Another fact is the roughness of the substrate surface affects the thin film quality. It is because of the evaporated atoms incident on the substrate from a single direction. For that reason, any blocking features on top of the substrate surface (e.g., roughness) may result in the formation of a non-uniform deposition of the thin film. This phenomenon is known as step coverage. The geometry of the evaporation chamber influences the thickness of the film. There are high possibilities for collisions of residual gases and the target atoms if the chamber is small; in that case, aggravates non-uniform thickness of the film arises [85].

3.5 Thickness Measurement Method: Profilometry

The thickness of the thin film can be measured by different techniques. Profilometry is one of the standard tools used to characterize topographic information from a surface, especially a thin film surface. Information about surface morphology, such as, step heights and surface roughness, can be extracted through a single point, line scan, or even a full scan of the surface that can be performed using the physical probe. This part of the report describes the basics of profilometry and the working principle for the step height measurements, which correspond to the layer thickness of the thin film.

There are two types of profilometers: stylus and optical profilometry. Among them, stylus profilometers use a diamond stylus or tip having a specific diameter, generally in a few μm. All of the stylus profilometry techniques consist of a gearbox for precise movement, a diamond stylus, a transducer, a sample holder, a predefined software-based control unit, and a data acquisition system, as shown in figure 16 [89]. All movement is performed through a gearbox unit that controls the stylus movement across the sample stage in the X, Y, and θ stage; define the scan speed, movement direction of the sample stage, etc. For movement purposes, a stepper motor can be used, which moves by a series of pulses in a configuration of 2 or 4 electrical winding. Generally, the stepper motor has excellent movement resolution; for example, 300 steps per revolution mean 1.2 degrees per step. This high

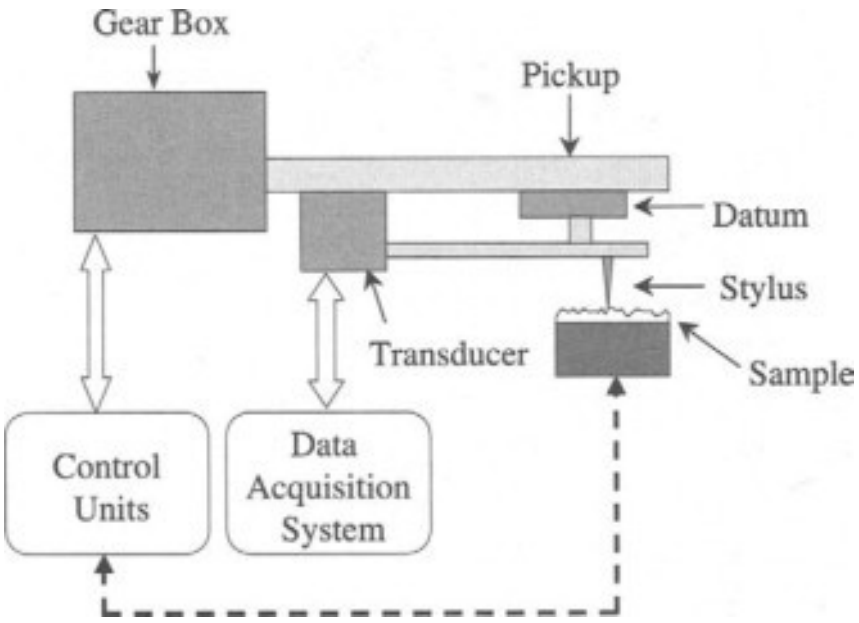

Figure 16: The major components of a stylus profilometry [89].

movement resolution of the stepper motor gives precise movement control of the stylus probe [87]. The even higher resolution of movement can be achieved using some mechanical translation system, such as worm screw or reduction gear. The transducer converts the mechanical steps different from the surface into an electrical signal, which feeds into the data acquisition unit. Depending on the movement, there are several sensing methods for converting the probe movement into an electrical signal. For example, capacitive sensing, inductive sensing, variable reluctance, piezoelectric transducers, etc. The whole system is controlled by a computer. The important central part of stylus profilometry is its precise mechanical movement of the stylus or tip, which is generally made of tough materials, for example, diamond. The mechanical movement of the stylus is converted into an electrical signal through the transducer [89].

The operation principle of a stylus profilometer:

The basic working principle of any stylus profilometry tool is based on the contact measurement of the sample surface. This type of profilometer requires force feedback over the scan area. A very sensitive and reliable contact stylus moves across the feature of the thin film surface where it to be characterized. A cantilever arm is used to holds the stylus in the one end, and its opposite end contains a counter-balanced weight. An actuated motor moves the counter-weight closer or away from the pivoting center of the cantilever arm resulting in the precise control of stylus force on the surface. The stylus physically scans in X, Y, and Z direction by maintaining contact with the surface, as shown in Fig. 17. During the dragging of the stylus over the surface, a minimal amount of constant force is applied on the stylus, which can be changed by changing the counter-weight on the cantilever arm. Due to the surface roughness, the cantilever moves at linear Z direction (up/down), and the force impinging over the sample is changed corresponding to the step height. The change of force is detected by the transducer, and it is converted to a measurable electric signal. If the sample is perfectly smooth,

the stylus force along the linear Z-axis does not change means the step height is zero. On the other hand, if the surface is rough, e.g., some hills and valley exist on the surface, the Z-axis displacements of the stylus induced some change of force, which is detected by the transducer. That means the vertical force difference between the high and low points of a surface is mechanically detected. A force feedback loop is used to monitors the changing of force from the sample pushing up against the probe [90]. Finally, a measurable output electric signal from the inductive transducer is amplified by an electronic amplifier and collected by an acquisition system to generate the surface profile. It is done through commercial computer software that evaluates the step height profile (thickness) of the thin-film surface.

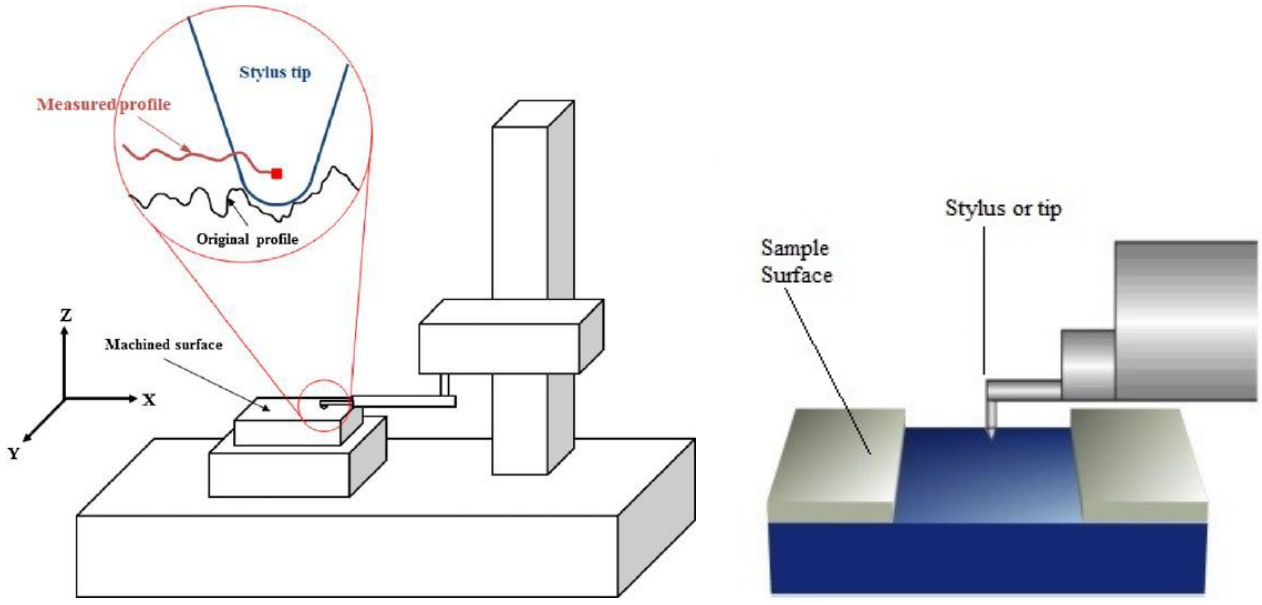

(a) (b)

Figure 17: (a) Setup and operation procedure of a stylus profilometer. The magnified part shows the stylus scans in X, Y, and Z direction over the sample surface which contains hills and valley (also known as step height) [90]. (b) Scheme of profilometer measurement on the surface of the sample having step height.

Any stylus profilometer encounters some common challenges. Since the stylus is extremely sensitive, any dust on the surface may interrupt the measurement. The lateral resolution also depends on the shape and size of the stylus/tip; thus, any dust on top of the cantilever tip may induce low lateral resolution. The probe/stylus can be contaminated by soft surface, or the probe can also be destructive to the soft surface by drawing unexpected scratching on it. Due to this reason, there is a high risk of damage to organic thin-film while measuring the thickness using contact stylus profilometry. Since the probe involves physical movements in X, Y and Z direction with surface contact, it is always slower than the non-contact techniques. Moreover, the accuracy of any stylus profilometry is limited by the linearity of the transducer used [91]. The hilly and valley surface profile of a polymer thin film from real-time thickness measurement is given in appendix A4.

4. Experimental Procedure

The whole experimental procedure has been performed into two major parts: the fabrication process and electrical measurements of OECTs. Both of them are describing here in this section step by step.

4.1 Fabrication Process of OECTs Memory Device

In this thesis project, the OECTs memory devices have been fabricated using cleanroom-based standard microfabrication techniques. Several fabrication steps have been performed to prepare a full-functional OECT memory device. The overview of subsequent fabrication procedures of the OECTs memory device is shown in Figure 18.

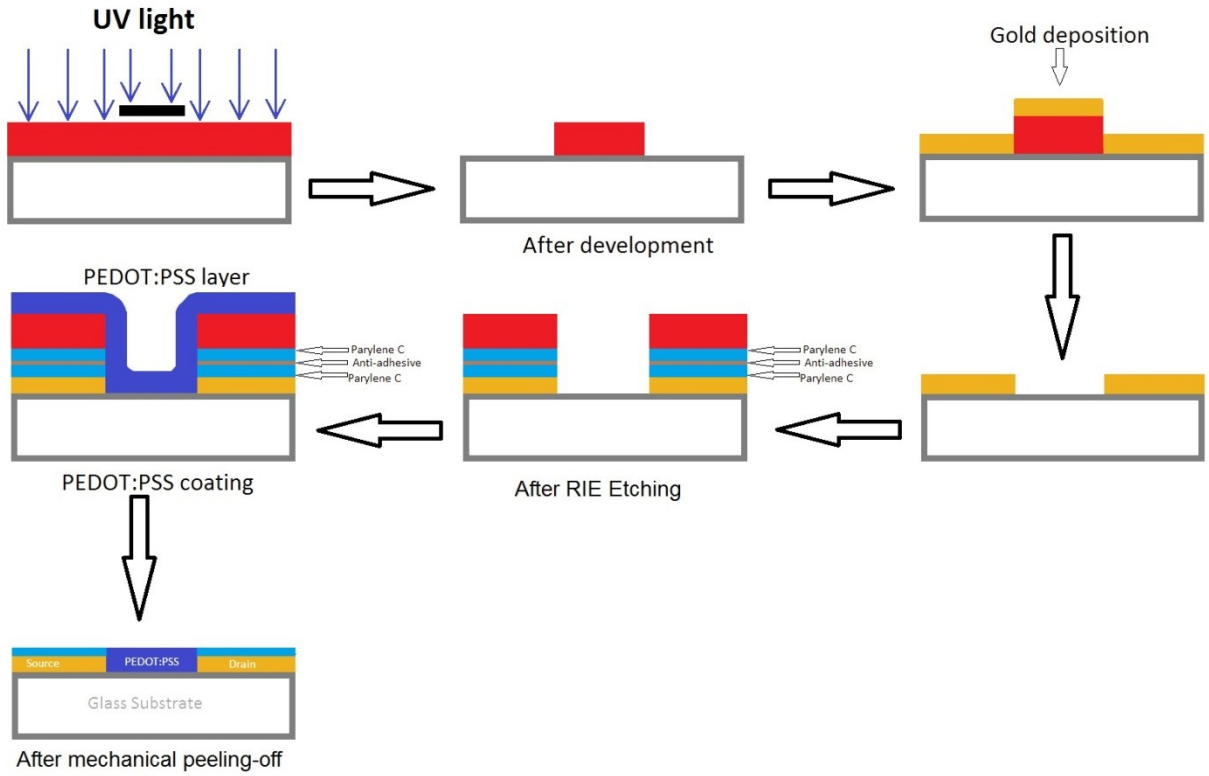

Figure 18: Schematic presentation of subsequent major fabrication steps of the OECTs memory device.

Preparing and Cleaning the Substrate:

The fabrication process has been started by cleaning the substrate that is one of the essential steps for the fabrication of any microelectronic device. Silicon wafers are a very commonly used substrate in the semiconductor industry. Other substrates such as glass slides, flexible organic materials (e.g., Parylene-C), or even textile, can be used as a substrate. However, in this project, rectangular shape glass slides with the dimensions 26mm×76mm×1mm (width, length, and height respectively) have been used. It is crucial to keep the glass substrates free of any contaminants since the degree of cleanness dramatically affects the quality of the thin film; even a micron-size particle may negatively affect the OECTs device. For that reason, cleaning it in a cleanroom environment ensures the minimum number of unwanted particles on the final fabricated device [10].

The cleaning process has been started by marking the slides on their backside with a diamond pen to indicate the front surface where the device to be fabricated. The next step involves the multiple sonication process of the slides. The first sonication was performed with a mixture of soap solution and distilled water with the volumetric ratio 1:10, respectively. The soup solution play role as a surfactant which helps to remove non-polar compound such as oil and greases from the substrate. To do it, all-glass slides were placed in a rack, which was then immersed in a beaker full of water-soap mixture solution and sonicate them for 15 minutes. They were taken out after the sonication and then cleaned by deionized (DI) water until the soap bubbles were washed off. Next to it, all-glass substrates have dried with nitrogen after the washing. After that, the dried substrates have been again sonicated in acetone and isopropanol mixture solution with the volumetric ratio 1:1 for 15 minutes. This sonication step is called organic cleaning. After the second sonication, the substrates were taken off the rack one by one and first washed with acetone. The acetone solution leaves some trace on the substrates, which have been removed by washing them separately with isopropanol solution. Again they were carefully dried by nitrogen gun and store in a box.

The sonication has been performed by a sonicator that uses ultrasound, from the range of 20 kHz to 40 kHz, to perturb the fluid. The ultrasound generator produces ultrasonic waves in the fluid, which oscillate at the ultrasound frequency. The subsequent oscillations of the ultrasounds create standing waves in the liquid, which induce many millions of microscopic void or partial vacuum bubbles, also known as cavitations. Those cavitations produce enormous energy, temperature, and forces which were collapsed on the substrate surface resulting in the clean surface from dirt. The cavitations are so tiny that they do not need more than cleaning, but sometimes they can penetrate the blind holes if the ultrasound frequency is high enough. During the sonication process, any blocking objects should not be placed on the bottom of the substrate as it may prevent the collapse of the cavitation on the substrate surface [93,94].

Deposition of 1st Photoresist Thin Film:

The cleaned glass substrates were followed by polymer photoresist deposition by a spin coating process. The idea for photoresist deposition is to create photoresist thin film, which helps to draw the predefined micro pattern on the substrate via UV photolithography in where the metallic contact lines will be defined later. First, a cleaned glass substrate was placed correctly in the spin coater rotating chuck. Then a small amount of positive photoresist (Microposit S1813 Photoresist DOW) was taken in a pipette in such a way so that it is sufficient to cover approximately $^3/_4$ of the surface area of the non-rotating substrate. Few drops of positive photoresist solution then left via static dispense methods on or near to the center of the substrate just before its rotations. It also called a static spin-coating process. Generally, 1 to 10 cc of photoresist is sufficient, although it depends on the viscosity of the fluid and size of the substrate. After that, the spin coater lid has been closed. The substrate was then rotated along with the rotating chuck at the speed 4000 revolution per minute with the acceleration at 3000 ms^{-2} for 40 seconds. The deposition parameters described above provides about 2 μm photoresist thin films. Centrifugal force compels to spreads the photoresist all over the substrate resulting in the uniform photoresist film. At the same time, the solvent evaporation provides stability to the film. But still, some solvent remains there in the film that needs to be removed by thermal treatment, also known as post-apply baking or soft baking. The soft baking steps of the resist coated substrates were then performed by putting them on a hot plate at 110^0C for 60 seconds. The idea behind this thermal treatment step was to evaporate the remaining solvents to densify the deposited thin film. This step also improves the photoresist film stability and firmly sticks with the substrate surface.

Mask Alignment and 1st Exposure to UV Light:

The photosensitive film-coated substrate is then exposed to a highly intense ultraviolet light to make the desired lines/patterns. A foil mask has been used to transfer the predefined pattern on the photosensitive film. To do it, at first, the top side of the substrate (the surface contains the thin film) was placed under a foil mask. Then the mask was carefully aligned according to the position and shape of the substrate. After that, the photosensitive thin film was brought into soft contact with the foil mask which was then fixed onto the chuck with a vacuum. This step is called soft contact mask alignment which was manually performed using MBJ4 Mask Aligner. Figure 19 shows the template of a foil mask that can be used to transfer the pattern on a photosensitive film surface. Depending on the substrate properties, this alignment can be performed either using the substrate's store position data or through the live image alignment [95]. The soft contact exposure mode offers a high resolution by minimizing the gap between the substrate and the foil mask. After finishing the foil mask alignment process, the whole system was then exposed to UV light for 10 seconds.

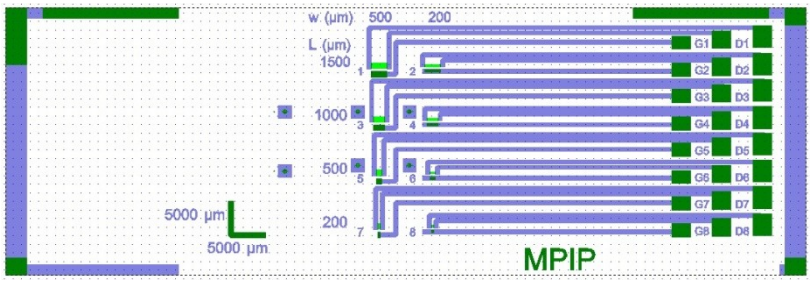

Figure 19: Template of a foil mask design. The blue and green areas are transparent in the foil mask that allows the UV light contact with the photo thin film [96].

Development:

After exposing the positive photoresist-film to UV light, the exposed parts became more soluble. A development step can reveal the patterns on the photo film surface. Development is one of the vital fabrication steps that may control the quality of the final device. The development approaches can be divided into:

- Wet development and
- Dry development, such as plasma etching.

In this case, wet development was carried out on the UV light treated positive photoresist coating glass slides. To do that, a liquid alkaline solution, such as tetramethylammonium hydroxide (TMAH or TMAOH), was used as a wet developer. The coated glass slides were then immersed in the bath of TMAH developer for 30 seconds, and simultaneously, they were gently shaken to eliminate the soluble residual photoresist. After 30 seconds of wet development activities, all coated glass slides were taken off from the development bath and placed them in a separated deionized water bath for 60 seconds. The slides were politely stirred in the DI water bath to clean the remaining residue. After the rinsing step, the photoresist thin film has been dried with a nitrogen gun. This step has to be performed carefully because a high flow of nitrogen gas from the gun may damage the photoresist film by creating some micro pinhole in the film.

Plasma Treatment and Post-Baking:

After the development and washing of the patterned photoresist film, it needs to clean with mild oxygen plasma. This step is also known as descumming [10]. The descumming process was started by placing the patterned glass slides in an oxygen plasma reactor/chamber, and the chamber had been closed. A 100 W of plasma power with 50 sccm of oxygen flow rate was applied for two minutes. The oxygen plasma removes any unwanted tiny particles without significantly damaging the desired patterns. Longer cleaning time or high plasma power may seriously damage the features of the pattern on photoresist film. To avoid any damaging severe of the pattern, the etching parameters were previously calibrated; thus, an optimized etching was ensured. However, the pre-patterned photoresists were slightly removed from its top surface. As long as the removal is a few hundred angstroms does not affect the fabrication processes.

After the oxygen plasma treatment, a post-baking step (also known as hard baking) was performed. The plasma-treated slides (as well as the patterned on the resist) were then placed on a hot plate at 120^0 C temperature. The hard baking temperature was settled in such a way so that it was slightly higher than the soft-baking temperature. The hard baking step increases the interfacial adhesion between the film and the glass surface through intermolecular interactions. Moreover, this hard baking temperature-induced some additional cross-links in the photoresist film resulting in harder and more etching resistant film. Care should be taken in this hard-baking step for temperature not to melt the photoresist. In every subsequent step, the fabricated part was monitored by an optical microscope.

Metal Evaporation & Pattern Transfer:

The previously accomplished all steps provide a clean negative image of the desired pattern on the photoresist. At this stage of the fabrication, the glass slide was ready for transferring the metal contact lines from the pre-patterned photoresist onto the substrate. This pattern transferring process has been rendered through the additive method in where the first negative image of the pattern was created by UV photolithography, and then its corresponding positive version (metal contact lines) was performed via metal deposition.

The thermal evaporation technique was used to deposit the metal contact lines on the substrate. At first, about 10 nm of the Chromium thin layer was deposited on the glass slides at an evaporation rate of 0.1 A/s using a metal evaporator. The idea behind the Chromium deposition was to improve the better adhesion of the gold layer on a glass substrate. Without the Chromium layer, there are high possibilities for delamination and detachment of the gold electrodes when it is in contact with electrolyte [66]. Then, about 100 nm gold film was deposited on top of the Chromium layer using the same thermal evaporation technique, as shown in Fig.18. The entire gold deposition process was performed into two individual evaporation rates: first, evaporate 10 nm of gold at the evaporation rate 0.1 A/s and then evaporate 90 nm gold at the rate of 2.5 A/s. At those evaporation rates, the 100 nm gold thin film deposition had been taken 6 minutes. During the thermal evaporation, the metal film was deposited over the entire top surface of the wafer. Thus, the gold layer was sitting both on top of the photoresist and in the pattern regions that have direct contact with the substrate through the opening of the photoresist mask. In this additive deposition method, the gold contact lines in the pattern regions are the desired electrodes of the device. Other parts, including the photoresist, need to be removed after this step.

Lift Off Step:

After the metal evaporation, the glass slides were taken out of the metal evaporator. The gold that stays on top of the photoresist is excessive material that needs to be removed along with the photoresist. This removal of excessive materials was accomplished by a wet etching process, also called the lift-off process. First, the glass slides were soaking in a mixture of acetone and isopropanol solutions bath with a volumetric ratio of 1:1 respectively for overnight. During this time, the action of chemical etching melts the photoresist structures, and as a consequence, the metallic layer deposited thereon was lifted-off that can be easily washed away in the ultrasonic bath. After the overnight immersion, the solution was replaced with a fresh mixture of the same recipe and the slides were sonicated for 15 minutes. This sonication step helped to remove the lifted-off metallic part and other tiny gold flakes from the substrates, which were finally washed by acetone and then by isopropanol solution, respectively. This washing left behind the desired gold contact lines with direct contact with the substrate through the chromium layer. If by chance, the lifted-off metallic part is not removed after the cleaning, a Q-tip or a small brush can be used to remove the remaining unwanted gold. After them drying at room temperature, they were observed under a light microscope to check any short circuit connections between the electrodes.

Cleaning with 2nd Plasma Treatment:

The gold contact lines on the developed glass substrates were then cleaned with oxygen plasma. To do that, glass slides were placed in a plasma chamber and applied a 100 W of plasma power with 50 sccm of oxygen flow for 2 minutes. The oxygen plasma removes any microscopic dust between the metal contact lines; thus, possibilities of any short circuit connections were reduced. Moreover, this plasma treatment improves the hydrophilicity of the substrate [66].

Parylene – C Deposition:

Parylene – C is a chemically inert, electrically insulator, and optically transparent biodegradable polymer. During the electrical measurements of the device, the liquid electrolyte may induce a short circuit connection throughout the metallic contact lines. A thin layer of Parylene – C polymer on the top can protect the contact lines from the electrolyte, and it also can define the OECTs device active area. To do that, two successive Parylene - C layer was formed with the separation of an anti-adhesive layer between them, i.e., the first layer of Pa-C on the gold, then anti-adhesive layer, and finally the second layer of Pa-C.

The first solid Pa-C dimer was placed in the molder compartment. Then, few drops of silane in the liquid form were taken with a cotton bud and carefully touched around the molder chamber. Silane is a toxic chemical, and it's volatile in the ambient atmosphere. It is important to stop breathing or use proper breathing mask while silane was applying in the chamber. The applied silane enhances adhesion between Pa-C and the glass substrate. After closing the chamber lid, the machine's cold finger was started for 15 minutes, and then a set of vacuum pump was used to create the vacuum in the chamber. At 8 mTorr chamber pressure and above 600^0 C furnace temperature, the Pa-C coating process has been started in the presence of nitrogen gas. After the first layer of Pa-C deposition, a thin soap (1 to 2%) soap solution layer was spin-coated and dried it at 100^0 C for 1 minute. This soap layer acts as an anti-adhesive promoter before the second layer of Pa-C, and thus, it allows strip-off the upper layers in the final step of fabrication. The second layer of Pa-C was deposited in the same way on the soap layer which plays a role as a sacrificial layer. 3g and 3.5g of solid Pa-C dimer were used to form the first layer with 1.5 μm thickness and a second layer with 2.0 μm of Pa-C thicknesses, respectively. Each layer of Pa-C polymer deposition takes around 3 hours. It was then ready for the next fabrication steps.

Deposition of 2nd Photoresist Film:

The Pa-C thin-film covered everywhere on top of the slides; even the active areas of the channel also covered with Pa-C film, which needs to be opened. A photolithography process followed by development and a plasma etching step was used to open the channel windows under the Pa-C layers. To do that, another layer of positive photoresist film was deposited on top of the Pa-C layer (sacrificial layer) by a spin coating, which was followed by soft baking at 110^0 C temperatures for 2 minutes. The second photoresist film deposition parameters were as follows: rotations 4500 RPM, acceleration 4000 m/s^2 and coating time 30 seconds.

2nd UV Photolithography Step:

The second photoresist film treated slides were then placed under a foil mask using the same mask aligner (MBJ4 Mask Aligner) technique as used before, i.e., soft contact exposure of UV light for 20 seconds. However, the patterns in the foil mask used in this time were exactly the opposite pattern of the previously used foil mask. As a result, this foil mask allowed the UV light direct contact with the channel region's photoresist only.

2nd Development:

The UV light treated positive photoresist slides were then developed using a similar alkaline solution that was used during the 1st development, i.e., tetramethylammonium hydroxide was used as the developer. To do it, the coated glass slides were immersed in the developer bath for 5 minutes. During this time, a pipet was used to blow the developer solution on the slides that help to remove the residual photoresist. After the development, the slides were taken out from the developer bath and immersed into DI water for 1 minute. This step removed the developer solutions from the device. Then the slides were rinsing by DI spray and dried by nitrogen gun.

Another Step of Plasma Etching:

The channel's window regions were not wholly opened even after the development process. Still now, a skinny layer of Pa-C was remaining in the channel regions that need to be removed. To open it completely, another plasma etching step was performed with the following etching parameters: plasma of power 160 W for 16 minutes, Oxygen and CHF_3 gases were used for etching at the flow rate of 50 sccm and 5 sccm respectively.

The oxygen plasma removal mechanism of Pa-C polymer is not well-understood yet [14]. The plasma removal of Pa-C is related to the opening of the benzene ring of the polymer. First, the ionic oxygen abstract the hydrogen atoms from the $=CH_2$ radical between the benzene rings in the polymer chain and hydroxyl radical is formed, as shown in reaction 4.1.

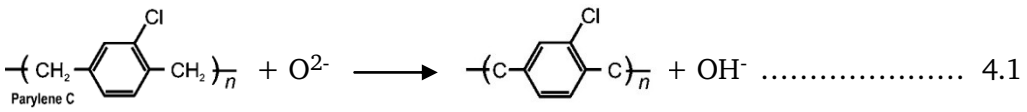

..... 4.1

Then the exposed unsaturated or reactive site absorbs the molecular or atomic oxygen to form an unstable peroxy radical. A few rearrangements of this unstable radical then produce carbon monoxide or carbon dioxide.

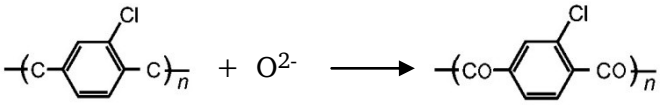

..... 4.2

The more oxygen plasma interaction on the radical site results in the formation of ring-opening. The presence of the chlorine atom in the Pa-C ring reduces the available reactive sites by one. Thus more oxygen is required for this polymer etching [14].

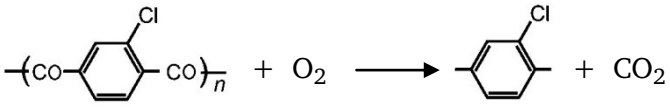

..... 4.3

Device Inspection:

The last plasma etching step described above successfully open the channel window regions and removed all residual partials. To ensure the devices were stched correctly, they were carefully checked in two ways. First, they were visually inspected under a light microscope, and then they were checked with a multimeter. The light microscope was used to check the device status in every step of the fabrication. To do that, the glass slides were placed under a microscope lens; the light was focused onto the surface, and the surface of the devices was magnified through the lenses. Moreover, checking with multimeter ensures that there were no short circuit connections and the devices were conducting. If by chance, the etching result is not satisfactory during the inspection, they need to etch a few more minutes again. In that case, care should be taken not to do over-etching.

The Polymer (PEDOT:PSS & p(g2T-TT)) Deposition by Spin Coating:

The previously etching step defines the channel regions for the polymer deposition. In this work, PEDOT:PSS & p(g2T-TT) polymer were used for the OECTs channel. Commercially PEDOT:PSS has several formulations; among them, *Clevios™ PH1000* was used with 5 wt% ethylene glycol (EG), 0.1 wt% dodecyl benzene sulfonic acid (DBSA) and 1 wt% of (3-glycidyloxypropyl–trimethoxysilane) (GOPS). The EG was used to enhance the channel's conductivity, DBSA decrease the surface tension of the polymer film, and GOPS reduce the delamination by increasing the bond between polymer chain [4, 66].

The OECTs channels were obtained by the spin-coating step, followed by the hard backing. Before starting the polymer spin-coating deposition, the liquid polymer was stirred with sonicator for about 15 minutes. This step helps to get a well-mixed polymer composition. Then the liquid polymer was taken in a syringe and filtered through a 0.45 μm cellulose acetate filter. A small amount, sufficient to cover the active area of the device, of filtered polymer (PEDOT:PSS or p(g2T-TT)) dispersion was placed on the glass slides. The next step was starting the spin coater with predefined spin-coating deposition parameters (rotations, times, and accelerations), which allow about 100 nm thin film depositions for the OECTs channel (see appendix A2 for additional spin coating data). A soft baking step was followed after the spin coating process. Since PEDOT:PSS and p(g2T-TT) polymers have individual physical and chemical properties, their spin-coating deposition parameters were different to achieve 100 nm thin film as given in table 1. Sometimes multiple spin-coating steps were performed with different rotating speeds to obtain a specific thickness of the film.

Polymers	Spin coating time (in seconds)	RPM	Acceleration	Soft baking (1 minute)
PEDOT:PSS	30	1500	1000	110^0 C
P(g2T-TT)	60	1000	3000	60^0 C

Table 1: Spin coating deposition parameters of PEDOT:PSS and p(g2T-TT) polymers (see appendix A2).

Mechanical Peeling Off:

The evaporated channel's polymer was deposited everywhere on the slides, even the sidewall of the glass slide was also covered by polymer thin film. The slide's edge was scratched with tweezers that helps the peeling off the unwanted parts of the polymer from the device. After that, a piece of Kapton tape was carefully placed on the upper surface of the slide in where PEDOT:PSS or p(g2T-TT) polymer film was formed. The tape was then gently taken off from the slide, which removes everything remaining on top of the anti-adhesive layer, i.e., the sacrificial Pa-C layer, photoresist, and unwanted polymer films were taken out of the surface. An only a protective layer of Pa-C film on the contact lines and polymer channel remains after this step. This step is known as a mechanical peel off that defines and exposes the active device area (channel). This peel-off step was done before performing the hard baking step. As a result, quick removal of the tape may cause the removal of the channel polymer; thus, care should be taken while removing the tape.

Hard Baking and Final Rinsing:

After the peeling off step, the devices were placed on a hot plate at 140^0 C temperatures for 1 hour. This hard baking step helps to dense the channel's polymer, thus firmly attached the polymer with the substrate. Some unwanted materials, such as non-polar soap from the anti-adhesive part, remain even after the peeling-off step that needs to be washed away. The devices were then immersed in a DI water bath overnight. Next to it, they were taken off the bath and carefully dried with a pressurized nitrogen gun. Now the devices are ready for its electrical characterization. Fig. 20 shows the final fabricated devices on a glass slide.

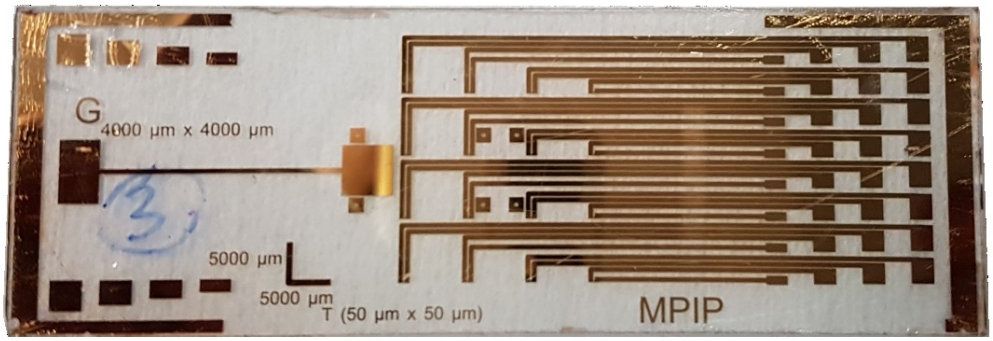

Figure 20: A glass slide contains multiple OECTs memory devices that are connected with metallic gold contact lines that play a role as a source and drain electrodes. All shinny lines are gold contact lines fabricated in the cleanroom-based metal evaporation process. Each end of the two neighbor contact lines (middle in the slide) holds the tiny OECTs channels with various dimensions. Picture courtesy [96].

4.2 OECTs Characterization Technique

After the fabrication, the devices were needed to electrically tested to analyze their full functional features, i.e., switching behavior, neuromorphic properties, etc. To do that, electrical transient response measurements were performed through a set of electrical instruments that interfaced with a custom program for the acquisition. In this thesis work, a semiconductor analyzer was mainly used to analyze the device's characteristics. Along with that, a mechanical probe station was used to precisely connect the devices with an external signal generator. A probe station consists of a stage; the user installs probe arm, thin needles into the manipulators, and a microscope. The manipulator allows the exact positioning of the needles to head onto the surface of metal contact lines (electrodes) of the devices. Once the needle tips have been settled in a precise position, the device was ready to be tasted.

The fabricated device architecture is presented in Fig. 20, which consists of 4 × 4 grid of two-terminal devices in the glass slide. All the devices were gated with an Ag/AgCl wire gate electrode serves as the global input through a liquid electrolyte. An aqueous solution of 0.1 M NaCl in DI water was used as the electrolyte. All electrical characterizations in this thesis study were performed using Ag/AgCl gate electrode and 100 mM NaCl liquid electrolyte. First, the liquid electrolyte was placed on the devices with a dropper at the testing sites (channel regions). A PDMS well was used to confine the liquid electrolyte within the testing sites, thus preventing them from moving around. It is always better to wait several minutes before testing the devices; this waiting period allows the sodium ions to cross-link the PEDOT:PSS film.

The electrical characterizations of the devices were carried out using a semiconductor analyzer unit, which was interfaced with customized software. For the investigation of OECTs neuromorphic behavior, the pre-synaptic signal was applied to the Ag/AgCl global gate electrode using a Keithley 2604B Arbitrary Function Generator, as shown in Fig. 21 (a). The source electrode of every OECT memory device was grounded, while a constant bias was applied within the source and drain. The response of the devices was investigated by measuring the drain current (also known as a post-synaptic signal) corresponding to the gate voltage. The output drain current was recorded using the Keithley's 2600B dual-channel source measure unit (SMU) instruments, Fig 21 (b). Everything was monitored and controlled by a customized LabVIEW computer-based program. Beside of this instrument, the resistivity data of the device's channel was measured using a DC powered multimeter.

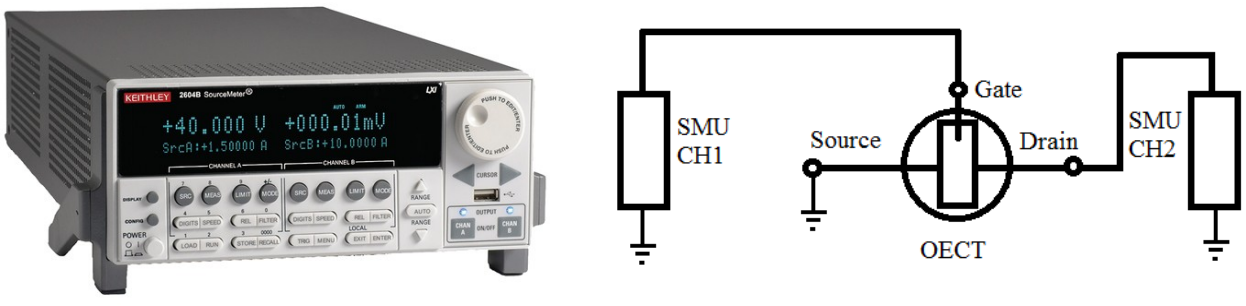

(a) (b)

Figure 21: (a) Keithley 2604B Arbitrary Function Generator that provides a gate voltage of OECTs devices [98]. (b) The dual-channel source measure unit (SMU) of this generator can simultaneously measure the gate current and drain current.

5. Results and Discussion

All the fabricated OECT devices were geometrically symmetric; they can be distinguished by applied potentials only. The source was always grounded. The Ag/AgCl gate electrode leads to the significant current modulations; as a result, it does not require any reference electrode due to their high double-layer capacitance. The electrochemical characterizations of the devices were performed over various measurement ranges dictated by polymer stability. For the electrical characterization, a train of pulses was applied at the gate electrode, and simultaneously, the drain current as a function of time/drain voltage was recorded. The resulting drain currents, therefore, reflect the characteristics of the OECTs memory device. In this section, all the characterizations were performed based on the response of the drain current of OECT which are discussed here.

5.1 Electrical Characterization of PEDOT:PSS Polymer OECT

Steady-State Characteristics:

The PEDOT:PSS polymer-based micro-OECTs on glass slides were electrically characterized by scanning various negative potentials at the drain-source electrodes while a fixed positive potentials were applied at the gate electrode. Figure 22 shows the output characteristics curves of a fabricated OECT device (W= 1500 µm, L=500 µm) in where the output drain current (I_D) is a function of potential between source and drain (V_D) at various constant positive gate voltages V_G varying from 0 V to +0.6 V. The OECT shows almost linear output curve at V_G = 0 V (top black curve) means the drain current linearly increases by increasing the drain voltage even in the absence of any gate potentials, the OECT is in the ″ON″ state. While ON state, about 1.09 kΩ channel resistance was found, which is very small compared to solid-state transistor counterparts. This linear behavior of the output curve is in good agreement with the high conductivity of PEDOT:PSS polymer film. The output curves also exhibit that at a specific negative drain voltage V_D, the drain current decreases by increasing positive gate potentials. For example, by applying +0.2 V at the gate reduces the drain current approximately

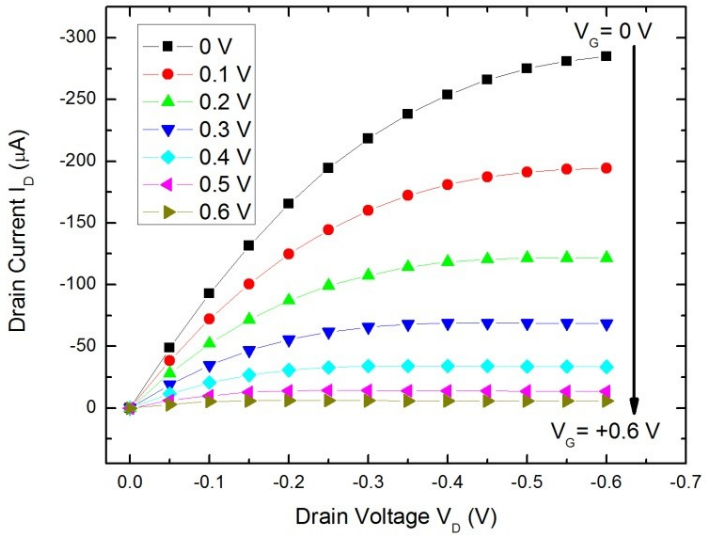

Figure 22: Output characteristics of single OECT device (PEDOT:PSS channel dimensions W= 1500 µm, L=500 µm, d=100 nm) with V_D swept from 0 V to -0.6 V and V_G varying from 0 V (top curve) to +0.6 V (bottom curve) with a step difference of 0.1 V.

by 57% of the initial I_D, although the drain voltage defines the exact percentage of decrement. It was reported by *Paschalis Gkoupidenis et al.* [5] that the saturation (steady-state) of drain current is possible only for negative drain voltages but not for a positive one. Previously the same information has also been reported by *Nilsson et al.* [99]. That's why negative drain voltage was applied to analyze the steady-state behavior of this output curve.

The output curve in Fig. 22 shows that at a fixed positive gate voltage, the drain current (I_D) reaches its saturation state at a certain level of negative drain voltage (V_D). This steady-state behavior of drain current is a good agreement with the work of other researchers [5,18,99,101]. In this output curve, steady-state phenomenon is observed at the gate voltage starting from 0.1 V to 0.6 V. But, at 0.6 V gate potentials (the bottom curve in Fig. 22), the OECT enter into a constant drain current-mode, further drain current increment is not possible at this state of OECT means the PEDOT:PSS polymer channel reaches at its minimum conductive state, also called ″OFF″ state. The non-conductive state of OECT was also proved by the transfer curve, as shown in Fig. 23. The transfer curve shows that +0.6 V is the switching gate potentials for which this OECT device turns into the OFF state. These low voltage operation characteristics are the remarkable hallmark of electrolyte gated OECTs compared to its solid-state transistor counterparts. Thus, the level of drain current can be controlled by controlling the positive gate potential. This feature turns OECT into a low operating voltage switching device. This type of gate-controlled switching behavior is analogous to the traditional silicon-based semiconductor transistors in where the ground state of the silicon transistor channel is in the OFF state. But in PEDOT:PSS polymer channel-based OECTs operated in depletion mode, i.e., in the ground state, the OECTs are in ON state. Although, the switching speed of OECT is slower than solid-state devices because the switching time in the molecular-based device (OECT) depends on the rate of chemical reactions, which is a time-consuming process, whereas no chemical reaction associated with solid-state devices. It was previously reported that the switching speed of OECT could be optimized with smaller lateral channel dimensions and film thickness of the channel, as large OECT with the thick channel has slow switching operations than small and thin ones [18, 39].

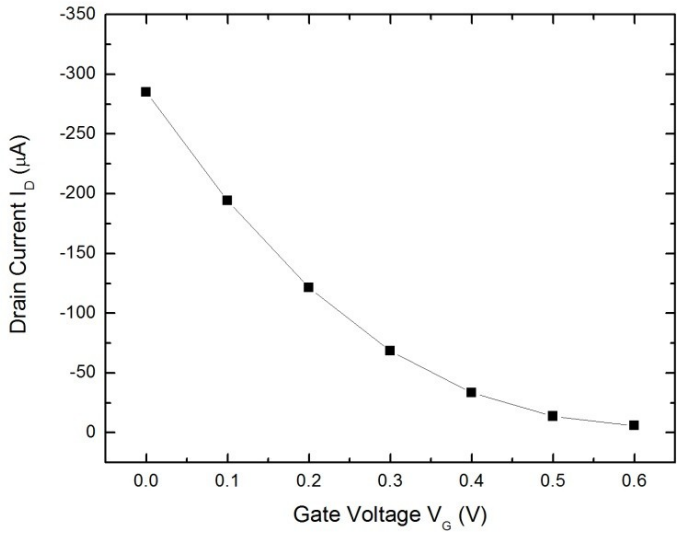

Figure 23: Drain current (I_D) vs positive gate voltage (V_G) of a fabricated OECT (for V_D = - 0.6 V). The transfer curve shows the depletion-mode of OECT in where the steady-state I_D as a function of V_G. The device reached its steady-state of output current at V_G = +0.6 V.

Volatile Characteristics of OECTs:

Besides the steady-state behavior of OECTs, its volatile characteristics were also investigated by reproducing different short-term functions, such as drain current. The reproducible behavior of PEDOT:PSS polymer channel-based OECTs was obtained by applying a repetitive cycle of gate pulses over time. Each cycle consists of two voltage pulses with opposite polarity (V_G =+0.3 V to -0.3 V) having 2 seconds of each pulse duration. In Fig. 24 (I-t plot), the volatile behavior of OECT was observed through the response of drain current I_D as a function of time. To do that, a cycle of the short pulse (V_G = ± 0.3 V and t_p = 2 seconds for each pulse) were applied at the gate electrode, and the corresponding drain current response over time was recorded. Throughout that measurement, the channel was biased with a fixed small potential V_D = - 0.2 V. The high channel biasing potential should not be used to avoid polymer degradation.

The I–t curve in Fig.24 shows that initially, the channel has high drain current even at V_G = 0 V, see the drain current vs. time on the bottom plot. This initial drain current was obtained, without any gate voltage in OECTs, because the PEDOT:PSS polymer film is naturally conductive even in the ground state of OECT. Whenever a positive gate pulse with magnitude V_G = +0.3 V was applied for 2 seconds, a decrement of drain current was immediately induced, as shown in the dotted box inside the plot. This reduction of drain current holds as long as the positive gate voltage remains for 2 seconds. After removal of the gate voltage, the drain current was returned to its initial state means the drain current response of this OECT was volatile over time. Thus a short term depression was observed in PEDOT-PSS channel OECTs. The fact behind this short-term depression event is the temporal changing of charge carrier concentration in the PEDOT:PSS polymer channel induced by the short pulse of gate

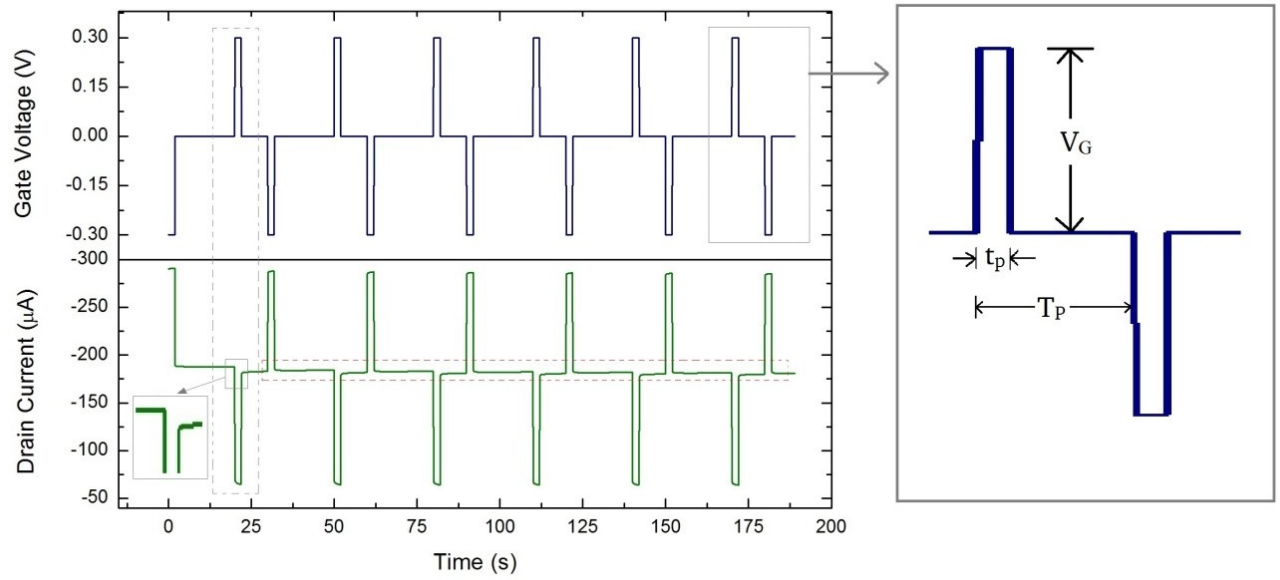

(a) (b)

Figure 24: (a) Drain current (I_D) vs. time (t) plot of the PEDOT:PSS channel-based NaCl electrolyte gated OECT with channel dimensions W×L = 1500×500 μm^2, gate voltage V_G = ± 0.3 V, pulse duration t_p=2 s and V_D = - 0.2 V. The vertical dotted box shows the reduced drain current pulse corresponding to the positive gate voltage. Inset: tiny stage difference of I_D after the application and removal of gate voltage. (b) A full cycle of gate voltage shows the pulse width (t_p) and pulse height (V_G), the time difference between two gate pulse $\Delta t = T_P - t_p$.

potentials. This volatile response phenomenon of drain current is attributed to the present understanding of the operation mechanism of OECTs. Due to the applied positive gate pulse, cations from the electrolyte were penetrated to the PEDOT:PSS polymer made channel and the sulfonate anions on the PSS were compensated. The sulfonate is thus inactive from interacting with the charge transporting holes in the channel. As a consequence, the PEDOT:PSS polymer thin film was developed that leads to a decrease of the hole density in the OECT channel, as well as increase the electrical resistance of the channel. The end resulting in the decreasing of the conductivity of the channel, and I_D was switched OFF. After removing the positive gate pulse, the injected cations naturally move back to the electrolyte, and the channel was reversibly doped again to its initial state.

Figure 24 also shows similar volatile drain current response for negative gate pulse with the same magnitude V_G = - 0.3 V. But in this case, the drain current was increased by application of the negative gate voltage. This increment of drain current can be explained as follows: The applied negative gate voltages force the anions to migrate from the electrolyte into the polymer channel. The OECT channel was hydrated; thus, the ions can penetrate from the liquid electrolyte into the bulk of the channel volume. Due to the anionic migration, an unstable charging environment is raised on the channel. The cations were extracted from the channel to compensate for the charges on the sulfonate. This event results in the ionic doping of the channel material, which increases the hole concentrations by accumulating the holes from the polymer backbone chain. The end was resulting in the increasing of the drain current I_D; meaning the electronic currents in the channel were modified by the ionic current; it is called electrochemical doping. Shortly, after cutoff the negative gate voltage, the migrated anions go back to the electrolyte. As a result, the increased drain current drops back to its initial state in the absence of positive gate voltage. This temporal increment of drain current can be referred to as short-term-potentiation (STP), which is analogous to the neuromorphic system. To ensure the short term depression and potentiation over an extended period of measurement time, a set of identical gate pulses with opposite polarity voltages (V_G = ± 0.3 V, t_p=2 s, and period of pulse T_P = 10 s) were repeated in multiple times, as shown in Fig. 24. From the entire I-t plot, a volatile asymmetric sequence of drain current responses was obtained. From the above discussion, it is clear that the drain current response has only appeared in the presence of applied gate potentials. After removing the gate voltage (both positive and negative), the injected ions into the OECTs channel no longer stay inside the bulk of the channel volume. The straight line in the horizontal dotted red box (bottom plot of Fig.24) is a clear indication that no ions were permanently stored into the PEDOT:PSS polymer channel. Due to this reason, PEDOT:PSS polymer-based OECTs are not attributed to the memory device.

Moreover, due to the volatile characteristics of its drain current, the PEDOT:PSS polymer channel-based OECTs can be used as a bio-electronics application based micro-switching device. However, it provides low switching speed compared to the semiconductor FET counterparts due to the few reasons (similar switching mechanism is given in Appendix A6). The main reason is the interactions of the migrated ions with the channel material. The effect of the ionic interaction is reflected in the inset picture of Fig. 24. The inset view indicates the stage difference of the drain current after the application and removal of gate voltage. There are two possible reasons behind this stage difference event. One reason could be the ion storing phenomena in the channel. But almost no ions were stored into the PEDOT:PSS polymer channel discussed previously. The final reason for the drain current's stage difference is attributed to the slow movement of migrated ions. Due to the short time difference ($\Delta t = T_P - t_{p,}$) between two back-to-back gate pulses, the migrated ions do not get enough time to return from channel polymer to the electrolyte in the absence of gate voltage. Sufficient time intervals

(Δt) between two gate pulses may optimize this stage difference of drain current because a longer time allows all the ions to move back to the electrolyte. Referring to Figure 24 (a), it should be mentioned that our fabricated OECT device shows faster switching since the drain current immediately drops to zero after removal of the gate potentials, which is analogous with the short-term synaptic depression. Previously it was reported this type of synaptic depressions as pair-pulsed-depression (PPD) [8]. As earlier reported for OECTs, some electrical characteristics (such as drain current) are a function of the dimensions of the channel [19]. Larger channel thickness of OECT provides high drain current as well as high transconductance but reduces the switching speed. Another important aspect of OECTs is the stability of the drain current over a more extended measurement period. As depicted in Figure 24, the drain current stability of PEDOT:PSS polymer channel-based OECTs device had also been investigated using a repetitive cycle of a square wave of gate voltage. When this device was switched from 0 V to +0.3 V, it exhibits excellent stability as evidence from the constant peak drain current of approximately -122 μA obtained in each positive gate pulses. Similarly, it also shows excellent stability when switched from 0 V to -0.3 V with constant peak drain current roughly -105 μA per negative gate pulses. In Figure 24 (a), the constant peak drains current levels tell that the device had an excellent drain current stability over the entire measurement time.

The above characterizations of PEDOT:PSS polymer channel OECTs show that STP and STD can be achieved with this device by applying an inhibitory potential to the gate terminal, which leads to an increment and reduction of channel conductance. This STP and STD of OECTs thus help to study about the neuromorphic system. Moreover, this OECTs device does not attribute to memory devices. Due to its volatile output current response, it can be used as a bi-stable switching device.

5.2 Electrical Characterization of p(g2T-TT) OECT Memory Device

Electrical characterizations of p(g2T-TT) polymer-based OECT memory device was also performed under the application of successive identical short pulses (~ 1 second) at the gate electrode. The p(g2T-TT) thin-film channel is pretty much vulnerable to higher potentials; thus, higher gate voltage may damage the device. To stand in a safe range of applied gate voltage to the channel, a set of resistors in series connection were used in the path of gate voltage is depicted in Fig. 25. The gate pulses were manually applied to makes the device analogous to real life-switching applications, such as in the artificial intelligent based robotic car applications.

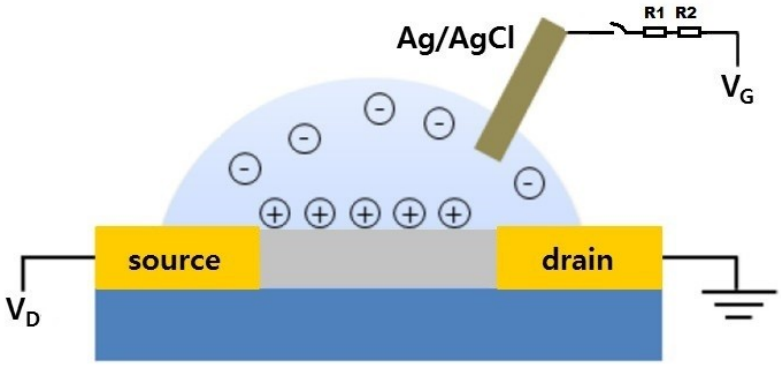

Figure 25: Schematic diagram of the p(g2T-TT) polymer-based OECT memory device. The gate potential is manually applied through a set of series resistors placed before the gate electrode [57].

Transient Behavior of OECT Memory Devices:

Transient characteristics of OECTs memory device is one of the crucial aspects in biological applications, especially in the study of neuromorphic systems. The transient behavior of OECTs is similar to the brain's nervous system in where the strength of a synapse is proportional to the pre-synaptic signal [5, 8, 67]. When the synaptic strength is considered in an electronic platform such as synaptic transistors, it is more convenient to consider the numerical weight as the synaptic strength. Thus, the synaptic weight in a transistor can be defined as the amplitude of the drain current (I_D) response concerning the gate voltage. Following this thesis protocol, the applied voltage at the gate electrode is defined as a pre-synaptic signal and the drain current is being treated as a postsynaptic signal in OECT memory devices. In this thesis study, the synaptic functions were reproduced in the p(g2T-TT) polymer thin film channel-based OECT by applying a pre-synaptic signal at the gate electrode. Depending on the polarity of pre-synaptic pulses (negative or positive gate bias), the synaptic strength can be increased or decreased in the form of potentiation or depression respectively.

To demonstrate the synaptic behavior in the organic transistors, the p(g2T-TT) organic polymer thin-film channel-based OECTs memory device with W × L = (2000 μm × 20 μm) active channel area were used. When a train of pre-synaptic short-pulses of negative current (with pulse height V_{pre} = -1.0 V, duration of each pulse t_p = ~ 1 second, interval between pulses Δt= 30 seconds) was applied at the gate terminal, a significant increase in the post-synaptic signal was obtained with the application of each set of pre-synaptic pulses, as shown in Fig. 26. Fig. 26 (a) shows a stepwise post-synaptic current due to the application of multiple square-wave pulses of pre-synaptic negative current at the gate electrode. Unlike the PEDOT:PSS polymer channel OECTs, every pre-synaptic negative short pulse gradually increase the channel's conductance in non-volatile way (see in Fig. 27 (c)), meaning gained synaptic weight of the device does not go back to the initial state even in the absence of pre-synaptic gate pulses as opposite behavior of PEDOT:PSS OECTs. The multi-steps drain current curve appears because the migrated anions from the electrolyte remain into the channel bulk volume (which changes its conductance) even after removing the gate voltage, meaning the ions were stored in the thin film channel due to the unique property of the p(g2T-TT) polymer structure. As a consequence, multi-steps post-synaptic (drain current I_D) signal relaxation over time was observed from the resulting curve, meaning this device store the ions in multi-steps. If we consider only one drain current step with the corresponding gate pulse, it tells that the system does not return to its initial post-synaptic drain current even after removal of negative gate current, which is an adaptation to long-term potentiation. The multi-steps drain current curve is a clear indication of non-volatile post-synaptic responses over time, which is attributed to the storing information in the p(g2T-TT) channel. Therefore, this device can be labeled as a multi-stage OECTs memory device. The main fact behind this ion storing event of this polymer is the side glycol chain that captures the injected ions with the main polymer backbone chain; the details mechanism was discussed in section 2.2.2 in this protocol.

By comparing two immediate steps of drain current, it was observed that the post-synaptic weight (drain current) in any step is slightly larger than the previous step, as shown in the bottom inset plot on the left side of figure 26 (a). It happened because each negative gate pulse injects a certain amount of anions that increase the charge carrier concentration in the channel by accumulating the holes from the polymer backbone chain. Hence, the increment number of holes reduces the channel's resistance and enhanced post-synaptic weight. Next, the applied pre-synaptic pulse again injects anions to the channel. The additional injected anions from the second gate pulse were added with the previously stored ions, which together enhance the post-synaptic current one step further ahead. For that reason, the amplitude of each next step drains current spike is on a higher level than the previous step, as

shown in the bottom inset curve. The enhanced post-synaptic weight may remain in the channel from few hours to few weeks, depends on some factors including the way of the polymerization process. It means a negative pre-synaptic gate pulse increases post-synaptic strength, which retains in the channel over a longer period in the form of long-term potentiation (LTP), which is analogous to the neuromorphic system.

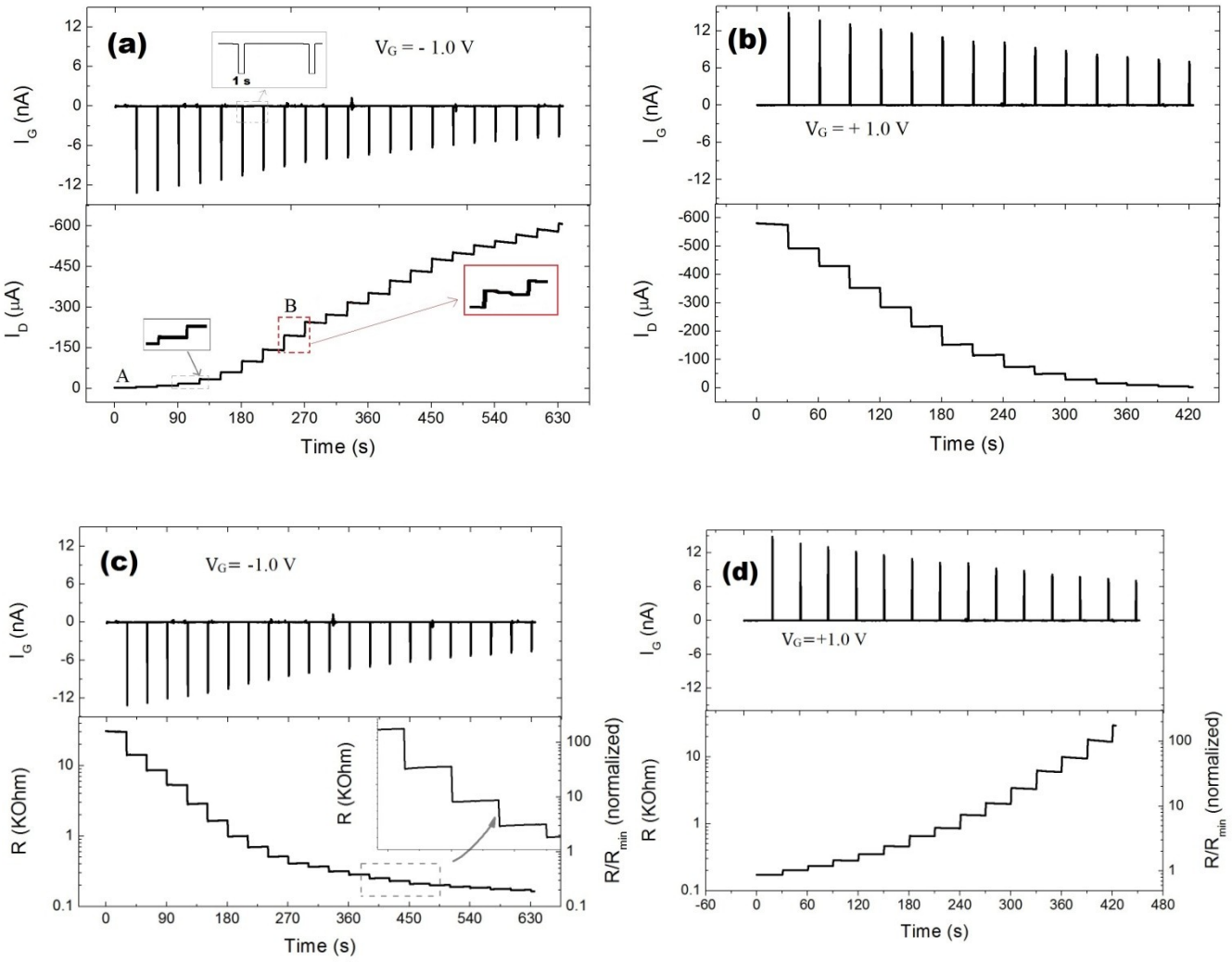

Figure 26: Transient characteristics of p(g2T-TT) OECT memory device with active channel dimensions W × L = (2000 μm × 20 μm) and d = 100 nm. The post-synaptic signal I_D changes exhibit LTP and LTD. The applied source-drain voltage V_D= -100 mV (a) Application of pre-synaptic negative gate current (for V_G = - 1.0 V) induced long-term potentiation. (b) Long-term depression was induced by positive gate current (for V_G = + 1.0 V) that reversibly brings the previously gained drain current to its initial state. (c) & (d) Resistance of the channel stepwise decrease and increase by application of the negative and positive gate pulses, respectively. For every plot, pulse time t_p = ~1 second/pulse, the interval between pulses Δt= 30 seconds.

The Fig. 26 (a) also shows the step-breaks of this device was started at the post-synaptic current level $I_{post} \approx I_D \approx$ - 196 μA. The initial step-breaks indicate the starting of the device's saturation level. The baseline increment of post-synaptic current continues up to a specified maximum level, known as saturation level, that is also the mark-line of maximum ion storing capacity of the polymer channel. The device was saturated when the drain current was at -196 μA, as shown in the dotted red box in Fig.

26 (a). After reaching the saturation level, no more ions were stored in the channel bulk volume, and the injected excess anions were naturally returned to the electrolyte after releasing the gate current between the pulses. As a result, the drain current exhibits a decreasing tendency, which makes the step-break shown in a red-colored inset plot. Besides, Figure 26 (a) also clearly exhibits that the ions storing phenomena of this device was initiated from I_D = -3 μA and terminated on the saturation point at -196 μA. There was no possibility to store the ions in the channel beyond this region (from point A to point B), meaning all ions were stored between points A to B. Thus the region from the baseline drain current (point A) to the saturation line (point B) can be treated as ion storing regime or memory window. A wide memory window provides a more significant number of multistep switching facilities, which is more favorable for practical applications. Although, the magnitude of the memory window mainly depends on the type of the polymer in the channel and their molecular structure. It also has been observed from this thesis study that the total number of drain current steps in the memory window regime can be increased by applying a short duration gate pulse, although the memory window remains the same. It is because the longer duration gate pulse pushes additional more ions at a time; thus, the device reaches saturation level within few gate pulses which gives a few numbers of drain current steps.

On the other hand, the reverse circumstance, long-term depression, can be obtained by applying a set of successive characterization spikes of positive gate current, as shown in Figure 26 (b). When a set of positive gate current pulses with V_G=+1.0 V, t_p = ~ 1 second, and Δt= 30 seconds was applied, the previously gained post-synaptic weight of the device was stepwise declined. It happens because of the positive pre-synaptic current reversibly doped the channel, and its conductivity reduces step by step with every positive gate pulses. Each reduced drain current step corresponding to an applied positive gate pulse. Thus the channel's memory status was also stepwise returned to the initial state. After reaching the initial post-synaptic weight I_D = -3 μA, no more drain current was remarkably reduced with further gate pulses. As a result, the I_D curve becomes a straight line at the end instead of multistep; the straight line of I_D is the saturation point for the positive gate potential of the OECTs memory device. By comparing the measurement time of the plot (a) and (b), a faster saturation event was observed when positive gate voltage was applied in this OECTs memory device. The possible reason for this faster saturation could be the radial structure of Na^+ is relatively more favorable for higher ionic mobility in the liquid compared to the mobility of Cl^- [60].

Besides those above characterizations, Fig. 27 (a) shows the channel resistance reduced from 30 kΩ to 0.185 kΩ over the measurement time concerning the negative gate voltages. It means the application of the negative pre-synaptic gate voltages turns the channel from a high resistive state to a low resistive state that can reversibly be returned into the initial high resistive state by application of positive gate potentials as shown in Figure 27 (b). Comparison of these two resistive curves (a & b) indicates that the resistivity as well as the conductance, on the other way around synaptic weight, of the p(g2T-TT) polymer channel are a reversible process. The multistep resistance-changing phenomena attributed to the multistage switching characteristics of the p(g2T-TT) channel OECTs device. Previously it was reported that p(g2T-TT) polymer OECTs show significantly faster switching time compared to the PEDOT:PSS polymer OECTs [16]. Beside it, Figure 27(c) shows the increment of channel conductance from 0.03 mS to 1.97 mS within the memory window, which was reversible with the application of negative polarity pulses, shown in the plot (d). By comparing Figure 27 (c) & (d), the multistage increment and decrement of the channel's conductance were observed, which is another indication that this device can be characterized as a multistage reversible-memory device.

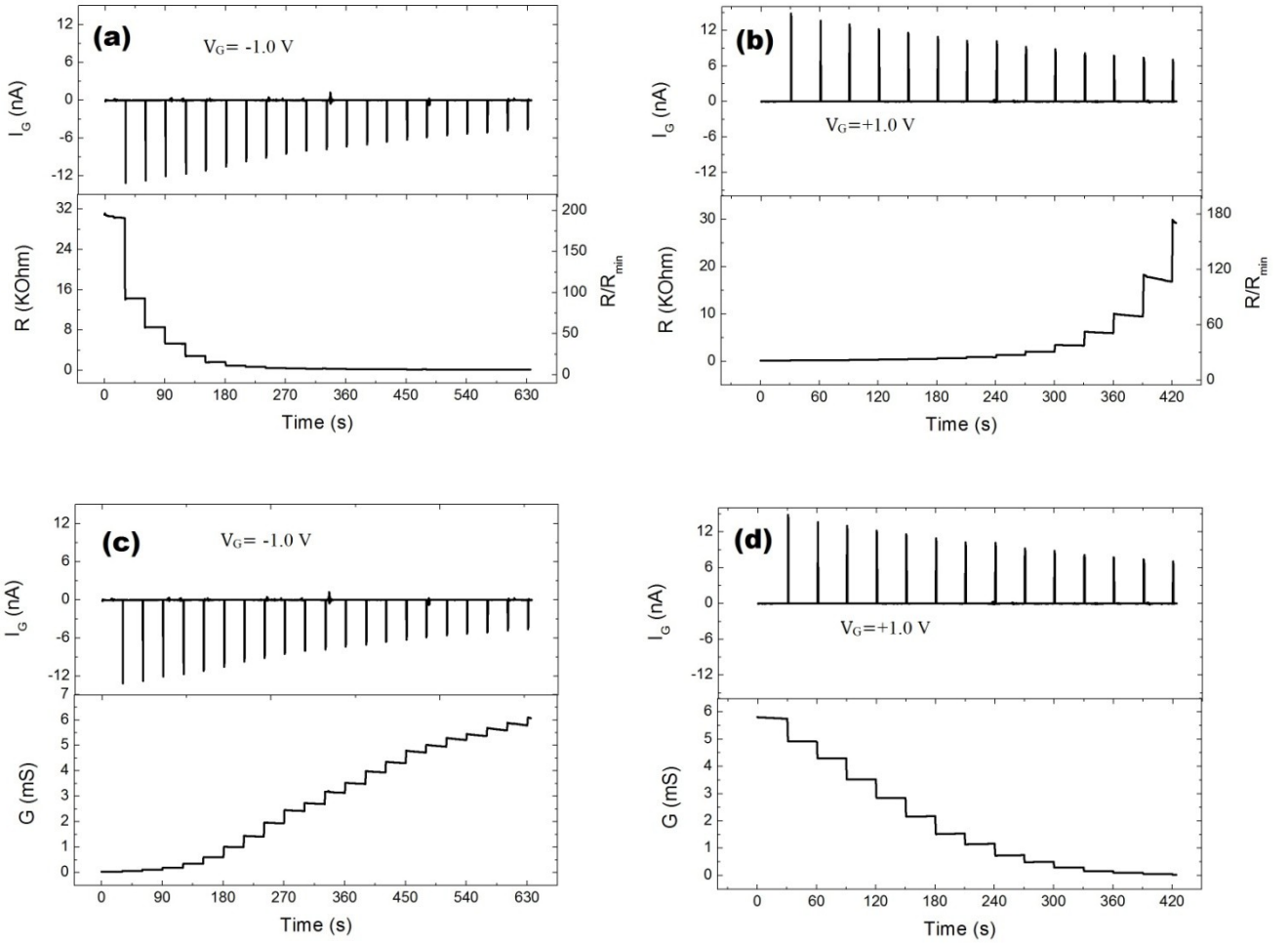

Figure 27: Multistage switching and memory phenomena in the p(g2T-TT) channel OECT with active channel dimensions W × L = (2000 µm × 20 µm) and d = 100 nm (for V_D= -100 mV). (a) & (b) Resistance vs. time response concerning the negative and positive gate current respectively with V_G=±1.0 V, (c) & (d) The reversible electrical conductance of the OECTs channel by application of opposite polarity voltage pulses.

Referring to the above discussion, it is clear that p(g2T-TT) polymer thin-film channel-based OECTs memory devices exhibit transient long-term potentiation and depression characteristics, which were fully reversible and can be modulated by changing the ionic concentrations within the OECT channel. The post-synaptic drain current (I_D) of this device was suppressed by 98.46 % within the memory window when V_G = +1.0 V was applied at the gate terminal, with comparing to the I_D = -3 µA at V_G = 0 V. The stability of the synaptic functions in this p(g2T-TT) transistors were evaluated by stressing the devices within 7.5 minutes of constant biasing. It was observed from other similar polymer channel dimension devices that at low (0.1 V) and moderate (0.6 V) gate potentials, the synaptic strengths were stable at a longer time. However, it was reported previously that higher gate potentials result in over-oxidation of the channel; thus, polymer transistor exhibits a stretched exponential decay, which is irreversible [16, 67]. This synaptic characteristic of this electronic device is analogous to the nervous system in our brain. Figure 28 (a) shows the I_D vs. time curve of one of the best OECT memory device which was fabricated during this thesis work. A larger memory window (from I_D= -0.47 µA to -498 µA) and high channel conductance G= 5.16 mS was found from this p(g2T-TT) channel-based OECT

device with V_G= -1.0 V. Nevertheless, it was the highest channel conductance of p(g2T-TT) polymer channel-based OECT synaptic device compared to other similar devices.

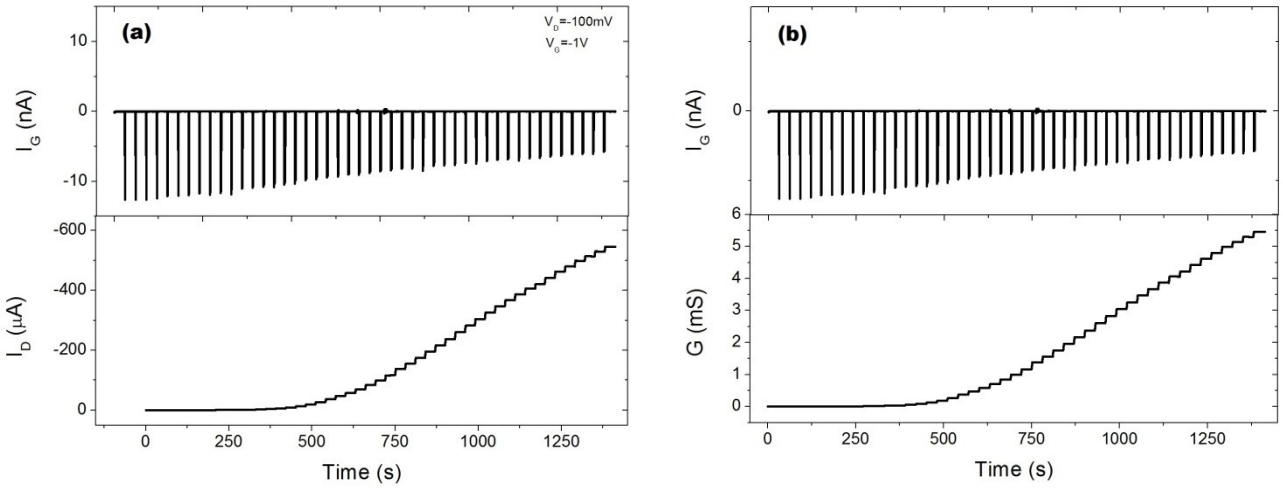

Figure 28: Long-term potentiation of p(g2T-TT) channel OECT device with active channel dimensions W×L = 2000 μA ×100 μA, d=100 nm. The gate pulse V_G= -1.0 V at Ag/AgCl floating gate electrode was applied through 0.1M NaCl liquid electrolyte. (a) I_D vs. time shows a larger memory window (from I_D= -0.47 μA to -498 μA). (b) Channel conductance G vs. measurement time.

5.3 Comparison between OECTs and Memory Device

Although, the working principle of the PEDOT:PSS thin-film channel-based OECT and p(g2T-TT) channel OECT memory device is similar, however, their neuromorphic functionalities are different. Both polymer-based OECTs channel bulk volume is electrochemically doped and de-doped by migrated ions from electrolyte due to the applied gate potentials, but their channel's conductivity tuned in different ways which individually makes both of them unique device for neuromorphic applications. However, the interaction mechanism between ions and the polymer are different due to their individual channel's polymer structure. The major difference between PEDOT:PSS channel OECT and p(g2T-TT) channel synaptic device are their ion storing capabilities, switching functionalities, swelling ability in contact with liquid, etc. That phenomenon makes a clear separation line between PEDOT:PSS channel OECTs and p(g2T-TT) channel OECTs neuromorphic memory device.

Comparison by Memory Functionalities:

It was previously discussed that the p(g2T-TT) thin-film channel-based OECTs could reproduce a phenomenon analogous with the long-term potentiation and depression which are directly correlated with its ion-storing capabilities for a more extended time. On the other hand, it was also observed in the previous section of this protocol that the PEDOT:PSS channel-based typical OECT reproduce short-term potentiation and depression since the polymer was incapable of storing the ions for a longer duration. The ion storing event or memory phenomenon of those two devices has been demonstrated below in the drain current vs. time curve. The drain current I_D vs. time plot of PEDOT:PSS channel OECT (on the top) and p(g2T-TT) thin-film channel memory device (on the bottom curve) is shown in Figure 29. In the upper red plot, the baselines drain current I_D remains on a constant level after

removing the gate potentials. The PEDOT:PSS polymer cannot store ions in the absence of external gate potentials, and hence constant baseline I_D appears. The straight baseline drain current tells that the PEDOT:PSS thin-film channel OECTs cannot store ions (actually its store very negligible number of ions) in its bulk-volume for a longer period. For that reason, PEDOT:PSS polymer thin-film channel-based OECTs are not attributed to the memory devices.

On the other hand, the baseline drain current of p(g2T-TT) channel OECTs memory device was declined step by step with the application of positive gate pulses, as shown in the bottom blue-colored plot in Figure 29. The multistep declined to drain current curve indicates that the injected cations were captured in the channel, and hence the electrical conductivity, as well as drain current of the channel, was reduced with each external gate pulses. Thus, the ion storing capabilities of this polymer channel generate a multistep drain curve. Due to the ion storing capabilities, p(g2T-TT) polymer channel-based OECT devices are attributed to the synaptic memory device.

Comparison by Information Processing and Switching Capabilities:

The red curve in Figure 29 shows that the synaptic information was lost between the pulses, which means continuous information processing and storing is not possible by using PEDOT:PSS channel OECTs. It happened because the outputs drain the current return to zero (OFF state of the device) after removing the gate pulse. This volatile property of I_D makes PEDOT:PSS channel OECTs as a bi-stable switching device. In the bottom curve, the I_D was not returned to the baseline level, which means synaptic information was not destroyed between pulses. Due to this reason, p(g2T-TT) channel OECTs memory device can perform continuous information processing and store at the same time until its saturation level. Moreover, the OECTs memory device can be used as a multistep switching device for biological applications.

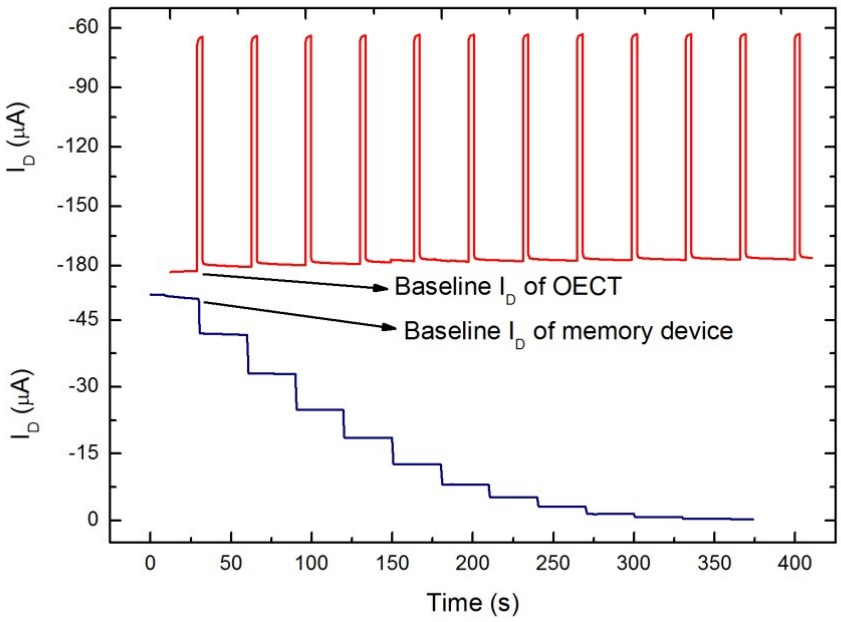

Figure 29: The drain current vs. time curves of a PEDOT:PSS channel OECT device (top red curve) with channel dimensions W×L = 1500×500 μm^2, gate voltage V_G = +0.3 V, pulse duration t_p=2 s and V_D = - 0.2 V. The bottom multistep drain current vs. time curve belongs to p(g2T-TT) channel OECT memory device with W×L = 2000×100 μm^2, V_G = +1.0 V, V_D = - 0.1 V.

Comparison by Swelling Abilities of the Channel:

The dehydrated channel of PEDOT:PSS OECTs and p(g2T-TT) memory devices can be hydrated in contact with liquid electrolyte. Both polymer's chain more or less expands in contact with a liquid solution. For that reason, polymer thin-film channel swelling phenomena appeared in OECTs that permit the penetration of ions into the polymer chain in contact with liquid electrolyte, and hence channel resistance as well as drain current changes. Figure 30 shows, the comparable swelling phenomenon of PEDOT:PSS and p(g2T-TT) thin-film polymer channel was observed through ion-transporting events into the channels without applying any gate potentials.

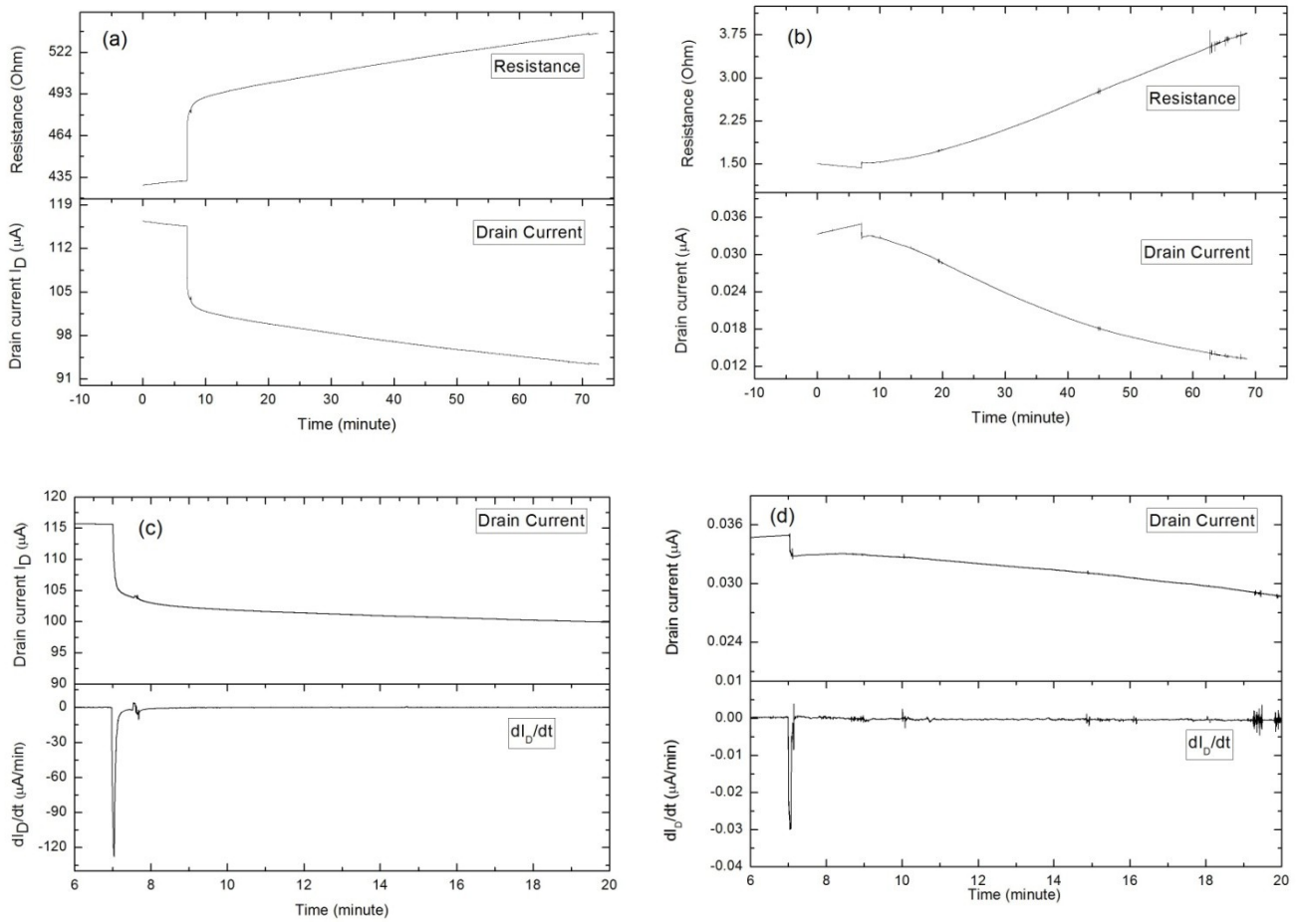

Figure 30: Swelling ability of (a) W×L=20 μm×100 μm PEDOT:PSS polymer thin-film channel and (b) W×L=200 μm×500 μm p(g2T:TT) thin-film channel OECTs. (c) & (d) Derivative drain currents of PEDOT:PSS and p(g2T-TT) channel. The channel was biased at V_D=+50 mV, V_G= 0 V, and applied liquid electrolyte was 100 mM NaCl.

Figure 30 (a) shows R_{ch} & I_D vs. measurement time of W×L=20 μm×100 μm PEDOT:PSS thin-film channel OECT with V_D=+50 mV and gate electrode was detached from the device during the entire measurement time, i.e., V_G=0 V. Initially, the drain current was measured without putting electrolyte onto the device channel, and hence resistance of the channel as well as the drain current was not remarkably changed which is reflected in the initial linear line of I_D & R_{ch}. During the continuous measurement, 100 mM NaCl liquid electrolyte was placed on the channel, and almost immediately, the channel resistance was increased, and the output drain current was dramatically decreased within a short period.

On the other hand, Figure 30 (b) shows the analysis results of W×L=200 μm×500 μm p(g2T-TT) channel OECTs memory device with similar measurement parameters, i.e., V_D=+50 mV and V_G=0 V. However, in this case, the channel resistance was also increased but in small number and a negligible amount of output drain current was decreased just after placing the electrolyte on the channel during the continuous measurement.

By comparing Figure 30 (a) and (b), it is clear that the drain current was decreased in both polymer channel contact with NaCl electrolyte. It means positive sodium ions (Na^+) was penetrated from NaCl electrolyte into the polymer chain even without applying any gate potentials. The Na^+ penetration and its barrier-less movement phenomena can be proved by electrochemical moving-front measurements, which were previously reported [102,103,104]. The presence of Na^+ in the channel results in the decrement of drain current as well as increased channel resistance (a list of Ri_{ch} before and after putting the electrolyte is given in Appendix A3). But the rate of I_D decrement was not on the same magnitude in both channels due to their different polymer structures. Figure 30 (c) and (d) represents the rate of drain current decrement in PEDOT:PSS channel was 125.7 μA/min and 0.029 μA/min for p(g2T-TT) channel memory device. The higher changing rate of output I_D in PEDOT:PSS thin-film channel was observed because of PEDOT:PSS thin-film channel composed of hydrophilic PSS chain with PEDOT segments that make it be expanded in contact with water. The hydrophobic PEDOT core region is enclosed by a hydrophilic PSS shell that is consists of loosely cross-linked polymer (Schematic picture is given in Appendix A5). In contact with liquid solutions, the loosely crosslinked polymer forms a swollen PSS network, which allows the penetration of ions into it [51]. On the other hand, p(g2T-TT) polymer also consists of the hydrophilic glycol side chain, but it does not remarkably expand as PSS does. As a consequence, PEDOT:PSS polymer thin-film channel's swelling ability is much higher than p(g2T-TT) polymer channel; on the other way around PEDOT:PSS thin film is more hydrophilic compared to p(g2T-TT) film.

5.4 Reproducibility of Memory Devices.

The reproducible memory phenomenon was investigated in OECTs memory devices. Figure 31 shows the reproducibility of four individual p(g2T-TT) channel OECTs memory devices with different channel dimensions, which were fabricated on various days. Those four memory devices were fabricated by using the same channel recipe (p(g2T-TT)), same fabrication parameters, and environment. Even same measurement parameters (V_G= -1V, V_D= -100 mV, 100 mM NaCl liquid electrolyte) were used during their all electrical characterization time. Only they were fabricated on different dates, even some of them were fabricated in two months gap from each other. In Figure 31, the memory device 1 and device 2 are two individual devices having the same polymer channel dimensions W×L=2000 μm × 100 μm, but they were fabricated on different days. Despite it, their resultant drain current and channel resistant are almost identical.

Similarly, device 3 and 4 having the same channel recipe and dimensions W×L=1000 μm × 100 μm, only they were made on separate dates. But both of them exhibit a closely similar magnitude of memory window, as shown in Figure 31 (b). Out of these four devices, a similar phenomenon happened with other fabricated devices in this thesis work. Based on these OECTs behaviors, it is easy to conclude that the memory phenomenon of p(g2T-TT) semiconductor polymer-based OECTs devices are reproducible.

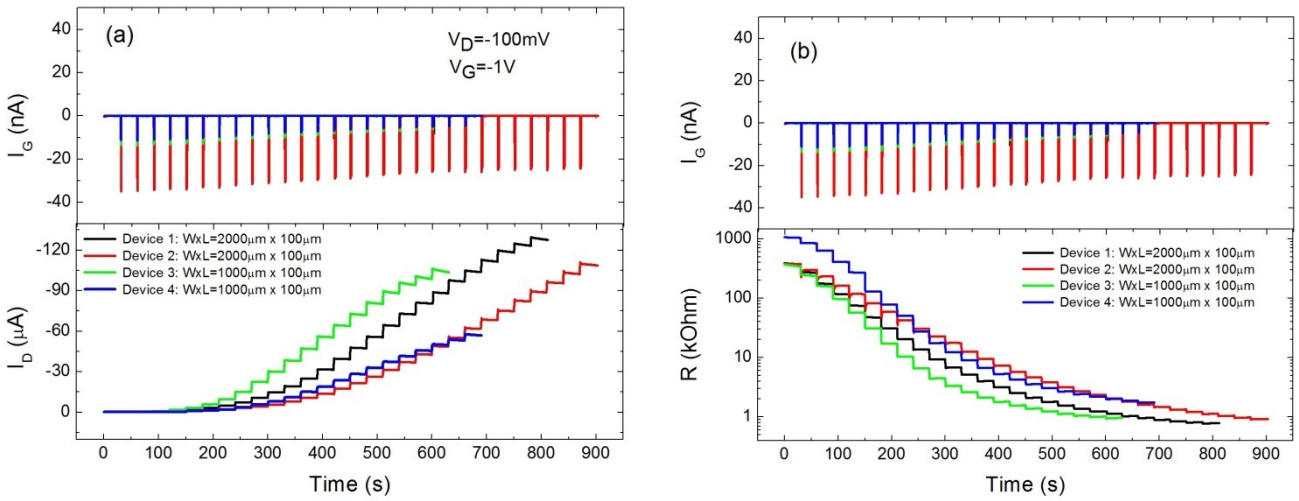

Figure 31: Reproducibility of p(g2T-TT) thin-film OECTs memory devices with individual channel dimensions. The applied channel potentials V_D= -100 mV, gate potentials V_G= -1V were applied at Ag/AgCl gate electrode through 100 mM NaCl liquid electrolyte.

5.5 Relationship between Channel Resistance and Dimensions

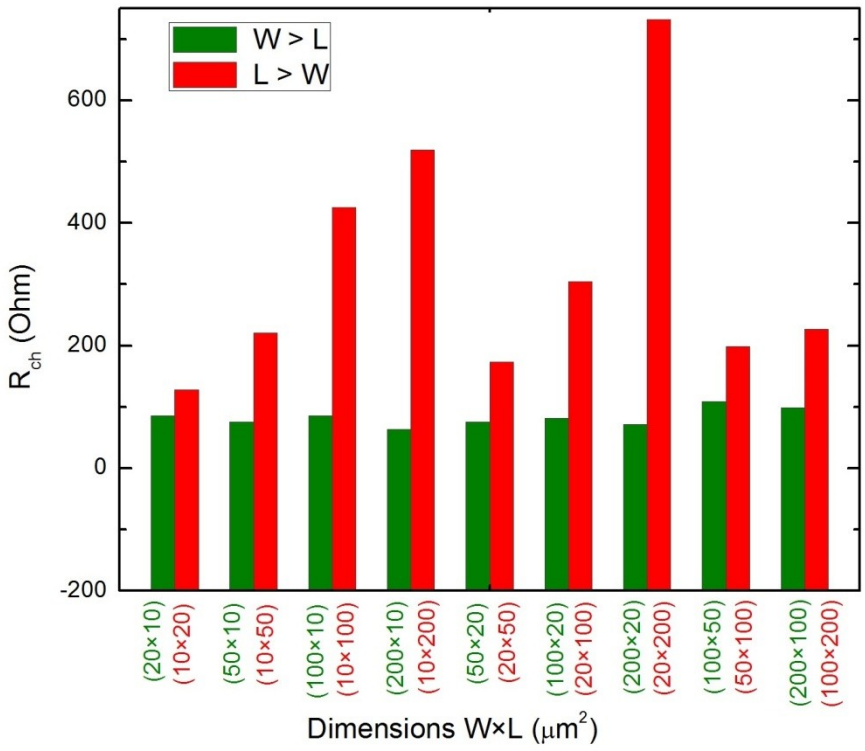

Figure 32: The channel resistance R_{ch} varies with the dimensions and their orientations on the device. All devices having PEDOT:PSS thin-film channel thickness of 100 nm. The resistances given here were measured without putting electrolytes on the device. For green color bars: W > L, for red color bars: L > W.

The channel resistance of the OECTs devices was also investigated with respect to various channel dimensions. A set of PEDOT:PSS polymer thin-film channel-based OECTs devices with individual channel dimensions were used to investigate this behavior. Figure 32 shows the channel resistance changes concerning the arrangement of individual channel dimensions. In this figure, every set of the vertical bar (pair of green and red color bar) represents the same channel dimensions of two devices, but their orientations on the device are different, i.e. $(10\times20)\mu m^2$ & $(20\times10)\mu m^2$. Their channel orientations give them different channel resistance. After a fruitful analysis of those results, it was observed that in the same set of two devices having similar channel dimensions but different orientations between the source and drain electrode, exhibit distinct channel resistances. In any set of the device, when the channel width (W) is larger than the length (L), in that case, the channel resistance (R_{ch}) become smaller compared to the device having L > W. That means R_{ch} is smaller when W > L and R_{ch} is larger when L > W.

This characteristic of the channel resistance is supported by the electrical resistivity formula given below:

$$R = \rho \frac{L}{A} \quad \text{.. 5.1}$$

Or $$R \; \alpha \; \frac{L}{A} \quad \text{.. 5.2}$$

The fabricated device channel thickness was 100 nm everywhere; thus, a uniform cross-sectional area (A) was maintained everywhere in the PEDOT:PSS channel. According to equation 5.1, longer the channel length means higher the channel resistance, which was obtained in PEDOT:PSS OECTs channel. Figure 32 shows that a larger cross-sectional area of a channel in PEDOT:PSS OECTs provides smaller channel resistance that is supported by equation 5.2. All these results tell that a comparatively wider channel provides smaller channel resistance R_{ch} and vice versa.

6. Conclusion

Typical OECTs and OECTs based neuromorphic memory devices were fabricated in this thesis work using two different polymer semiconductors as their channel materials; PEDOT:PSS and p(g2T-TT), respectively. The entire fabrication process was performed in a cleanroom-based fabrication environment. This work shows that synaptic functions of biological memory can be reproduced with a liquid electrolyte-gated organic electrochemical transistors (OECTs). And later on, neuromorphic functionalities of those devices were studied throughout the conventional laboratory-based electrical characterization techniques.

In this work, it has been demonstrated that the OECTs channel made of bio-compatible PEDOT:PSS polymer exhibits a high channel conductance with low operating voltages. That property makes PEDOT:PSS channel OECTs device suitable as a biological signal amplifier with low input voltages. Beside it, this polymer channel OECTs demonstrate volatile post-synaptic drain current, which can be temporarily increased or decreased by applying selected pre-synaptic gate stimuli. Due to this reason, this device unfolds volatile post-synaptic functionalities including short-term depression and short-term potentiation, which are analogous with the biological synaptic systems. In this PEDOT:PSS OECTs device, the information cannot be processed into the long-term states, because the information was lost between the gate pulses which is attributed to its inability to store the ions in the channel, and hence PEDOT:PSS polymer thin-film channel-based OECTs are a non-memory device. The channel's conductance can be modulated only in the bi-stable way, on the other way around ON and OFF modulation. This phenomenon makes it suitable as a reversible electrochemical switching device, although its switching speed is slower compared to its semiconductor counterparts.

On the other hand, the present work also demonstrated that the biological synaptic features could be reproduced in p(g2T-TT) polymer channel based OECT memory device. During this work, non-volatile drain current responses and multiple discrete memory states were reproduced in p(g2T-TT) channel OECTs device. The ion-capturing capabilities of the channel make it as a memory device. The channel conductance was modulated and demodulated by capturing and releasing the ions in multiple steps. For that reason, p(g2T-TT) channel OECTs has been displayed reversible memory phenomena in this work. On the other way around, the post-synaptic weight was tuned in several steps. The multistage tuning provides steep threshold switching behavior of this memory device. Beside it, this work also demonstrated that the entire modulation of channel conductance occurred within a low operating gate voltage that is an excellent hallmark of low power consumption neuromorphic memory devices. Due to the reversible ion storing abilities, p(g2T-TT) channel OECTs exhibits long-term potentiation and long-term depression, which are analogous to the neuromorphic system. This work also represents that memory phenomena of this device were reproducible over time. But the stability of the memory window was not well satisfactory due to the ion loss from the channel. The stability of the memory window could be improved by applying a blocking and tunneling dielectric layers in between channel and electrolyte, respectively [1]. Thus, the injected ions may stay on the channel for an extended period, which would provide longer memory stability.

In conclusion, this thesis work showed that the integration of electronic and biological memory is possible that can be realized with OECTs. Moreover, it showed that the neuro-inspired synaptic functions could be generated with typical OECTs and OECTs memory device, which can lead the way of development of the neuro-inspired computational platforms. The tunable-memory features of this device meet the expectations to build the artificial neuromorphic information processing circuits. This

work also demonstrated that information processing and storing can be performed at the same time by using p(g2T-TT) thin-film channel-based OECT memory devices that can create platforms suitable for non-von Neumann computer architecture. Those results may open a new emerging ground of organic-based neuromorphic computational engineering systems.

Appendix

Additional Data:

A 1:
Comparison of transconductance of various transistors [101].

Active material	Dielectric material	W (μm)	L (μm)	$\|V_G\|$ (V)	$\|V_D\|$ (V)	g_m (μS)	g_m/W ($S\,m^{-1}$)	$g_m/\|V_D\|$ ($\mu S\,V^{-1}$)
Aqueous electrolyte								
PEDOT:PSS (best)	NaCl	10	10	0.2	0.6	4,020	402	6,700
PEDOT:PSS (typical)	NaCl	10	5	0.275	0.6	2,700	270	4,500
Graphene	PBS + NaCl	40	20	0.25	0.1	420	11	4,200
Diamond	PBS + KCl (*in vitro*)	~20	~5–20	0.22	0.2	18	0.9	90
Silicon	SiO_2/TiO_2 (*in toto*)	20	20	0.25	0.25	15	0.75	60
Silicon NW	SiO_2, PBS	20	2	~0.4	0.03	5	0.25	167
Ionic liquid/gel, solid electrolyte								
ZnO	IL (DEME/TFSI)	200	500	1.2	0.1	160	0.8	1,600
ZnO NW	Solid electrolyte ($PVA/LiClO_4$)	0.018	0.94	~1.5	0.5	2.79	155	5.58
Organic semiconductor: P3HT	IL (EMIM/TFSI) gel (PS-PEO-PS)	100	20	~4	1	50	0.5	50
Solid-state								
ZnO	Al_2O_3	50	1	5.1	4	1,400	28	350
Graphene	SiO_2 (BG); Y_2O_3 (TG)	2.7	0.31	~1.2	2	1,863	690	932
III–V NW: n-InAs NW	SiN_x	0.05	2	0.56	1	97.5	1,950	98
III–V Bulk: GaN/InAlN	SiN_x	NR	0.06	1.75	2	NR*	1,105	NR
Carbon nanotube (mat)	HfO_2	10	1.5	~1	0.5	50	5	100
Organic semiconductor: DNTT	AlO_x/SAM	10	1	~2	2	12	1.2	95
Silicon NW	SiO_2	0.01	0.8–2	~2–4	NR	2	200	NR

Abbreviations: BG, bottom gate; NR, not reported; TG, top gate; NW, nanowire; PBS, phosphate buffered saline; SAM, self-assembled monolayer.
When BG/TG are both listed the device is operated in the dual gate configuration, and the applied gate voltage listed is the larger of the two. For this statement to hold, the changes described in the table regarding reference citations needs to be returned to the format of the as-submitted table.
*The GaN/InAlN device shown here shows the highest g_m/W, but the paper does not report W, and therefore g_m cannot be calculated. It should be noted that III–V bulk devices with channel widths of 10–100 μm can achieve g_m values of 30–50 mS .

A 2:
Various thickness of PEDOT:PSS thin-film polymer can be achieved using distinct RPM of spin-coater.

Nr.	Coating time in sec	Acceleration	Soft backing at 110 C in min	Hard baking at 140 C in min	RPM	Thin-film thickness In nm
1	30 sec	1000	1 min	60 min	200	701
2	30 sec	1000	1 min	60 min	500	283
3	30 sec	1000	1 min	60 min	650	223
4	30 sec	1000	1 min	60 min	1000	167
5	30 sec	1000	1 min	60 min	1500	116
6	30 sec	1000	1 min	60 min	1700	62
7	30 sec	1000	1 min	60 min	2000	53
8	30 sec	1000	1 min	60 min	3000	66
9	30 sec	1000	1 min	60 min	4000	53
10	30 sec	1000	1 min	60 min	5000	54

A 3:
The relationship between channel dimensions and resistance of PEDOT:PSS polymer channel.

Channel Dimensions W×L in μm^2	Channel Resistance in Ω	
	Without electrolyte on channel	After putting the electrolyte
10×20	127.6	140.9
20×10	85.4	89.5
10×50	221.2	244.9
50×10	75.7	77.0
10×100	426.0	445.0
100×10	85.5	85.9
10×200	519.0	545.0
200×10	63.4	63.3
20×50	173.6	192.4
50×20	76.0	78.9
20×100	304.3	322.0
100×20	81.3	82.0
20×200	732.0	774.0
200×20	71.9	72.9
50×100	198.7	203.9
100×50	108.7	110.5
100×200	227.1	131.5
200×100	98.7	97.4
10×10	115.0	123.0
20×20	92.6	108.0
50×50	114.0	119.8
100×100	163.3	163.7
200×200	179.2	177.5

A 4:
The surface profile of a scratched thin film. The step height difference is the film thickness.

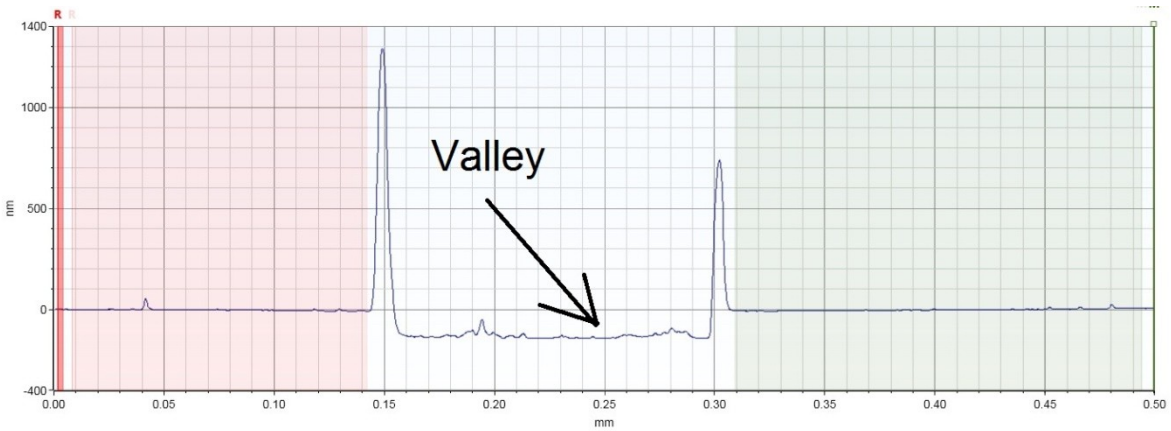

A 5:
Structure model of PEDOT:PSS micelle in where hydrophilic PEDOT polymer core is surrounded by hydrophobic PSS shell [51].

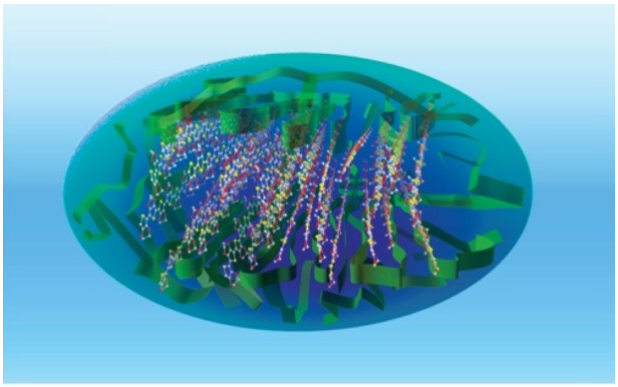

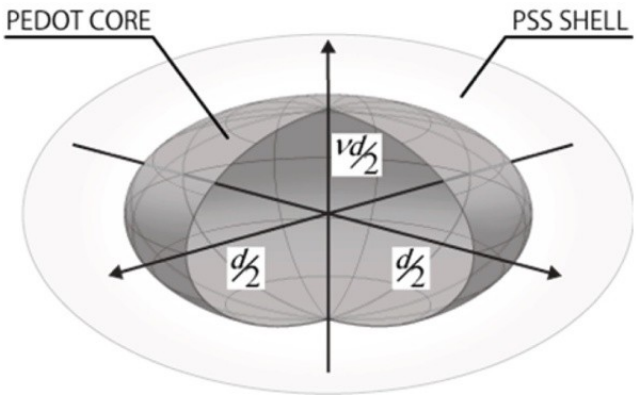

A 6:
Switching mechanisms and the materials used in organic neuromorphic devices [2].

Principle	Material / electrolyte	Number of states / tuning[a]	Memory mechanism	State retention[b] / demonstrated cycles[c]	Reference
Electrochemical doping	poly(3-methyl thiophene) / poly(ethylene oxide-propylene oxide) + $LiClO_4$	4 / continuous	Counter-redox reaction + separation read/write	~hours / -	
	PANI / PEO	>2	Slow kinetics	- / 10^4	
	MEH-PPV / $RbAg_4I_5$	8 / continuous	Diffusion disparity	~20 ms for STP and >240 h for LTP / -	
	PQT / PEO + $EV(ClO_4)_2$	2	Counter-redox reaction + separation read/write	14 h[d] / > 100	
	PEDOT:PSS / NaCl	>2	Slow kinetics	<1 s / -	
	PEDOT:PTHF / NaCl	Continuous	Slow kinetics + structural rearrangement of the polymer	<1 s / -	
	BTPA-F / PEO + $EV(ClO_4)_2$	Continuous	Counter-redox reaction	~seconds / -	
	P3HT / P(VDF-HFP) P3HT / P(VDF-TrFE)	>2	Slow kinetics	<10 s / -	
	P3HT / PEO	Continuous	Slow kinetics	<5 s / 60	
	PEDOT:PSS / NaCl PEDOT:PSS / Nafion	512 / continuous	Counter-redox reaction + separation read/write	100 s / >15	
Charge trapping	Pentacene (Au)	Continuous	Charge trapping nanoparticles	24 h / 800	
	DNTT (Al)	Continuous	Charge trapping nanosheet	~1 s / -	
Ion migration	Ti/PEDOT:PSS/TiAg/PEDOT:PSS/Ta	Continuous	Compound formation	~seconds / -	
Light-assisted reaction	P3HT / diarylethene	256	Energy level modification	>500 days / 70	

List of abbreviation and symbols

OECTs	Organic Electrochemical Transistors.
PEDOT:PSS	Poly(3,4-ethylenedioxythiophene):poly(styrenesulfonate).
p(g2T-TT)	Poly(2-(3,3´-bis(2-(2-(2-methoxyethoxy)ethoxy)ethoxy)-[2,2´-bithiophen]-5-yl)thieno[3,2-b]thiophene).
EDOT	3,4-ethylenedioxythiophene
(2T-TT)	Bithiophene-thienothiophene
FET	Field Effect Transistor
CMOS	Complementary Metal Oxide Semiconductor
EG	Ethylene Glycol
STDP	Spike-Time-Dependent Plasticity
STP	Short-term Potentiation
LTP	Long-term Potentiation
STD	Short-term Depression
LTD	Long-term Depression
AA	Ascorbic Acid
DA	Dopamine
PSA	Prostate Specific Antigen
DNA	Deoxyribonucleic Acid
RNA	Ribonucleic Acid
RIE	Reactive-Ion Etching
DRIE	Deep Reactive Ion Etching
ICP	Inductively Coupled Plasma
RF	Radio Frequency
UV	Ultraviolet
DIW	Deionized water
TMAH	Tetramethylammonium hydroxide
Pa - C	Parylene –C
DBSA	Dodecyl Benzene Sulfonic Acid
GOPS	3-GlycidylOxyPropyl – trimethoxySilane
PDMS	Poly-dimethyl-siloxane
V_G	Gate voltage
V_D	Drain voltage
I_D	Drain current
W	Channel width
L	Channel length
d	Thickness
t_p	Pulse width
Δt	Time interval between pulses
T_P	Period of pulse
g_m	Mutual transconductance
I_{post}	Post-synaptic current
ω	Angular spinning speed
ρ	Solvent density
η	Solvent viscosity
e_r	Rate of evaporation

List of Figures

List of Tables

List of Materials used for OECTs & Memory Device Fabrication.

- Substrate: Microscope glass slides (VWR)
- Photoresist: Microposit S1813 Photoresist (DOW)
- Developer: AZ 9260 Microchemicals (Cipec Spécialités)
- Developer : MF26A
- Insulator: Parylene –C (SCS coatings)
- Polymer 1: PEDOT PSS (Clevios)
- Polymer 2: p(g2T-TT)
- Alcohol: Ethylene Glycol (Sigma Aldrich)
- Organic Acid: Dodecylbenzene sulfonic acid (DBSA) (Sigma Aldrich)
- Silane : 3-glycidoxypropyltrimethoxysilne (GOPS) (Sigma Aldrich)
- SOAP: MICRO-90(Sigma Aldrich)
- Solvent: Aceton
- Solvent: IPA
- Metal: Chromium
- Metal: Gold

Bibliography

[1] Sun, Jia; Fu, Ying; Wan, Qing (2018): Organic synaptic devices for neuromorphic systems. In *J. Phys. D: Appl. Phys.* 51 (31), p. 314004. DOI: 10.1088/1361-6463/aacd99.

[2] van de Burgt, Yoeri; Melianas, Armantas; Keene, Scott Tom; Malliaras, George; Salleo, Alberto (2018): Organic electronics for neuromorphic computing. In *Nat Electron* 1 (7), pp. 386–397. DOI: 10.1038/s41928- 018-0103-3.

[3] Rivnay, Jonathan; Inal, Sahika; Salleo, Alberto; Owens, Róisín M.; Berggren, Magnus; Malliaras, George G. (2018): Organic electrochemical transistors. In *Nat Rev Mater* 3 (2), p. 99. DOI: 10.1038/natrevmats.2017.86.

[4] Gkoupidenis, Paschalis; Rezaei-Mazinani, Shahab; Proctor, Christopher M.; Ismailova, Esma; Malliaras, George G. (2016): Orientation selectivity with organic photodetectors and an organic electrochemical transistor. In *AIP Advances* 6 (11), p. 111307. DOI: 10.1063/1.4967947.

[5] Gkoupidenis, Paschalis; Schaefer, Nathan; Strakosas, Xenofon; Fairfield, Jessamyn A.; Malliaras, George G. (2015): Synaptic plasticity functions in an organic electrochemical transistor. In *Appl. Phys. Lett.* 107 (26), p. 263302. DOI: 10.1063/1.4938553.

[6] Gkoupidenis, Paschalis; Koutsouras, Dimitrios A.; Malliaras, George G. (2017): Neuromorphic device architectures with global connectivity through electrolyte gating. In *Nature communications* 8, p. 15448. DOI: 10.1038/ncomms15448.

[7] Gkoupidenis, Paschalis; Koutsouras, Dimitrios A.; Lonjaret, Thomas; Fairfield, Jessamyn A.; Malliaras, George G. (2016): Orientation selectivity in a multi-gated organic electrochemical transistor. In *Scientific reports* 6, p. 27007. DOI: 10.1038/srep27007.

[8] Gkoupidenis, Paschalis; Schaefer, Nathan; Garlan, Benjamin; Malliaras, George G. (2015): Neuromorphic Functions in PEDOT:PSS Organic Electrochemical Transistors. In *Advanced materials (Deerfield Beach, Fla.)* 27 (44), pp. 7176–7180. DOI: 10.1002/adma.201503674.

[9] Koutsouras, Dimitrios A.; Malliaras, George G.; Gkoupidenis, Paschalis (2018): Emulating homeoplasticity phenomena with organic electrochemical devices. In *MRC* 8 (02), pp. 493–497. DOI: 10.1557/mrc.2018.53.

[10] Koutsouras, Dimitrios A.; Bihar, Eloïse; Fairfield, Jessamyn A.; Saadaoui, Mohamed; Malliaras, George G.: Fabrication Approaches for Conducting Polymer Devices. In (Book) Green Materials for Electronics. ISBN: 9783527692958. Wiley-VCH Verlag GmbH & Co. KGaA. ch2. pp. 55-69. DOI: 10.1002/9783527692958.

[11] Gualandi, I.; Marzocchi, M.; Achilli, A.; Cavedale, D.; Bonfiglio, A.; Fraboni, B. (2016): Textile Organic Electrochemical Transistors as a Platform for Wearable Biosensors. In *Scientific reports* 6, p. 33637. DOI: 10.1038/srep33637.

[12] Hall, David B.; Underhill, Patrick; Torkelson, John M. (1998): Spin coating of thin and ultrathin polymer films. In *Polym. Eng. Sci.* 38 (12), pp. 2039–2045. DOI: 10.1002/pen.10373.

[13] Zhang, Fengjiao; Di, Chong-an; Berdunov, Nikolai; Hu, Yuanyuan; Hu, Yunbin; Gao, Xike et al. (2013): Ultrathin film organic transistors: Precise control of semiconductor thickness via spin-coating. In *Advanced materials (Deerfield Beach, Fla.)* 25 (10), pp. 1401–1407. DOI: 10.1002/adma.201204075.

[14] Meng, Ellis; Li, Po-Ying; Tai, Yu-Chong (2008): Plasma removal of Parylene C. In *J. Micromech. Microeng.* 18 (4), p. 45004. DOI: 10.1088/0960-1317/18/4/045004.

[15] Lingstedt, Leona V.; Ghittorelli, Matteo; Lu, Hao; Koutsouras, Dimitrios A.; Marszalek, Tomasz; Torricelli, Fabrizio et al.

(2019): Effect of DMSO Solvent Treatments on the Performance of PEDOT. PSS Based Organic Electrochemical Transistors. In *Adv. Electron. Mater.* 26, p. 1800804. DOI: 10.1002/aelm.201800804.

[16] Giovannitti, Alexander; Sbircea, Dan-Tiberiu; Inal, Sahika; Nielsen, Christian B.; Bandiello, Enrico; Hanifi, David A. et al. (2016): Controlling the mode of operation of organic transistors through side-chain engineering. In *Proceedings of the National Academy of Sciences of the United States of America* 113 (43), pp. 12017–12022. DOI: 10.1073/pnas.1608780113.

[17] Venkatraman, Vishak; Friedlein, Jacob T.; Giovannitti, Alexander; Maria, Iuliana P.; McCulloch, Iain; McLeod, Robert R.; Rivnay, Jonathan (2018): Subthreshold Operation of Organic Electrochemical Transistors for Biosignal Amplification. In *Advanced science (Weinheim, Baden-Wurttemberg, Germany)* 5 (8), p. 1800453. DOI: 10.1002/advs.201800453.

[18] Havener, R., Boyea, J., Malone, E., Bernards, D., DeFranco, J., Malliaras, G., & Lipson, H. (2007, August). Freeform fabrication of organic electrochemical transistors. In *Proceedings of the 18th Solid Freeform Fabrication Symposium* (pp. 60-73).

[19] Inal, Sahika; Malliaras, George G.; Rivnay, Jonathan (2017): Benchmarking organic mixed conductors for transistors. In *Nature communications* 8 (1), p. 1767. DOI: 10.1038/s41467-017-01812-w.

[20] Piro, Benoît; Mattana, Giorgio; Zrig, Samia; Anquetin, Guillaume; Battaglini, Nicolas; Capitao, Dany et al. (2018): Fabrication and Use of Organic Electrochemical Transistors for Sensing of Metabolites in Aqueous Media. In *Applied Sciences* 8 (6), p. 928. DOI: 10.3390/app8060928.

[21] Franssila, S. and Sainiemi, L., 2015. Reactive Ion Etching (RIE). In *Encyclopedia of Microfluidics and Nanofluidics*, pp.2911-2921.

[22] Mengi, E.; Tai, Yu-Chong (2005): Parylene Etching Techniques for Microfluidics and Miomems. In 18th IEEE International Conference on Micro Electro Mechanical Systems technical digest, pp. 568–571. DOI: 10.1109/MEMSYS.2005.1453993

[23] Friedlein, Jacob T.; Shaheen, Sean E.; Malliaras, George G.; McLeod, Robert R. (2015): Optical Measurements Revealing Nonuniform Hole Mobility in Organic Electrochemical Transistors. In *Adv. Electron. Mater.* 1 (11), p. 1500189. DOI: 10.1002/aelm.201500189.

[24] Koutsouras, Dimitrios A.; Hama, Adel; Pas, Jolien; Gkoupidenis, Paschalis; Hivert, Bruno; Faivre-Sarrailh, Catherine et al. (2017): PEDOT. PSS microelectrode arrays for hippocampal cell culture electrophysiological recordings. In *MRC* 7 (2), pp. 259–265. DOI: 10.1557/mrc.2017.34.

[25] Wang, Chenxi; Suga, Tadatomo (2012): Investigation of fluorine containing plasma activation for room-temperature bonding of Si-based materials. In *Microelectronics Reliability* 52 (2), pp. 347–351. DOI: 10.1016/j.microrel.2011.09.005.

[26] Friedlein, Jacob T.; Shaheen, Sean E.; Malliaras, George G.; McLeod, Robert R. (2015): Optical Measurements Revealing Nonuniform Hole Mobility in Organic Electrochemical Transistors. In *Adv. Electron. Mater.* 1 (11), p. 1500189. DOI: 10.1002/aelm.201500189.

[27] Engel, Sabrina; Spitzer, Daniel; Rodrigues, Leona Lucas; Fritz, Eva-Corinna; Straßburger, David; Schönhoff, Monika et al. (2017): Kinetic control in the temperature-dependent sequential growth of surface-confined supramolecular copolymers. In *Faraday discussions* 204, pp. 53–67. DOI: 10.1039/c7fd00100b.

[28] van Doremaele, Eveline R. W.; Gkoupidenis, Paschalis; van de Burgt, Yoeri (2019): Towards organic neuromorphic devices for adaptive sensing and novel computing paradigms in bioelectronics. In *J. Mater. Chem. C* 16, p. 414. DOI: 10.1039/C9TC03247A.

[29] Backus, John (2007): Can programming be liberated from the von Neumann style?: A functional style and its algebra of programs. In : ACM Turing Award Lectures. New York: Association of Computing Machinery, p. 1977. DOI: 10.1145/1283920.1283933

[30] https://www.welove.ai/en/blog/post/neuromorphic-chips-moores-law.html

[31] https://en.wikipedia.org/wiki/Neuromorphic_engineering

[32] Lee, Myoung-Jae; Park, Gyeong-Su; Seo, David H.; Kwon, Sung Min; Lee, Hyeon-Jun; Kim, June-Seo et al. (2018): Reliable Multivalued Conductance States in TaO x Memristors through Oxygen Plasma-Assisted Electrode Deposition with in Situ-Biased Conductance State Transmission Electron Microscopy Analysis. In *ACS applied materials & interfaces* 10 (35), pp. 29757–29765. DOI: 10.1021/acsami.8b09046. Image courtesy: DGIST (Daegu Gyeongbuk Institute of Science and Technology)

[33] Kergoat, Loïg; Piro, Benoît; Berggren, Magnus; Horowitz, Gilles; Pham, Minh-Chau (2012): Advances in organic transistor-based biosensors. From organic electrochemical transistors to electrolyte-gated organic field-effect transistors. In *Analytical and bioanalytical chemistry* 402 (5), pp. 1813–1826. DOI: 10.1007/s00216-011-5363-y.

[34] https://www.corial.com/en/technologies/reactive-ion-etching-rie/

[35] Vitoratos, E., Sakkopoulos, S., Dalas, E., Paliatsas, N., Karageorgopoulos, D., Petraki, F., Kennou, S. and Choulis, S.A. (2009): Thermal degradation mechanisms of PEDOT. PSS. In *Organic Electronics* 10 (1), pp. 61–66. DOI: 10.1016/j.orgel.2008.10.008.

[36] Zeglio, Erica; Inganäs, Olle (2018): Active Materials for Organic Electrochemical Transistors. In *Advanced materials (Deerfield Beach, Fla.)* 30 (44), e1800941. DOI: 10.1002/adma.201800941.

[37] Kim, Youngseok; Lim, Taekyung; Kim, Chi-Hyeong; Yeo, Chang Su; Seo, Keumyoung; Kim, Seong-Min et al. (2018): Organic electrochemical transistor-based channel dimension-independent single-strand wearable sweat sensors. In *NPG Asia Mater* 10 (11), pp. 1086–1095. DOI: 10.1038/s41427-018-0097-3.
[38] Bai, Liming; Elósegui, Cristina García; Li, Weiqi; Yu, Ping; Fei, Junjie; Mao, Lanqun (2019): Biological Applications of Organic Electrochemical Transistors. Electrochemical Biosensors and Electrophysiology Recording. In *Frontiers in chemistry* 7, p. 313. DOI: 10.3389/fchem.2019.00313.
[39] White, Henry S.; Kittlesen, Gregg P.; Wrighton, Mark S. (1984): Chemical derivatization of an array of three gold microelectrodes with polypyrrole. Fabrication of a molecule-based transistor. In *J. Am. Chem. Soc.* 106 (18), pp. 5375–5377. DOI: 10.1021/ja00330a070.
[40] Zhu, Zheng-Tao; Mabeck, Jeffrey T.; Zhu, Changcheng; Cady, Nathaniel C.; Batt, Carl A.; Malliaras, George G. (2004): A simple poly(3,4-ethylene dioxythiophene)/poly(styrene sulfonic acid) transistor for glucose sensing at neutral pH. In *Chemical communications (Cambridge, England)* (13), pp. 1556–1557. DOI: 10.1039/b403327m.
[41] Paul, Elizabeth W.; Ricco, Antonio J.; Wrighton, Mark S. (1985): Resistance of polyaniline films as a function of electrochemical potential and the fabrication of polyaniline-based microelectronic devices. In *J. Phys. Chem.* 89 (8), pp. 1441–1447. DOI: 10.1021/j100254a028.
[42] Bartlett, P. N.; Birkin, P. R. (2002): A Microelectrochemical Enzyme Transistor Responsive to Glucose. In *Anal. Chem.* 66 (9), pp. 1552–1559. DOI: 10.1021/ac00081a031.
[43] Nilsson, D., Chen, M., Kugler, T., Remonen, T., Armgarth, M. and Berggren, M., 2002. Bi-stable and dynamic current modulation in electrochemical organic transistors. *Advanced Materials*, *14*(1), pp.51-54.
[44] Epstein, A.J., Hsu, F.C., Chiou, N.R. and Prigodin, V.N., 2002. Electric-field induced ion-leveraged metal–insulator transition in conducting polymer-based field effect devices. *Current Applied Physics*, *2*(4), pp.339-343.
[45] Malti, Abdellah; Edberg, Jesper; Granberg, Hjalmar; Khan, Zia Ullah; Andreasen, Jens W.; Liu, Xianjie et al. (2016): An Organic Mixed Ion-Electron Conductor for Power Electronics. In *Advanced science (Weinheim, Baden-Wurttemberg, Germany)* 3 (2), p. 1500305. DOI: 10.1002/advs.201500305.
[46] Bartlett, P. N. (1998): Measurement of low glucose concentrations using a microelectrochemical enzyme transistor. In *Analyst* 123 (2), pp. 387–392. DOI: 10.1039/a706296f.
[47] Bartlett, P. N.; Birkin, P. R.; Wang, J. H.; Palmisano, F.; Benedetto, G. de (1998): An Enzyme Switch Employing Direct Electrochemical Communication between Horseradish Peroxidase and a Poly(aniline) Film. In *Anal. Chem.* 70 (17), pp. 3685–3694. DOI: 10.1021/ac971088a.
[48] Wei, Qingshuo; Mukaida, Masakazu; Naitoh, Yasuhisa; Ishida, Takao (2013): Morphological change and mobility enhancement in PEDOT:PSS by adding co-solvents. In *Advanced materials (Deerfield Beach, Fla.)* 25 (20), pp. 2831–2836. DOI: 10.1002/adma.201205158.
[49] Greczynski, G.; Kugler, Th; Keil, M.; Osikowicz, W.; Fahlman, M.; Salaneck, W.R (2001): Photoelectron spectroscopy of thin films of PEDOT–PSS conjugated polymer blend. A mini-review and some new results. In *Journal of Electron Spectroscopy and Related Phenomena* 121 (1-3), pp. 1–17. DOI: 10.1016/S0368-2048(01)00323-1.
[50] Alemu, Desalegn; Wei, Hung-Yu; Ho, Kuo-Chuan; Chu, Chih-Wei (2012): Highly conductive PEDOT. PSS electrode by simple film treatment with methanol for ITO-free polymer solar cells. In *Energy Environ. Sci.* 5 (11), p. 9662. DOI: 10.1039/c2ee22595f.
[51] Takano, Takumi; Masunaga, Hiroyasu; Fujiwara, Akihiko; Okuzaki, Hidenori; Sasaki, Takahiko (2012): PEDOT Nanocrystal in Highly Conductive PEDOT. PSS Polymer Films. In *Macromolecules* 45 (9), pp. 3859–3865. DOI: 10.1021/ma300120g.
[52] Elschner, A., Kirchmeyer, S., Lövenich, W., Merker, U. & Reuter, K. in PEDOT, Principles and Applications of an Intrinsically Conductive Polymer. Pp: 113–166 (CRC Press, 2010).
[53] Peper, Ferdinand (2017): The End of Moore's Law. Opportunities for Natural Computing? In *New Gener. Comput.* 35 (3), pp. 253–269. DOI: 10.1007/s00354-017-0020-4.
[54] Kim, J. Y.; Jung, J. H.; Lee, D. E.; Joo, J. (2002): Enhancement of electrical conductivity of poly(3,4-ethylenedioxythiophene)/poly(4-styrenesulfonate) by a change of solvents. In *Synthetic Metals* 126 (2-3), pp. 311–316. DOI: 10.1016/S0379-6779(01)00576-8.
[55] Ashizawa, S.; Horikawa, R.; Okuzaki, H. (2005): Effects of solvent on carrier transport in poly(3,4-ethylenedioxythiophene)/poly(4-styrenesulfonate). In *Synthetic Metals* 153 (1-3), pp. 5–8. DOI: 10.1016/j.synthmet.2005.07.214.
[56] Proctor, Christopher M.; Rivnay, Jonathan; Malliaras, George G. (2016): Understanding volumetric capacitance in conducting polymers. In *J. Polym. Sci. Part B: Polym. Phys.* 54 (15), pp. 1433–1436. DOI: 10.1002/polb.24038.
[57] Choi, WooSeok; An,Taechang; Lim, Geunbae (2011): Organic electrochemical transistors based on a dielectrophoretically aligned nanowire array. In *Nanoscale Research Letters* 6(1), p.339.DOI: 10.1186/1556-276X-6-339.
[58] ElMahmoudy, Mohammed; Inal, Sahika; Charrier, Anne; Uguz, Ilke; Malliaras, George G.; Sanaur, Sébastien (2017): Tailoring the Electrochemical and Mechanical Properties of PEDOT. PSS Films for Bioelectronics. In *Macromol. Mater.*

Eng. 302 (5), p. 1600497. DOI: 10.1002/mame.201600497.
[59] Kim, D.-H. et al. in Indwelling Neural Implants: Strategies for Contending with the In-Vivo Environment (ed. Reichert, W. M.) 165–207 (CRC Press/Taylor & Francis, 2008).
[60] Impey, R. W.; Madden, P. A.; McDonald, I. R. (1983): Hydration and mobility of ions in solution. In *J. Phys. Chem.* 87 (25), pp. 5071–5083. DOI: 10.1021/j150643a008.
[61] Friedlein, Jacob T.; Rivnay, Jonathan; Dunlap, David H.; McCulloch, Iain; Shaheen, Sean E.; McLeod, Robert R.; Malliaras, George G. (2017): Influence of disorder on transfer characteristics of organic electrochemical transistors. In *Appl. Phys. Lett.* 111 (2), p. 23301. DOI: 10.1063/1.4993776.
[62] Thiburce, Quentin; Giovannitti, Alexander; McCulloch, Iain; Campbell, Alasdair J. (2019): Nanoscale Ion-Doped Polymer Transistors. In *Nano letters* 19 (3), pp. 1712–1718. DOI: 10.1021/acs.nanolett.8b04717.
[63] Nielsen, Christian B.; Giovannitti, Alexander; Sbircea, Dan-Tiberiu; Bandiello, Enrico; Niazi, Muhammad R.; Hanifi, David A. et al. (2016): Molecular Design of Semiconducting Polymers for High-Performance Organic Electrochemical Transistors. In *Journal of the American Chemical Society* 138 (32), pp. 10252–10259. DOI: 10.1021/jacs.6b05280.
[64] McCulloch, Iain; Heeney, Martin; Bailey, Clare; Genevicius, Kristijonas; MacDonald, Iain; Shkunov, Maxim et al. (2006): Liquid-crystalline semiconducting polymers with high charge-carrier mobility. In *Nature Materials* 5 (4), pp. 328–333. DOI: 10.1038/nmat1612.
[65] Piro, Benoît; Mattana, Giorgio; Zrig, Samia; Anquetin, Guillaume; Battaglini, Nicolas; Capitao, Dany et al. (2018): Fabrication and Use of Organic Electrochemical Transistors for Sensing of Metabolites in Aqueous Media. In *Applied Sciences* 8 (6), p. 928. DOI: 10.3390/app8060928.
[66] Vurro, Vito (2017): Organic Electrochemical Transistor: A Tool for Cell Tissue Monitoring. In Master Thesis Protocol, Università di Bologna, Corso di Studio in Fisica, https://amslaurea.unibo.it/13502/
[67] Gerasimov, Jennifer Y.; Gabrielsson, Roger; Forchheimer, Robert; Stavrinidou, Eleni; Simon, Daniel T.; Berggren, Magnus; Fabiano, Simone (2019): An Evolvable Organic Electrochemical Transistor for Neuromorphic Applications. In *Advanced science (Weinheim, Baden-Wurttemberg, Germany)* 6 (7), p. 1801339. DOI: 10.1002/advs.201801339.
[68] Bernards, D. A.; Malliaras, G. G. (2007): Steady-State and Transient Behavior of Organic Electrochemical Transistors. In *Adv. Funct. Mater.* 17 (17), pp. 3538–3544. DOI: 10.1002/adfm.200601239.
[69] Snook, Graeme A.; Kao, Pon; Best, Adam S. (2011): Conducting-polymer-based supercapacitor devices and electrodes. In *Journal of Power Sources* 196 (1), pp. 1–12. DOI: 10.1016/j.jpowsour.2010.06.084.
[70] Koch, C., 2004. *Biophysics of computation: information processing in single neurons*. Oxford university press. ISBN: 978-0-19-510491-2
[71] Aikens, D. A. (1983): Electrochemical methods, fundamentals and applications. In *J. Chem. Educ.* 60 (1), A25. DOI: 10.1021/ed060pA25.1.
[72] Wu, Fei; Yu, Ping; Mao, Lanqun (2017): Self-powered electrochemical systems as neurochemical sensors. Toward self-triggered in vivo analysis of brain chemistry. In *Chemical Society reviews* 46 (10), pp. 2692–2704. DOI: 10.1039/c7cs00148g.
[73] Qing, Xing; Wang, Yuedan; Zhang, Yang; Ding, Xincheng; Zhong, Weibing; Wang, Dong et al. (2019): Wearable Fiber-Based Organic Electrochemical Transistors as a Platform for Highly Sensitive Dopamine Monitoring. In *ACS applied materials & interfaces* 11 (14), pp. 13105–13113. DOI: 10.1021/acsami.9b00115.
[74] Giordani, Martina; Berto, Marcello; Di Lauro, Michele; Bortolotti, Carlo A.; Zoli, Michele; Biscarini, Fabio (2017): Specific Dopamine Sensing Based on Short-Term Plasticity Behavior of a Whole Organic Artificial Synapse. In *ACS sensors* 2 (12), pp. 1756–1760. DOI: 10.1021/acssensors.7b00542.
[75] Peng, Jing; He, Tao; Sun, Yulian; Liu, Yawen; Cao, Qianqian; Wang, Qiong; Tang, Hao (2018): An organic electrochemical transistor for determination of microRNA21 using gold nanoparticles and a capture DNA probe. In *Mikrochimica acta* 185 (9), p. 408. DOI: 10.1007/s00604-018-2944-x.
[76] Nilsson, D.; Robinson, N.; Berggren, M.; Forchheimer, R. (2005): Electrochemical Logic Circuits. In *Adv. Mater.* 17 (3), pp. 353–358. DOI: 10.1002/adma.200401273.
[77] Braendlein, Marcel; Pappa, Anna-Maria; Ferro, Marc; Lopresti, Alexia; Acquaviva, Claire; Mamessier, Emilie et al. (2017): Lactate Detection in Tumor Cell Cultures Using Organic Transistor Circuits. In *Advanced materials (Deerfield Beach, Fla.)* 29 (13). DOI: 10.1002/adma.201605744.
[78] Norrman, K.; Ghanbari-Siahkali, A.; Larsen, N. B. (2005): 6 Studies of spin-coated polymer films. In *Annu. Rep. Prog. Chem., Sect. C* 101, p. 174. DOI: 10.1039/b408857n.
[79] https://de.wikipedia.org/wiki/Datei:Spin-coater_for_resist_coating_(DE).svg, Used under creative-common Licenses.
[80] Mack, C., 2008. *Fundamental principles of optical lithography: the science of microfabrication*. John Wiley & Sons. ISBN: 978-0-470-01893-4
[81] Madou, Marc J. (2012): Fundamentals of microfabrication and nanotechnology. Volume II, Manufacturing techniques for microfabrication and nanotechnology. Third edition. Boca Raton, FL: CRC PRESS. ISBN: 978-1-4398-9530-6
[82] Bordonaro, G.J., 2012. DUV Photolithography and Materials. *Encyclopedia of Nanotechnology*, pp.590-604. DOI: 10.1007/978-90-481-9751-4_370

[83] The Basics of Microlithography. http://www.lithoguru.com/scientist/lithobasics.html
[84] Willson, C.G., Dammel, R.R. and Reiser, A., 1997, July. Photoresist materials: a historical perspective. In *Metrology, Inspection, and Process Control for Microlithography XI* (Vol. 3050, pp. 38-51). International Society for Optics and Photonics. DOI: 10.1117/12.275921
[85] Jaeger, Richard C. (1988): Introduction to microelectronic fabrication. pp: 17-38. Reading, Mass.: Addison-Wesley Pub. Co. 2nd ed. ISBN: 0-201-14695-9
[86] Angstrom Engineering Inc. https://angstromengineering.com
[87] Cha, S.; Lin, P. C.; Zhu, L.; Sun, P. C.; Fainman, Y. (2000): Nontranslational three-dimensional profilometry by chromatic confocal microscopy with dynamically configurable micromirror scanning. In *Applied optics* 39 (16), pp. 2605–2613. DOI: 10.1364/ao.39.002605.
[88] Brand, U.; Hillmann, W. (1995): Calibration of step height standards for nanometrology using interference microscopy and stylus profilometry. In *Precision Engineering* 17 (1), pp. 22–33. DOI: 10.1016/0141-6359(94)00003-I.
[89] Koutsouras, Dimitrios A.; Gkoupidenis, Paschalis; Stolz, Clemens; Subramanian, Vivek; Malliaras, George G.; Martin, David C. (2017): Impedance Spectroscopy of Spin-Cast and Electrochemically Deposited PEDOT. PSS Films on Microfabricated Electrodes with Various Areas. In *ChemElectroChem* 4 (9), pp. 2321–2327. DOI: 10.1002/celc.201700297.
[90] Lee D, Cho N.: *Assessment of surface profile data acquired by a stylus profilometer*, Meas. Sci. Technol. 23 (2012) 105601-105613
[91] Veeco Instruments: *Dektak 8 Advanced Development Profiler Manual*, 2005
[92] User manual guide of RIE-1701 Plasma System, Nordson March Inc.
[93] Henglein, A., & Gutierrez, M. (1993). Sonochemistry and sonoluminescence: effects of external pressure. *The Journal of Physical Chemistry*, *97*(1), 158-162.
[94] *Azar, Lawrence (February 2009).* Cavitation in ultrasonic cleaning and cell disruption.
[95] User manual guide of MJB4 mask aligner, Süss Microtech Se. https://www.suss.com/en/products-solutions/mask-aligner
[96] Paschalis Gkoupidenis, Molecular Electronics Department, Max-Planck-Institute for Polymer Research, Mainz
[97] Inal, Sahika; Malliaras, George G.; Rivnay, Jonathan (2016): Optical study of electrochromic moving fronts for the investigation of ion transport in conducting polymers. In *J. Mater. Chem. C* 4 (18), pp. 3942–3947. DOI: 10.1039/C5TC04354A.
[98] Avalon Test Equipment, https://avalontest.com/tektronix-2604b-sourcemeter-200-w-2-ch/
[99] Nilsson, D.; Robinson, N.; Berggren, M.; Forchheimer, R. (2005): Electrochemical Logic Circuits. In *Adv. Mater.* 17 (3), pp. 353–358. DOI: 10.1002/adma.200401273.
[100] Zhang, Shiming; Hubis, Elizabeth; Girard, Camille; Kumar, Prajwal; DeFranco, John; Cicoira, Fabio (2016): Water stability and orthogonal patterning of flexible micro-electrochemical transistors on plastic. In *J. Mater. Chem. C* 4 (7), pp. 1382–1385. DOI: 10.1039/C5TC03664J.
[101] Khodagholy, Dion; Rivnay, Jonathan; Sessolo, Michele; Gurfinkel, Moshe; Leleux, Pierre; Jimison, Leslie H. et al. (2013): High transconductance organic electrochemical transistors. In *Nature communications* 4, p. 2133. DOI: 10.1038/ncomms3133.
[102] Stavrinidou, Eleni; Leleux, Pierre; Rajaona, Harizo; Khodagholy, Dion; Rivnay, Jonathan; Lindau, Manfred et al. (2013): Direct measurement of ion mobility in a conducting polymer. In *Advanced materials (Deerfield Beach, Fla.)* 25 (32), pp. 4488–4493. DOI: 10.1002/adma.201301240.
[103] Rivnay, Jonathan; Inal, Sahika; Collins, Brian A.; Sessolo, Michele; Stavrinidou, Eleni; Strakosas, Xenofon et al. (2016): Structural control of mixed ionic and electronic transport in conducting polymers. In *Nature communications* 7 (1), p. 11287. DOI: 10.1038/ncomms11287.